Dipl. Ing. Peter Böhling B. Eng.

Numerical Investigation of Pharmaceutical Coating Processes at the Industrial Scale

DISSERTATION

zur Erlangung des akademischen Grades

Doktor der technischen Wissenschaften

eingereicht an der

Technischen Universität Graz

Betreuer

Univ.-Prof. Dipl. –Ing .Dr. tech. Johannes G. Khinast

Institute for Process and Particle Technology

Graz, Februar 2020

EIDESSTATTLICHE ERKLÄRUNG

Ich erkläre an Eides statt, dass ich die vorliegende Arbeit selbstständig verfasst, andere als die angegebenen Quellen/Hilfsmittel nicht benutzt, und die den benutzten Quellen wörtlich und inhaltlich entnommenen Stellen als solche kenntlich gemacht habe. Das in TUGRAZonline hochgeladene Textdokument ist mit der vorliegenden Dissertation identisch.

20.2.2020
Datum

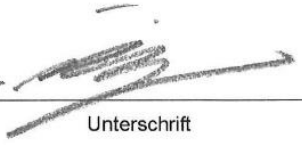
Unterschrift

Aus großer Verantwortung
erwachsen große Dinge.

Steven Fister,

Abstract

Coating processes are ubiquitously used in the pharmaceutical industry. Often as the last process steps to modify the final product. It is used to enhance performance. Coatings are applied for a wide variety of reasons. But is more often than not an afterthought during product development. Therefor the goal is to find process conditions that can deliver the desired product quality and little attention is paid to optimization possibilities. The goal of this work is to introduce and show the application of state of the art simulation for coating processes. It should be shown that process simulation can be used to develop or improve the coating process while simultaneously reducing the number of experiments

In this work state of the art, discrete element methods and computational fluid dynamics simulations are used to describe coating processes. DEM is used to simulate the movement of granular material, in this work, tablets and granules. DEM solves Newton's second law through time discretization. Computational fluid dynamics solves the Navier stokes equation through resolving the considered volume in small subvolumes and solving for each subvolume the Navier stokes equation. CFD and DEM algorithms can be coupled to exchange momentum, heat, and mass. In this work pure DEM simulation is used to describe tablet coating processes as well as coupled CFD-DEM simulations to characterize a Wurster coating and novel tablet coating process.

This work is structured into 5 main sections that are either already published or planned for publishing. In the first part, a tablet-coating process in a drum batch coater is analyzed. The influence of the material parameters on the tablet bed dynamic is shown in the laboratory and pilot scale. Through validating the simulation approach the tablet coating process is scaled from the laboratory to the industrial scale using the two most commonly used scale-up rules, scaling by keeping either the circumferential velocity or Froude number constant. Showing the influence of the scaling parameters a multidimensional analysis of the tablet coating process is performed at the industrial scale. These three parts are connected through similarity in the coater design and simulation approach. Afterward, the coating process inside a Glatt 15-30 Wurster coater is simulated. In this work, the influence of the fluidization airflow, particle size, and Wurster gap height are shown. In the last part of this work, we validated our developed model to simulate a novel continuous tablet coating process. The simulation results of the tablet movement, coating quality, outlet air temperature, and humidity agree well with experimental results.

This work shows how to apply state of the art simulation techniques for the process development. This way developing and improving existing coating process can be simplified by replacing time and material consuming experiments with simulations and only run experiments on the most promising settings.

Zusammenfassung

Coatingverfahren sind allgegenwärtig in der pharmazeutischen Industrie. Oft bilden sie den letzte Prozessschritte in dem das Produkt noch modifiziert wird. Coatings werden aus einer Vielzahl von Gründen verwendet. Meistens wird der Coatingprozess aber erst am Ende des Produktentwicklungszyklus betrachtet. Das Ziel ist oft Prozessbedingungen zu finden, die die gewünschte Produktqualität liefern können, dabei werden Optimierungsmöglichkeiten wenig betrachtet. Ziel dieser Arbeit ist Coatingverfahren *in silico* zu modellieren. Es soll gezeigt werden, dass durch Prozesssimulation die Coatingverfahren otpimiert werden können, bei gleichzeitiger Reduzierung der Anzahl von Experimenten.

In dieser Arbeit werden modernste Simulationen verwendet, diskrete Elementmethoden und Computational Fluid Dynamics, um Coatingprozesse zu simulieren. Mit DEM wird die Bewegung von Partikeln simuliert, in dieser Arbeit Tabletten und Granulate. DEM löst Newtons zweites Gesetz durch zeitliche Diskretisierung. Computational Fluid Dynamics löst die Navier-Stokes-Gleichung durch Auflösen des betrachteten Volumens in kleine Teilvolumina und löst für kedes Teilvolumen die Navier-Stokes-Gleichungen. CFD- und DEM-Algorithmen können gekoppelt werden, um Impuls, Wärme und Masse auszutauschen. In dieser Arbeit werden reine DEM-Simulationen zur Beschreibung von Tablettencoatingverfahren sowie gekoppelte CFD-DEM-Simulationen zur Simulation eines Wurster-Coater und eines neuartigen Tablettencoatingverfahren verwendet.

Die Arbeit gliedert sich in fünf Hauptabschnitte, die entweder bereits veröffentlicht sind oder veröffentlicht werden sollen. Im ersten Teil wird ein Tablettencoatingverfahren in einem Trommelcoater analysiert. Der Einfluss der Materialparameter auf die Tablettenbettdynamik wird im Labor- und Pilotmaßstab gezeigt. Durch die Validierung des Simulationsansatzes wird der Tablettencoatingverfahren mithilfe der beiden am häufigsten verwendeten Scale-up-Regeln vom Labor auf den industriellen Maßstab skaliert, wobei entweder die Umfangsgeschwindigkeit oder die Froude-Zahl konstant gehalten werden. Nach dem der Einflusses der Skalierungsparameter gezeigt wurde, wird eine mehrdimensionale Analyse des Tablettencoatingverfahren im industriellen Maßstab durchgeführt. Diese drei Teile sind durch Ähnlichkeit im Ansatz des Tablettencoatingverfahren und der Simulation miteinander verbunden. Anschließend wird der Beschichtungsprozess in einem Glatt 15-30 Wurster Coater simuliert. In dieser Arbeit wird der Einfluss des Fluidisierungsluftstroms, der Partikelgröße und der Wurster-Spalthöhe gezeigt. Im letzten Teil dieser Arbeit haben wir unser entwickeltes Modell validiert, um einen neuartigen kontinuierlichen Tablettencoatingverfahren zu

simulieren. Die Simulationsergebnisse der Tablettenbewegung, der Beschichtungsqualität, der Auslasslufttemperatur und der Luftfeuchtigkeit stimmen gut mit den experimentellen Ergebnissen überein.

Diese Arbeit zeigt, wie modernste Simulationstechniken für die Prozessentwicklung angewendet werden. Auf diese Weise kann die Entwicklung und Verbesserung bestehender Coatingverfahren vereinfacht werden, indem zeit- und materialaufwendige Experimente durch Simulationen ersetzt und nur Experimente mit den vielversprechendsten Einstellungen durchgeführt werden.

Scope

A. Introduction

The pharmaceutical industry is currently undergoing rapid changes in terms of process development and operation procedure. This is not only due to the pressure of globalization and the associated cost pressure but also to internal changes in the pharmaceutical industry.

Expiring patents for their blockbuster drugs over the last years hit the pharmaceutical industry hard. The so-called patent cliff. New discoveries targeted often smaller population and could not reach the same market as the former blockbuster. This forces the pharmaceutical industry to innovate or streamline its processes to increase the yield of the production and decrease the cost at the same time, e.g. through switching to continuous processes [1]. Another possibility to increase the duration of blockbuster sales is to improve product quality. Song and Han [2] advise that the pharmaceutical industry should follow multiple paths to ensure profitability.

Regulating agencies changed their strategy to improve the quality of the pharmaceutical production process due to increased recalls and drug shortages[3]. A focus was laid on allowing for continuous improvement of the production and good manufacturing practice. Manifold initiatives were launched and broadly discussed to achieve this goal [4]. Up to this date, the pharmaceutical industry is still in the transition phase to apply the possibilities and requirements.

Granular processes can widely vary and the same process can behave differently when operated at different sites. Understanding the mechanisms behind the granular material behavior allows to set-up and run processes safer and for a more precise process control strategy which in return enables for more flexible process space.

These factors force the pharmaceutical industry to rethink its production process development. Old batch processes are often outdated and poorly understood. Production was often an afterthought in the process development. The focus in research and development of new APIs was the discoveries of new molecules. Nowadays the trend is to catch up to other industries in production capabilities through increased process understanding [5] e.g. six sigma processes in the semiconductor industry.

Pharmaceutical coating processes are widely used to enhance the product recognizability, stability or functionality. Coatings can be applied to granules or tablets. Granules are coated in fluidized bed systems. In the case of granule coating, the Wurster coater is predominantly used as it allows for a defined coating cycle and minimizes the risk of granulation. The Wurster coater is a special form of the bottom spray fluidized bed coater[6]. The drying air simultaneously provides drag for the particle

movement. Tablets are another typical target for coating. In comparison to granules, tablets are seldom coated in fluidized bed systems. The bulk of tablets are coated in rotating drum batch coaters. In the rotating drum batch coater tablets are agitated through the rotation of the drum concurrently baffles and anti-slip bars are installed in the coater to increase tablet movement and the mixing of the tablet bed. The coating is applied from a central axis of the coater and angled to spray the tablet bed surface at around 1/3 of its height. In the tablet coating process, the drying air is introduced independently from the drum movement and does not influence the tablet movement. Both coating processes are investigated numerically in this work.

The goal of this work is to introduce and display the capabilities of numerical simulations in understanding and improving coating processes. Normally coating processes are developed at the end of the process development and seldom much thought is put into improving existing processes due to prohibitive costs either due to material or lost production time. Process understanding is key when creating new or enhancing old processes. Most of the time laboratory experiments are performed to extend the process understanding. Afterward, dimensionless numbers are used to transfer the process behavior to different scales. But to truly understand and control a process mechanistic understanding is the key [7], [8]. Mechanical understanding of the underlying processes allows for accurate measurements and control strategy as well as running the process more efficiently. Creating a mechanical understanding of the process is often hard, as measuring all needed information during and after the process is challenging and often very costly. Simulation can help to bridge the gap between the observed effects and the resulting behavior[9]. In this work numerical models are used to describe the movement of tablets, granules and the drying airflow. In the first half, the discrete element method is used to investigate tablet coating processes. A focus was laid is used to describe the tablet movement at different scales and process settings. The idea is to use simulation showing the relationship between process input parameters and the process responses. It is shown how simulation can help to understand the tablet coating process and it shows how simulation could be used to select better process settings. Similar thoughts were put into the simulation of a Wurster coater process. The influence of the process settings and even the granule size were considered when investigating it. In the end, a model was developed that allows to include the heat and mass transfer inside the simulation. The performed simulations allowed to investigate coating processes at the industrial scale. Performing the same investigation experimentally is either impossible or not feasible due to cost. Therefore simulations allow for profound insights of processes involving granular material materiahere exemplified through the simulation of coating processes.

A-1. Coating Processes

Coating processes are often employed in the pharmaceutical industry. A solid is coated onto substrate particles. In the pharmaceutical industry mainly three types of coating processes are in use, sugar coating, batch film coating, and fluidized bed coating [10]. All coating process types in common are that the suspension is applied via one or multiple spray nozzles. Through high atomization air pressure, a fine mist is created and the particles pass through the designated spray zones. The spray zones are defined through the applied pattern pressure and depend on the overall process strategy and layout [11]. The advantage of the liquid coating process is the flexibility and frequency of use. The disadvantage is the necessity to evaporate the coating liquid and the possibility of coating defects as well as the after-treatment to evaporate the excess liquid. Sugarcoating originated in the confectionery production and was adopted for the pharmaceutical industry to mask the often bitter taste of the drug. Nowadays film coating is the primary form of tablet coating. Fluidized bed coating is used mainly to coat pellets or micro tablets.

A-1.1. Coating process goals

Reasons for coating in the pharmaceutical industry range from adding color, a functional layer either, for environmental protection or delayed-release, or a secondary functionality, e.g. active pharmaceutical ingredient (API) [17]. Sometimes all the above-mentioned motives have to taken into consideration when designing a coating process. Color coating is done for brand recognition, ease of use or to mask tablet defects e.g. dark spots due to the tableting process. A functional layer is applied to protect the API from environmental influences e.g. humid conditions, sunlight or heat. Delayed-release is used to help transport the API to the part of the digestive tract to allow for the most beneficial ways of administration or to release the API over a well defined period of time. This is done through pH active coatings that either protect from the acid environment of the stomach and release the API in the small and large intestines or through a coating that allows the slow diffusion of the API. This is done by coating an API onto the substrate particle either as the main or as a secondary API that supports the main API in its functionality.

A-1.2. Coater types

Coater types are typically defined through the direction in which the coating is applied. Similar to the coating types there exist four main coater types, these are the top, bottom, Wurster and side coater [18], see Figure 1. In the top coater, the coating is applied from the top. A typical top coating would be a fluidized bed or drum tablet coater. In the bottom coater, the coating is applied through a nozzle at

the bottom of the coater. An often used bottom spray coater is the so-called Wurster coater [6]. In the side coater, the spray nozzle is positioned at the side of the coater. Independent of the direction of the spray all coaters have to apply mechanisms to provide mixing of the particle bed to avoid overwetting and guarantee an evenly consistent application of the coating.

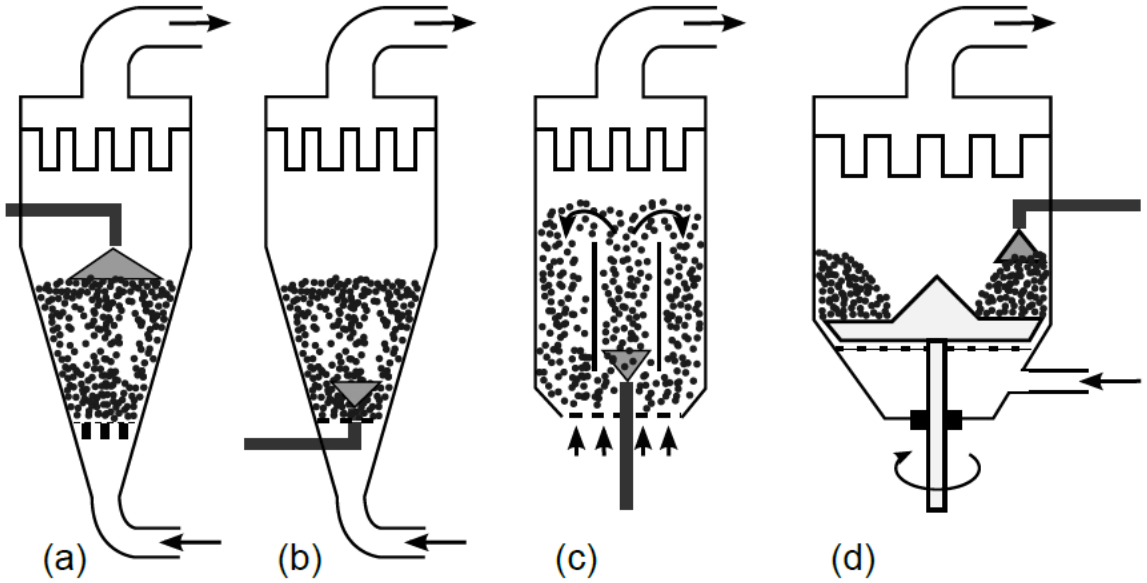

*Figure 1: Different types of fluidized bed coaters: Top (a), Bottom (b), Wurster (c), and side (d) fluidized bed coater. Figure is taken from **[18]***

A-1.3. Tablet Coating

Tablets are the most commonly taken dosage forms. Tablets simplify the administration, especially self-administration, as usually a tablet is one dosage [19]. Tablets are easy to store and can be differentiated due to shape, size or color. Tablets are coated for the reasons mentioned in the chapter Coating process goalsA-1.1. A typical tablet coating process is set in a drum coater, which rotates slowly around its lateral axis [20]. An image of the simulation of a typical coating process is shown in Figure 2. Through the rotation movement, the tablets are lifted up along the outer drum wall. When they reach a certain angle which is defined through the rotation rate, tablet shape, tablet material properties, and drum design the tablets fall down the top of the tablet bed [21]. To provide an even tablet bed height the lifting can be supported through anti-slip bars along the drum hull. The spray coating is applied through a spray nozzle stationed at roughly the drum center axis. The number and exact position of the spray nozzles depends on the scale, drum design and mode of operation. The spray is applied via a top spray approach. When the tablets reach the end of the tablet bed surface they get remixed into the tablet bed and are transported again to the spray zone. To ensure a good mixing the drum coater typically

also employes baffles. Baffles can have spiral, paddle or helical shapes. The baffles provide additional lift as well as provide axial and radial mixing of the tablet bed. In most tablet coating processes, the coating is provided through a liquid-solid suspension. Therefore the liquid has to be removed during and after the coating process. Drying air is usually introduced in such a way that it enters the coater outside the tablet bed and is sucked out through the tablet bed. This way the tablet – air contact time or drying time is maximized.

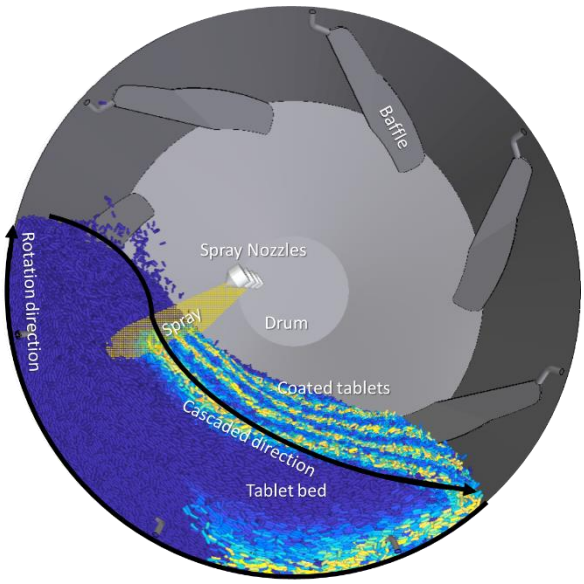

Figure 2: Typical tablet coating process in an industrial drum batch coater

A-1.4. Wurster coater

Another typically employed coating unit is the Wurster coater [6]. The Wurster coater is a special kind of a fluidized bed coater in which the coating is applied through one or more bottom spray nozzles (Figure 3). Above the spray nozzle, a tube is located. The bottom plate is perforated and through a varying number of perforation holes and diameters, the gross of the fluidization air is directed through the riser tube. Thus the particles are directed to pass through the Wurster tube through a chimney effect and thus a well adjustable cycle time between spray events can be achieved compared to conventional fluidized bed coaters. The particle-particle, particle-geometry and particle-air interactions are very complex and defining a process that fully fulfills all CQAs is challenging. Especially the scaling between the laboratory and larger process scales is not yet fully understood.

Figure 3: Wurster coater process. The particles are colored according to their velocity.

A-1.1. Laboratory experiments

During process development, the amount of available material is limited. Therefore initial experiments are performed in small laboratory coaters which can have a load between a few hundred grams up to a few kilograms [22], [23]. These initial experiments give first impressions about the tablet bed behavior and the slippiness of the tablet material. Also, the absorbency of the tablets as well as the drying behavior of the tablets is initially investigated. All these factors influence the tableting process and can be optimized if initial experiments show the necessity. But seldom laboratory experiments give insights into the tablet bed behavior at larger scales due to changes in material, geometry and drying behavior. Often dimensionless numbers are used to transfer the coating process from the smaller to larger scales. Agrawal et al. give an extensive overview of the dimensionless number used to scale the complete tablet coating process including thermal effects and spray nozzle setup [26].

A-1.2. Definition good coating process

The goal of the tablet coating process development is to guarantee that all critical quality attributes (CQAs) can be reached [27], [28]. Therefore the understanding of how to influence and achieve the CQAs should be demonstrated through experiments and models of the existing process. Then the process space should be chosen such that the CQAs can be achieved in a short period of time to maximize the throughput rates and production capacity and to allow a consistent product output quality for a wide variety of process input parameters.

A coating process is often described through two parameters the inter- and intraparticle coating variability. Interparticle coating variability (CoV_{inter}) is the standard deviation σ_{mc} of the coating mass distributed over all tablets divided by the mean of the coating mass μ_{mc} [12]:

$$CoV_{inter} = \frac{\sigma_{mc}}{\mu_{mc}} \quad (1)$$

An optimal tablet coating process has a consistently low $CoV_{inter.}$ In a typical coating process, the CoV_{inter} is measured through weighting randomly chosen sample particles. The intraparticle coating variability (CoV_{intra}) is the variability on the particle itself [13]. CoV_{intra} can be measured through the variability in the coating thickness over the particle surface or the calculated coating mass difference over the whole tablet. Typically the CoV_{intra} is measured through cutting the particle and doing microscopic measurements of the coating layer. Nowadays this process can be simplified for some coating processes by employing terahertz spectroscopy [14] or optical coherence measurements of the coating (OCT) [15]. These approaches also allow to rapidly measure the CoV_{intra} of a lot of particles. Other quality attributes for a good coating process are no defects, blistering, peeling, and no particle sticking to each other or the processing unit [16].

A-2. Process simulation,

Process simulation allows predicting process outcomes for a varying amount of process settings by reducing the demand for actual experiments [29]. There exist two main types of process simulation models, empirical and mechanistic. Empirical models use experimental gathered data to connect the process settings to the process outcomes via more or less complex mathematical fitting equations. The advantage of the empirical models is that the model fitting can nowadays be done via a wide variety of tools, beginning from simple excel sheet interpolations to complex multi-variant model analysis. The main disadvantage is that the empirical models typically do not give insight into the process mechanisms. This means that most empirical models are only valid for a narrowly defined process space or device. Mechanistic models, on the other hand, try to describe the physical laws inside the process units and thus predict the process outcome from a physical point of view. Describing physical laws in real processes is a complex task as a lot of different phenomena take place at roughly the same time during the process. The advantage of mechanistic models is that once set up and validated they should hold up for all possible process conditions. The discrete element method (DEM) is a typical mechanistic model that describes the behavior of granular material in all possible process units and conditions and allows to investigate processes in experimental impossible or very challenging ways. Another mechanistic simulation model employed in this work i is computation fluid dynamics(CFD). Other worth

mentioning models are the Lattice Boltzmann Models (LBM), direct numerical simulation (DNS), and molecular dynamics (MD). As these other models are not used in this work only the DEM and CFD-DEM will be explained in more detail.

A-2.1. CFD-DEM Simulation

CFD-DEM simulations model the fluid-solid material interactions. Both phases are simulated separately and information is exchanged via source terms. Both simulation methods are iterative in nature. In the DEM the time is discretized through small difference. In the CFD the volume is spatially resolved and the time can be discretized as well. Source terms allow exchanging momentum, heat and mass information between the fluid and solid phase. CFD models the fluid phase by solving the volume-averaged Navier-Stokes equations. All variables are locally volume-averaged quantities over the control volume V, which has to be at least one order of magnitude larger than the particle volume VP [30]. The conservation of mass can be written as follows:

$$\frac{\partial}{\partial t}(\varepsilon_F \cdot \rho_F) + \nabla \cdot (\varepsilon_F \cdot \rho_F \cdot v_F) = 0 \tag{2}$$

where ρ_f is the fluid density, ε_F is the local volume fraction of the fluid, v_F is the fluid velocity vector and t is the time. S_m represents the mass source term The conservation of the momentum is

$$\frac{\partial}{\partial t}(\varepsilon_F \cdot \rho_F \cdot v_F) + \nabla(\varepsilon_F \cdot \rho_F \cdot v_F \cdot v_F) = -\varepsilon_F \cdot \nabla p - \nabla \cdot (\varepsilon_F \cdot \tau_F) + \varepsilon_F \cdot \rho_F \cdot g - S_M \tag{3}$$

In CFD-DEM the fluid phase and the granular phase are modeled and the simulation can exchange information about the momentum, energy and even mass. Similar to equation 4 the source term can be used to transfer mass and energy between the granular and fluid phases. This allows simulating the coating process in even more detail as it allows to track the wetness and temperature of the particles during the coating process, showing zones of low and high energy/temperature. This helps to indicate possible weaknesses of the investigated processes and also more detailed scaling/changing of process size and settings.

The discrete element method (DEM) was developed by Cundall and Strack [31] in 1979. It solves Newton's second law by resolving particle-particle and particle–wall interactions [32], [33]. For the motion of each particle, the following equation is solved:

$$m_P \frac{dv_P}{dt} = -V_i \nabla p + \vec{F}_i^d + \sum_0^{N_P} F_{P \to P} + \sum_0^{N_W} F_{P \to W} + m_p g \tag{4}$$

where m_P is the particle mass, $\mathbf{v}_P$ is the particle velocity, $-V_i \nabla p$ is the pressure gradient force, $\vec{F}_i^d$ is the drag force, $\mathbf{F}_{P->P}$ is the particle-particle force and $\mathbf{F}_{P->W}$ is the particle-wall force. Here the fluid-particle interaction is already integrated in the equation. The three-dimensional angular momentum of the particle is calculated as

$$I_P \frac{d\omega_P}{dt} = \sum_0^{N_c} M_P + M_W + M_F \tag{5}$$

where $\boldsymbol{\omega}_P$ is the angular velocity, $\mathbf{M}_P$ is the torque coming from other particles $\mathbf{M}_w$ is the torque coming from particle–wall interactions and $\mathbf{M}_F$ is the torque coming from the surrounding fluid and $\mathbf{I}_P$ is the moment of inertia. Typically particles are represented as spheres in the simulation. There exist several ways to calculate the contact forces. The two main types are the hard- and soft-sphere model. The hard-sphere approach is an event-driven method while the soft-sphere approach is time step driven. This work only uses soft-sphere models to resolve particle contact. In soft sphere contact models, the contact events are timely resolved and the time step size has to be chosen such that the average contact has a duration of 10 to 20 time-steps.

A-2.2. DEM usage in the pharmaceutical industry

DEM is increasingly used in the pharmaceutical industry [32]–[35]. Initially, only small or simple processes could be investigated due to the high computational costs. One of the first processes to be investigated was the tablet coating process on the laboratory scale. Often coarse-graining[36], [37] methods are applied to reduce the number of particles to simulate. This holds true up to date for the simulation of powders where even in a small sample the number of particles reaches the hundred millions. For the tablet coating process, the particle shape was not taken into consideration when simulating pharmaceutical processes. But due to increasing computational power in combination with more advanced models realistic simulations of even large scale processes are possible.

Publications show the influence the material interaction parameters have on the bulk material behavior [38], [39]. Changing the parameters of material interaction can result in completely different results. Thus calibrating and choosing the right parameters is of utmost importance if the goal is to correctly predict process outcomes.

A-2.3. Advanced DEM

Similar to the material parameters, the shape of the granular material can influence the bulk behavior in the simulation. While some effects can be replicated through choosing the right material interaction

parameters other phenomena can only be simulated by trying to replicate the particle shape. Different ways of introducing particle shapes exist. The simplest form is the so-called glued sphere approach [40]. In this approach, the particle shape is emulated through gluing several spheres together. The accuracy of the modeled particle depends on the number of used sub spheres. This approach has the advantage of using the same contact detection and force calculation algorithm as for spheres and the disadvantage of needing a high number of sub spheres to realistically emulate the particle shape. It also introduces an artificial roughness to the particle which has to be taken into consideration when calibrating the material properties. A special case of the glued sphere model is the so-called real tablet shape. In this approach, biconvex tablets are described through three overlapping spheres. The tablet is described as the volume where the three spheres overlap [41].

Another approach to model nonspherical particles is to use ellipsoidal or super ellipsoidal particle shape [42]. This has the advantage of mathematical describing particle shape but is limited to ellipsoidal particles. Further is the contact and force calculation algorithm more complex than for simple spheres or glued sphere particles. A more widely applicable shape representation is the super quadric [43]approach. This allows representing a very wide type of particle shape mathematical through three parameters. Again the contact and force calculation is more complex. Both approaches, the ellipsoidal and super quadrics approach allow to even further increase the accuracy of the particle shape through multi-element models. The polyeder particles allow specifying arbitrary particle shape by defining the outer surfaces of the particle as planes[44]. By connecting several planes around a volume the particle shape is mimicked. This approach allows to model nearly all possible particle shapes but again the contact and force algorithms are increasingly complex.

A-3. Goal

The goal of this work is to use simulations, DEM and CFD-DEM to investigate granular processes in the pharmaceutical industry. In the next three chapters (B-D) a tablet-coating process is investigated, in chapter E a Wurster coating process at the industrial scale is investigated. In chapter F a model for a fully coupled, meaning momentum, heat and mass transfer, CFD-DEM simulation of a new tablet bed coater is validated.

In chapter B, the influence of the material properties on the tablet bed behavior is shown. The tablet bed surface velocity was experimentally evaluated through a novel high-speed camera combined with an image analysis algorithm. This approach eliminates the necessity to use tracer tablets to measure the tablet bed surface velocity. The performed experiments in the lab and pilot-scale were repeated in

silico. Through varying the tablet-tablet, tablet-wall friction, tablet stiffness, restitution, and simulation time step the material properties were calibrated. The tablet stiffness has the largest influence on the tablet surface velocity. At last, the change in the tablet bed behavior and process outcome were illustrated. This chapter was published [45].

After the influence of the material properties is shown the developed DEM model is used to scale a tablet-coating process from the lab to pilot and industrial scale. Here the focus was on the mechanical tablet bed behavior. The work focuses on the change in tablet surface velocity, spray residence time, coating quality, and cycle time through the varying coater scales. Thermal effects, e.g. tablet heating and drying were neglected as only the tablets were simulated. It could be shown that scaling by the circumferential velocity is not favorable compared to the Froude scaling as it would result in long (high) process durations. This chapter was published as [46].

After the effects of the scale-up rules on the tablet bed behavior were demonstrated a multi-variant study of the tablet coating process at the industrial scale was performed. The study was performed in silico to show the influence of the drum load, rotation rate, spray rate and number of spray nozzles on the coefficient of inter tablet coating variability. The simulation allowed an in-depth analysis of the changes in tablet bed behavior. Additionally, the calculated results for the CoV agreed well with the experimental investigated ones. It could be shown that increasing the spray nozzle number has the highest influence on coating mass distribution. As thermal effects were not included here as well there are be no predictions made regarding the drying behavior. This paper was published as [47].

An industrial-scale Wurster coating process was simulated to introduce the fluid-particle coupling at the industrial scale. A Glatt 15-30 Wurster coater with a load of 40 kg was simulated using our simulation approach. The simulations show the influence of the fluidization air flow rate, particle size, on the coating quality, cycle time, residence time and particle velocity. This chapter was published as [48].

In chapter G, a validation of a CFD-DEM simulation of the newly developed ConsiGma tablet coater is presented. The ConsiGma® tablet coater handles small batches, coherent to the ConsiGma production philosophy. During the coating process, the tablets are centrifuged to the drum wall and detached at around 2-3 o'clock positions through so-called air knives. Therefore to replicate the coating process in silico the air has to be included. This allows to also model the heat and mass transfer. The used models are validated against performed experiments and correlate very well. This part is planned for publishing.

A-4. Bibliography

[1] FDA, "Quality Considerations for Continuous Manufacturing Guidance for Industry Quality Considerations for Continuous Manufacturing Guidance for Industry(draft)," no. February, 2019.

[2] C. H. Song and J. W. Han, "Patent cliff and strategic switch : exploring strategic design possibilities in the pharmaceutical industry," *Springerplus*, pp. 1–14, 2016.

[3] K. Plumb, "Continuous Processing in the Pharmaceutical Industry: Changing the Mind Set," *Chem. Eng. Res. Des.*, vol. 83, no. June, pp. 730–738, 2005.

[4] L. X. Yu *et al.*, "Review Article Understanding Pharmaceutical Quality by Design," vol. 16, no. 4, 2014.

[5] W. Hsiao *et al.*, "Feeding of particle-based materials in continuous solid dosage manufacturing : a material science perspective," *Drug Discov. Today*, vol. 00, no. 00, 2019.

[6] D. E. Wurster, "Air-suspension technique of coating drug particles. A preliminary report," *J. Am. Pharm. Assoc.*, vol. 48, no. August, pp. 451–454, 1959.

[7] P. R. Wahl, D. Treffer, S. Mohr, E. Roblegg, G. Koscher, and J. G. Khinast, "Inline monitoring and a PAT strategy for pharmaceutical hot melt extrusion.," *Int. J. Pharm.*, Jul. 2013.

[8] S. Adam, D. Suzzi, C. Radeke, and J. G. Khinast, "An integrated Quality by Design (QbD) approach towards design space definition of a blending unit operation by Discrete Element Method (DEM) simulation.," *Eur. J. Pharm. Sci.*, vol. 42, no. 1–2, pp. 106–15, Jan. 2011.

[9] E. Sahni and B. Chaudhuri, "Experiments and numerical modeling to estimate the coating variability in a pan coater.," *Int. J. Pharm.*, vol. 418, no. 2, pp. 286–96, Oct. 2011.

[10] R. Turton and X. X. Cheng, "The scale-up of spray coating processes for granular solids and tablets," *Powder Technol.*, vol. 150, no. 2, pp. 78–85, Feb. 2005.

[11] G. Toschkoff, D. Suzzi, W. Tritthart, F. Reiter, M. Schlingmann, and J. G. Khinast, "Detailed Analysis of Air Flow and Spray Loss in a Pharmaceutical Coating Process," *Aiche J.*, vol. 58, pp. 399–411, 2012.

[12] A. Dubey *et al.*, "Improvement of tablet coating uniformity using a quality by design approach.," *AAPS PharmSciTech*, vol. 13, no. 1, pp. 231–46, Mar. 2012.

[13] B. Freireich, R. Kumar, W. Ketterhagen, K. Su, C. Wassgren, and J. A. Zeitler, “Comparisons of intra-tablet coating variability using DEM simulations , asymptotic limit models , and experiments,” *Chem. Eng. Sci.*, vol. 131, pp. 197–212, 2015.

[14] J. M. A. Mauritz, R. S. Morrisby, R. S. Hutton, C. H. Legge, and C. F. Kaminski, “Imaging pharmaceutical tablets with optical coherence tomography.,” *J Pharm Sci*, vol. 99, no. 1, pp. 385–91, Jan. 2010.

[15] D. Treffer *et al.*, “In-line implementation of an image-based particle size measurement tool to monitor hot-melt extruded pellets.,” *Int. J. Pharm.*, vol. 466, no. 1–2, pp. 181–189, Mar. 2014.

[16] A. R. Muliadi and P. E. Sojka, “A REVIEW OF PHARMACEUTICAL TABLET SPRAY COATING,” *At. SPRAYS*, vol. 20, pp. 611–638, 2010.

[17] G. Cole, J. Hogan, and M. E. Aulton, *Pharmaceutical Coating Technology*. Taylor and Francis, 2002.

[18] E. Teunou and D. Poncelet, “Batch and continuous fluid bed coating – review and state of the art,” *J. Food Eng.*, vol. 53, pp. 325–340, 2002.

[19] EU-Regulations, “2.9.40. uniformity of dosage units,” *Eur. PHARMACOPOEIA*, vol. 5.2, pp. 3117–3120.

[20] G. W. Smith, G. S. Macleod, and J. T. Fell, “Mixing efficiency in side-vented coating equipment.,” *AAPS PharmSciTech*, vol. 4, no. 3, p. E37, 2003.

[21] A. R. Muliadi and P. E. Sojka, “A Review of Pharmaceutical Tablet Spray Coating,” vol. 20, no. 7, pp. 611–638, 2014.

[22] S. Tobiska and P. Kleinebudde, “Coating uniformity and coating efficiency in a Bohle Lab-Coater using oval tablets,” *Eur. J. Pharm. Biopharm.*, vol. 56, pp. 3–9, 2003.

[23] a Faure, P. York, and R. C. Rowe, “Process control and scale-up of pharmaceutical wet granulation processes: a review.,” *Eur. J. Pharm. Biopharm.*, vol. 52, no. 3, pp. 269–77, Nov. 2001.

[24] W. R. Ketterhagen, “Modeling the motion and orientation of various pharmaceutical tablet shapes in a film coating pan using DEM.,” *Int. J. Pharm.*, vol. 409, no. 1–2, pp. 137–49, May 2011.

[25] A. Kalbag, C. Wassgren, S. Sumana Penumetcha, and J. D. Pérez-Ramos, “Inter-tablet coating

variability: Residence times in a horizontal pan coater," *Chem. Eng. Sci.*, vol. 63, no. 11, pp. 2881–2894, Jun. 2008.

[26] A. M. Agrawal and P. Pandey, "Scale Up of Pan Coating Process Using Quality by Design Principles," *J. Pharm. Sci.*, vol. 104, no. 11, pp. 3589–3611, 2015.

[27] E. Pharmacopoeia, "European Pharmacopoeia (PhEur) chapter 2.9.40 Uniformity of dosage units," *Eur. Pharmacop.*, vol. 8.8, pp. 3117–3120.

[28] S. Harmonization, "⟨ 905 ⟩ UNIFORMITY OF DOSAGE," *United States Pharmacopoeia*, vol. 3, pp. 4–6, 2011.

[29] J. Rantanen and J. Khinast, "The Future of Pharmaceutical Manufacturing Sciences," *J. Pharm. Sci.*, vol. 104, no. 11, pp. 3612–3638, 2015.

[30] D. Jajcevic, E. Siegmann, C. Radeke, and J. G. Khinast, "Large-scale CFD–DEM simulations of fluidized granular systems," *Chem. Eng. Sci.*, vol. 98, pp. 298–310, Jul. 2013.

[31] P. A. Cundall and O. D. L. Strack, "A discrete numerical model for granular assemblies," *Géotechnique*, vol. 29, no. 1, pp. 47–65, Jan. 1979.

[32] P. Toson and J. G. Khinast, "Data in brief Particle-level residence time data in a twin-screw feeder," *Data Br.*, vol. 27, p. 104672, 2019.

[33] P. Toson *et al.*, "Detailed modeling and process design of an advanced continuous powder mixer," *Int. J. Pharm.*, vol. 552, no. 1–2, pp. 288–300, 2018.

[34] L. Li *et al.*, "Residence time distributions of different size particles in the spray zone of a Wurster fluid bed studied using DEM-CFD," *Powder Technol.*, vol. 280, pp. 124–134, 2015.

[35] J. Ban, R. Kumar, and S. Agarwal, "Scaling Inter-Tablet Coating Variability in a Horizontal Rotating Drum," vol. 63, no. 9, pp. 3743–3755, 2017.

[36] A. Ozel, J. Kolehmainen, S. Radl, and S. Sundaresan, "Fluid and particle coarsening of drag force for discrete-parcel approach," *Chem. Eng. Sci.*, vol. 155, pp. 258–267, 2016.

[37] T. Weinhart, C. Labra, S. Luding, and J. Y. Ooi, "In fluence of coarse-graining parameters on the analysis of DEM simulations of silo flow," *Powder Technol.*, vol. 293, pp. 138–148, 2016.

[38] S. Luding, "Cohesive, frictional powders: contact models for tension," *Granul. Matter*, vol. 10,

no. 4, pp. 235–246, Mar. 2008.

[39] D. Höhner, S. Wirtz, and V. Scherer, “A numerical study on the influence of particle shape on hopper discharge within the polyhedral and multi-sphere discrete element method,” *Powder Technol.*, vol. 226, pp. 16–28, Aug. 2012.

[40] A. O. Favier, J.F., Abbaspour Fard M.H. , Kremmer, M. and Raji, “Shape representation of axi-symmetrical, non-spherical particles in discrete element simulation using multi element model particles,” *Eng. Comput.*, vol. 16, no. 4, pp. 467–480, 1999.

[41] H. Kureck, N. Govender, E. Siegmann, P. Boehling, C. Radeke, and J. G. Khinast, “Industrial scale simulations of tablet coating using GPU based DEM: A validation study,” *Chem. Eng. Sci.*, 2019.

[42] G. Morris, S. J. Neethling, and J. J. Cilliers, “A model for investigating the behaviour of non-spherical particles at interfaces.,” *J. Colloid Interface Sci.*, vol. 354, no. 1, pp. 380–385, Feb. 2011.

[43] A. Podlozhnyuk, S. Pirker, and C. Kloss, “Efficient implementation of superquadric particles in Discrete Element Method within an open-source framework,” *Comput. Part. Mech.*, vol. 4, no. 1, pp. 101–118, 2017.

[44] N. Govender, R. K. Rajamani, S. Kok, and D. N. Wilke, “Discrete element simulation of mill charge in 3D using the BLAZE-DEM GPU framework,” *Miner. Eng.*, vol. 79, pp. 152–168, 2015.

[45] P. Boehling *et al.*, “Comparison of video analysis and simulations of a drum coating process,” *Eur. J. Pharm. Sci.*, vol. 104, no. March, pp. 72–81, 2017.

[46] P. Boehling *et al.*, “Simulation of a tablet coating process at different scales using DEM,” *Eur. J. Pharm. Sci.*, vol. 93, pp. 74–83, 2016.

[47] P. Boehling *et al.*, “Analysis of large-scale tablet coating : Modeling , simulation and experiments,” *Eur. J. Pharm. Sci.*, vol. 90, pp. 14–24, 2016.

[48] P. Böhling *et al.*, “Computational Fluid Dynamics-Discrete Element Method Modeling of an Industrial-Scale Wurster Coater,” *J. Pharm. Sci.*, vol. 108, pp. 538–550, 2018.

B. Comparison of Video Analysis and Simulations of a Drum Coating Process

Published as: P. Boehling *et al.*, "Comparison of video analysis and simulations of a drum coating process," *Eur. J. Pharm. Sci.*, vol. 104, no. March, pp. 72–81, 2017.

B-1. Abstract

Tablet coating is a common unit operation in the pharmaceutical industry. To improve currently established processes, it is important to understand the influence of the process parameters on the coating quality. One of the critical parameters is the tablet velocity. In this work, numerical results are compared to results obtained experimentally.

Tablet movement in the drums was simulated using the Discrete Element Method (DEM). The simulation parameters were adapted to fit the simulation to the experimental data. A comparison of the experimental and simulation results showed that the simulation correctly represents the real tablet velocity. A change in the velocity over time and its dependence on the rotation rates and the baffle position in the simulation were similar to the experimental results.

In summary, simulations can improve the understanding of tablet coating processes and will thus provide insights into the underlying process mechanics, which cannot be obtained via ordinary experiments.

B-2. Introduction

In the pharmaceutical industry, tablet coating is commonly performed as the last step of the drug production process. Perforated pan coaters are generally the equipment of choice since they provide a gentle yet effective mixing of the tablet bed. Mixing, spraying and drying may occur simultaneously during coating. Understanding the underlying processes involved results in a better quality of the final product. A low coating variability is often required, especially for active coatings. Coating variability is significantly affected by the drum design, the rotation rate, the number of nozzles, the spray rate, the coating time and the drying temperature [1]–[3]. Good mixing in the tablet bed is essential for the homogeneous quality of the end product. Mixing is influenced by the pan speed, which in turns controls the mechanical energy introduced into the system.

Image analysis software for particle tracking, in combination with tracer tablets, was used in previous studies [4-7] to automate the analysis of tablet motion. The effects of pan loading, pan speed and

particle shape on the circulation times, surface appearance times, projected area of particles per pass and cascading velocities were investigated. Most of these studies were only performed on the laboratory scale. Some studies reported rules that govern the cascading velocities [5] when the process is scaled up. In this work, we propose an alternative approach, which combines a high speed camera with an image analysis spatial cross-correlation algorithm, to calculate the velocity fields in the tablet bed without tracer tablets. By computing the difference in the tablet position between two images, the velocity of the tablets can be calculated.

Experiments are expensive and can be material- and time-consuming. Furthermore, dedicated experiments are generally unfeasible after implementing final changes to the process. When planning a new process or optimizing an existing one, simulations can be used to reduce the number of experiments required [6]. The Discrete Element Method (DEM), which is increasingly applied in the pharmaceutical industry to simulate various processes [7], can help to improve the understanding of granular material flows. Due to a low number of particles and a relatively large size of tablets, tablet coating is particularly suitable for the DEM analysis [8]–[10]. When applying DEM, matching the simulations with experiments is crucial [11]. Spheres were often used to simplify the tablet shape in the simulations [9], [12]. However, since the tablet shape influences the bulk behavior and the validity of the simulation results [13][14] , the way the tablet shape is modeled greatly influences the simulation outcome. There are several methods to imitate the shape of the real tablets. In this work, we followed the glued-sphere approach (also termed the multi-element model) [15], which was successfully used in numerous works [13], [14], [16], [17]. It involves several simple shapes (spheres) arranged to mimic the real tablet shape. In this work, we employed the “eXtended Particle System” (XPS), an in house developed DEM software that uses the CUDA programming language to parallelize DEM on graphics processing units (GPUs) [18], [19].

The validity of the experimental results is shown first. A base configuration was chosen and the simulation material parameters were fitted to best reflect the experimental results. A full numerical DOE was performed on the laboratory and pilot scales using the parameters that fit the experiments best. The results show that it is possible to realistically simulate the behavior of a tablet bed and determine the tablet velocity. Moreover, they can predict the tablet velocity on larger scales. Finally, we investigated the influence of the material on the process outcome (coefficient of variation) and established that the elastic properties have a major effect on this quality parameter.

B-3. Material and Methods

B-3.1. Drum and Tablets

This work is a part of an active-coating-process optimization for the production of tablets that contain two active pharmaceutical ingredients (APIs): one with immediate release in the coating layer (active coating) and the other with sustained release in the core. For studying the process of tablet-core coating, gastrointestinal therapeutic systems (GITS 30) were used as a starting material (Bayer Pharma AG, Leverkusen, Germany). GITS 30 are round biconvex two-layer tablets that contain the API Nifedipine. They have a diameter of 9 mm and a height of 5 mm and are pre-coated with cellulose acetate and polyethylene glycol. The tablet shape used in the simulations can be seen in Figure 4 which is taken from [20].

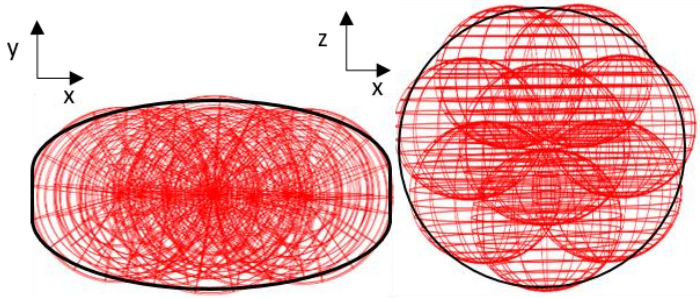

Figure 4: Tablet shape modeled via the glued sphere approach taken from [20].

The tablet velocity assessment experiments were performed on the laboratory scale using a perforated drum coater BFC 5 with a 5kg drum and on the pilot scale using a BFC 50 using a 25kg drum (both L.B. Bohle Maschinen + Verfahren GmbH, Ennigerloh, Germany). The 5 kg and 25 kg coating drums for the experiments and the detailed geometry of the drums were provided by the manufacturer.

B-3.2. Experimental Determination of Tablet Velocity

Drum filling degrees of 12.6% and 16.9% were used in the experimental part of our study. Experiments were done in cooperation with Dreu et al. [21]. Rotation rates of the 5 kg and 25 kg coating drums were varied in order to achieve circumferential drum speeds of 8.3, 16.5, 24.8, 33.1, 41.1 cm/s and for the 25 kg-coating drum, additionally, of 49.6 cm/s. In order to determine tablet surface flow velocities, a 560 or 1180 mm borescope (88590DF, 88770DF, Karl Storz GmbH, Germany) was inserted sideways into the coating drum and mounted to a high-speed camera (MotionBLITZ EoSens mini 2, Mikrotron GmbH, Germany). A high-speed video of the externally-illuminated tablet surface flow was taken at a frame rate of 1 kHz and with a shutter time of 350 or 450 µs. Image pairs from the high-speed tablet surface flow video were analyzed via a cross-correlation algorithm (VidPiv 4.7, ILA GmbH, Germany).

High-speed video data were imported as successive image pairs with a time gap of 1 ms and masked for the area of ~ 300 x 300 pixels that had sufficient sharpness and illuminance. To extract a velocity vector field for each time step, we first applied a cross-correlation algorithm with an interrogation area of 128 x 128 pixels and an interrogation grid separation of 20 pixels and continued with an adaptive cross-correlation algorithm with the same grid settings. A window filter was used to filter out velocity vector outliers. The minimum downward tablet surface flow velocity was set to one half of the drum circumferential speed. To determine the maximum threshold for the downward tablet velocity, tablets that moved to the highest location in the drum were used and a free-fall trajectory was assumed, yielding the maximum possible velocity. In order to attain the correct captured image magnification, the borescope-to-tablet-bed distance was measured in-line by an ultrasonic distance sensor (UM18, SICK, Germany). Representative tablet bed dynamic angles of repose were established by analyzing a separate sideways video (24 fps) of the tablet bed surface contour movement. The obtained spatially averaged velocities in pixels/s were transformed to velocity units by applying a distance-dependent scale and corrected for misalignment between bed dynamic angle of repose and optical axis angle, using equation 6.

$$|\vec{v}| = \frac{|\vec{u}|}{\cos(\Theta - \alpha)}, \tag{6}$$

where $|\vec{v}|$ is the tablet surface flow velocity magnitude aligned with the tablet bed, $|\vec{u}|$ is the video-extracted tablet velocity, α is the optical axis angle of inclination measured from the vertical line and Θ is the local dynamic angle of repose measured from the horizontal line. The whole model is describe and shown by Dreu et al.([21] Figure 1). The time averaged tablet bed distance and dynamic angle of repose was used in the transformation to determine from video the final absolute tablet velocity.

B-3.3. Simulation Setup

B-3.3.1. Simulation Experimental Setup

After initializing the simulation, the tablet bed was allowed to settle for the first 10 seconds, followed by a simulation run of additional 20 seconds (total process time of 30 seconds). 3 seconds during which the baffle position in the simulation matched that in the experiments were used for comparing the tablet velocity. For the simulation parameter, a fill level of 12.6 % and a rotation rate of 15 rpm were chosen as the base case.

Drum filling degrees of 12.6% and 16.9% were used in the simulation part of the study. The rotation rates of the 5 kg and 25 kg coating drums were varied in order to attain coating drum circumferential

speeds of 8.3, 16.5, 24.8, 33.1, 41.1 cm/s and, additionally, of 49.6 cm/s for the 25 kg coating drum. An overview over the different process settings is given in Table 1

Table 1. The position and velocity of every tablet were saved every 0.02 seconds of the simulated process time.

Table 1: Design of Experiment

Drum load in kg	Drum Fill level in %	Rotation rate in rpm	circumferential velocity in cm/s
3.00	12.6	5.00	8.25
3.00	12.6	10.30	16.99
3.00	12.6	15.40	25.40
3.00	12.6	20.70	34.14
3.00	12.6	25.40	41.89
4.00	16.9	5.00	8.25
4.00	16.9	10.30	16.99
4.00	16.9	15.40	25.40
4.00	16.9	20.70	34.14
4.00	16.9	25.40	41.89
16.11	12.6	2.88	8.29
16.11	12.6	5.69	16.39
16.11	12.6	8.61	24.80
16.11	12.6	11.51	33.15
16.11	12.6	14.44	41.58
16.11	12.6	17.25	49.68

21.48	16.9	2.88	8.29
21.48	16.9	5.69	16.39
21.48	16.9	8.61	24.80
21.48	16.9	11.51	33.15
21.48	16.9	14.44	41.58
21.48	16.9	17.25	49.68

The experimental design with a fill level of 12.6 % and rotation rate of 15 rpm in the BFC 5 was used to investigate how varying the spring constant influences the tablet coating process in terms of spray residence time, bed cycle time and coefficient of inter-tablet coating variation. To that end, cases with a spring constant of 2,500 N/m and 25,000 N/m were run for 156 seconds, discarding the first 6 seconds as the initialization phase.

B-3.3.2. Simulation Software

The “eXtended Particle System” (XPS) is a commercial discrete element software that primarily relies on the parallelization technology of nVidia graphics cards (GPUs), which are designed for direct programming using the CUDA language GPUs [22] and are intrinsically designed for massive calculation thread parallelization. This is especially interesting for cases where many simple calculations have to be performed independently from each other, as it is the case when calculating the movement of many independent particles. Modern GPU architectures allows over 2000 CUDA cores in parallel and a simulation of over 70 million single spheres on a single GPU. The glued-sphere [15] approach makes it possible to simulate non-spherical shapes, such as tablets. The XPS –DEM algorithm applied in this study uses a linear spring-dashpot system. The forces calculation and the integration scheme are detailed in [18] for both the normal and tangential force calculation a linear spring dash pot model is used. Although previous works [23] and [24]showed that the glued sphere approach is less accurate when simulating a single sphere or cylinders it was already used in various other studies to simulate tablet shaped particles. In these investigations it was shown that the glued sphere approach works well when used for a large number of tablets ([11], [13], [25], [26])

The investigated process parameters (with the values used for the comparison of experimental and simulation results in brackets) used in the simulations are shown in Table 2. The initial contact settings were taken from [11] (time step size and sliding friction) and the spring constant was chosen to match

the results. For the variation studies the spring constant was varied between 2,500 N/m and 25,000 N/m, the particle-particle friction coefficient between 0.13 to 0.78 and the time step between 10^{-4} s and 10^{-6} s.

The critical time step was calculated for each spring constant using Eq7. It is defined by the tablet mass (m) and the particle stiffness (k) and a α-value which should be lower than 0.4[27].

$$\Delta t_{crit} = \alpha \cdot \sqrt{\frac{m}{k}} \tag{7}$$

Table 2 Simulation Parameters.

Tablet properties:	
Spring constant	2,500-25,000 N/m
Density	1150 kg/m^3
Tablet Weight	0.000282 kg
Interaction Tablet – Wall:	
Coefficient of restitution	0.78
Sliding friction coefficient (pw)	0.55
Rolling friction coefficient	0.01
Interaction tablet – tablet:	
Coefficient of restitution	0.78
Sliding friction coefficient	0.13-0.78 (0.39)
Rolling friction coefficient	0.01
Simulation:	
Time step duration	10^{-6} - 10^{-4} ($4 \cdot 10^{-5}$) s
Cell size (X,Y,Z)	0.0061 m, 0.0058 m, 0.0061 m

B-3.3.3. Velocity Measurement

The saved simulation files were read into a post processing software written in Python and the velocity of the tablets in the area of interest was extracted. In the simulation the camera view was recreated as a bundle of rays with a geometrical range that resembles the size of the analyzed tablet surface flow video. Since the position (distance and angle) of the ray bundle is the same as the borescope optics position and orientation in the experiments, the same spatial point in the tablet bed was investigated. A ray-tracing algorithm was applied to find the tablets that were on top of the tablet bed. The velocity of the detected tablets was saved. The mean velocity per time step was established based on the number of rays hitting each tablet. This approach considers the influence of the tablets' visibility on the measured velocity in the experiments. The rays and camera position are shown in Figure 5. The exact location coordinates are presented in Table 3.

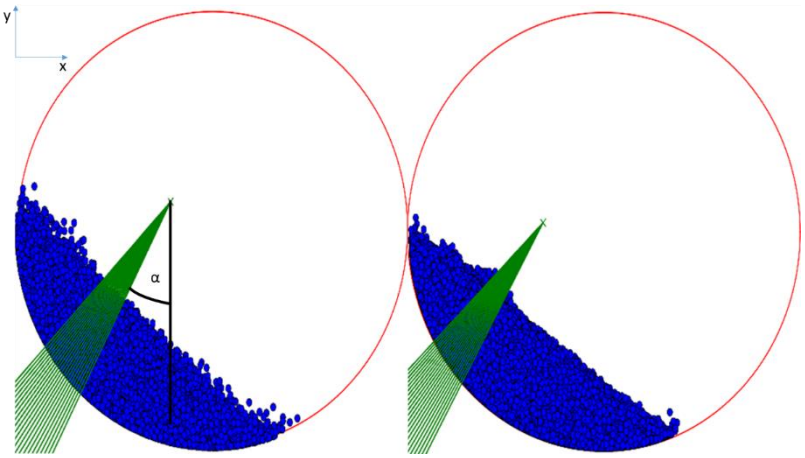

Figure 5: Tablet bed (blue) and rays (green) used in the post processing algorithm in the cases of BFC 5 (left) and BFC 50 (right). The angle of the camera is α.

Table 3: Position and angle (with respect to the vertical direction) of the camera and ray in the simulation and experiment.

	BFC 5	**BFC 50**
Position (X,Y,Z) in mm	-33.4, 19.6, 296	-85.2, 11.5, 550
Angle in °	33.5	33.2

B-3.4. Process Properties

The influence of various spring constants (i.e., various mechanical properties of the tablets) on the results is discussed in the last part of the study. Tablet coating was simulated for a total of 36 s (up to 156s for spring constants of 2,500 and 25,000 N/m), discarding the first 6 seconds of each simulation. During post-processing, the spray was simulated using the same ray-tracing algorithm that was applied

to identify the tablet in the spray zone. Two spray zones (Figure 6) were analyzed to determine the tablet velocity, the spray residence time and the bed cycle time.

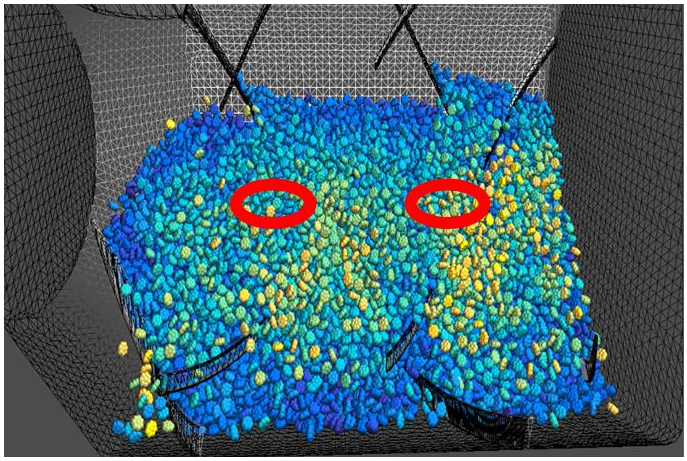

Figure 6: Spray nozzle position (red ellipses) in BFC 5 drum with the tablets colored according to their velocity.

B-4. Results and Discussion

B-4.1. Validity of Experimental Results

The experimental methodology for determining the tablet surface velocity was tested and validated in [28]. Specifically, this novel approach of measuring the tablet velocity via a high speed camera was validated by comparing the results with literature data using the same laboratory tablet coater BFC 5. For the literature values the tablet tracer technique was employed [5]. In Figure 7, we compare tablet velocity results for biconvex GITS 30 tablets, which are used in this study, to oblong tablets [5]. Both experiments had similar filling levels of 16.9 % and 18 % (of the total drum volume) and similar static bed angles of 34.1° for oblong tablets and of 36° for GITS 30. One can observe a fairly good agreement between both sets of experimental data, validating the new experimental approach.

The advantage of high speed camera imaging and subsequent image analysis over the more common approach of tracing color-tagged tablet is the statistical relevance of the obtained data and the ability to follow the dynamic changes of the average tablet velocity caused by the drum and baffle movement (i.e., an extra step of time aligning the tablet bed distance and dynamic angle of repose data with the surface flow image data).

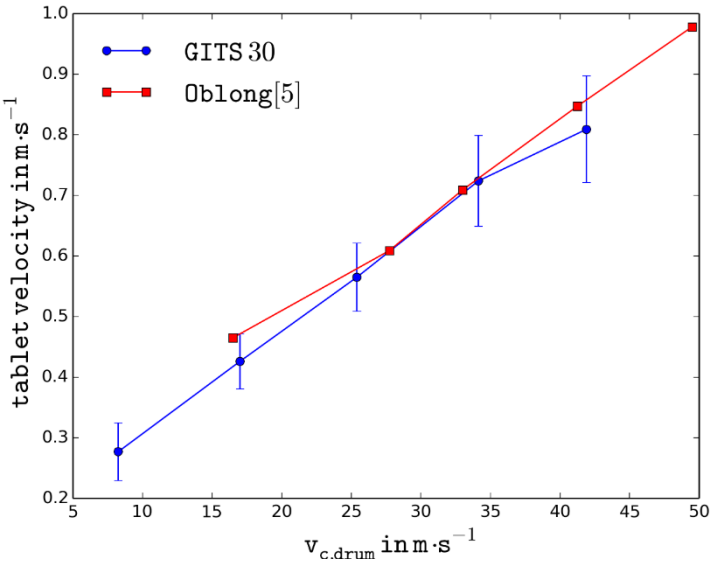

Figure 7: Comparison of average tablet velocity as a function of drum circumferential speed, obtained for GITS 30 and oblong tablets [5] in BFC down bed 5 laboratory coater.

B-4.2. Influence of Simulation Parameters on the Tablet Velocity

We studied the influence of the particle-particle (pp) friction, the spring constant (stiffness of tablets) and the DEM time step size on the tablet velocity. Each parameter was varied separately. First, the value of the particle-particle (pp) friction was changed and its influence on the tablet velocity was investigated. Theoretically, the velocity should increase with the decreasing pp friction. The initial value for the pp friction was 0.39. The friction coefficient was varied between 0.13 and 0.78. The tablet velocity increased with the decreasing pp friction as can be seen in Figure 8. As can be seen, the experimental velocity ranges could not be matched. However, the influence of the pp friction overall is insignificant. This is caused in part by the shape of the simulated tablets as the non-smooth surface provides additional friction and possibilities for interlocking, thus reducing the effect of the friction coefficient.

Since the tablet velocity failed to reach the experimentally measured tablet velocity, the pp friction was chosen to be 0.39, an experimentally determined value that, in an earlier simulation study, delivered good results for the dynamic angle of repose in combination with particle-wall friction coefficient (pw) value of 0.55 [29]. A relatively high value of particle-wall friction was selected due to a perforated type of the drum wall and the roughness of GITS coating.

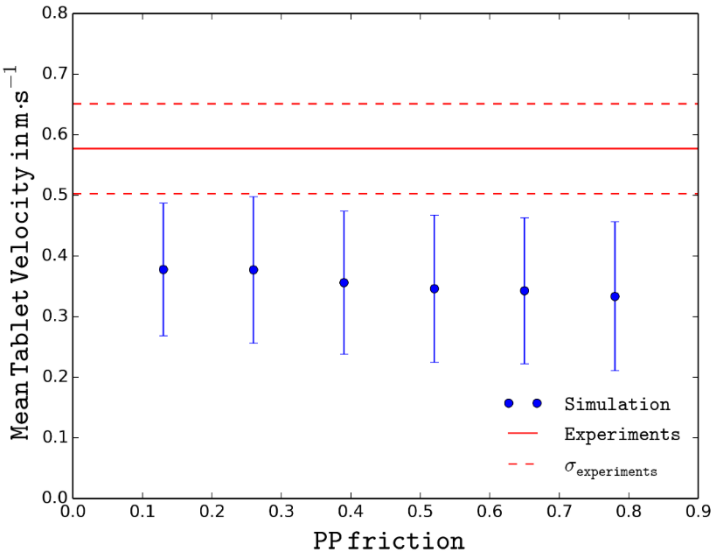

Figure 8: Mean down-bed tablet velocity for various values of the particle-particle friction coefficient (BFC 5, 12.6 % fill level, 15rpm). The red line is the mean tablet velocity and the dashed red line is the standard deviation of the experiment (k = 2,500, pw = 0.55, time step = $4 \cdot 10^{-5}$s).

Next, the influence of the spring constant on the tablet velocity in the simulation was investigated. Increasing the spring constant increases stiffness and thus, the impact dynamics, and results in an increased tablet velocity. A possible explanation is that the contact time decreases with increasing spring constant, thus leading to more effective gliding of the tablets over each other. The computational disadvantage of an increased spring constant value is that the simulations become time-consuming, as very small time steps have to be chosen and simulations easily become unstable. Thus, smaller values are used frequently. A realistic spring constant would be in the range of 10^5 N/m and would require a very small time step, which would significantly increase the wall clock time of the simulation. See Just et al. [29] for further information about the tablet material properties used in this work. Here a Young's modulus of 31.9 MPa was chosen.

Initially, a spring constant of 2,500 N/m was chosen, since it provided a good fit to earlier simulations [30], which fitted well other experimental data. The spring constant was steadily increased. In Figure 9, the results for the tablet velocity are shown. The mean velocity for spring constants over 10,000 N/m are within the standard deviation of the lab results. While a value of 25,000 N/m matches the experimental observation perfectly, values over 25,000 N/m could not be studied at this time step size ($4*10^{-5}$). A higher stiffness would require a lower simulation time step size. Otherwise the forces resulting from the contacts (particle-particle or particle-wall) are too large and the particles accelerate to quickly, being ejected from the simulation domain. Thus, the spring constant for all simulations was

set to 25,000 N/m. These results agree with the finding of Freireich et al. [31] which also found a correlation between increased particle stiffness and particle velocity in the DEM.

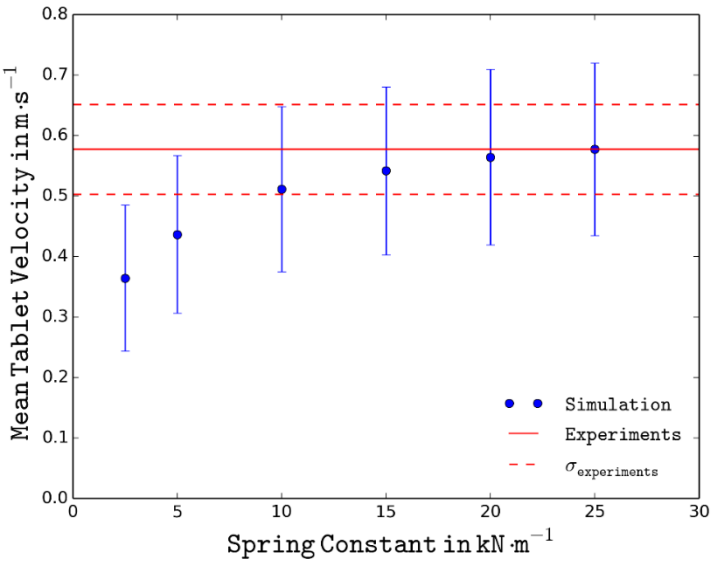

Figure 9: Mean down-bed tablet velocity as a function of spring constant (BFC 5, 12.6 % fill level, 15rpm). The red line is the mean tablet velocity and the dashed red line is the standard deviation in the experiments (pp = 0.39, pw = 0.55, time step = $4 \cdot 10^{-5}$s).

To confirm that the tablets still behave realistically while increasing the spring constant, the composition of the velocity vector was investigated. The ratio between the velocity vector components in the horizontal and vertical direction should stay constant as to not distort the simulation results. Both velocity components in the radial direction of the drum (x (horizontal), y (vertical)) increased with the increasing spring constant, yet the ratio between the components stayed constant (Figure 10, left column). The velocity in axial direction of the drum (z) remained constant, independent of the spring constant. This leads to less axial mixing in the tablet bed since the tablets move relatively slower along the axial direction, travel shorter distances and spend a shorter time on top of the tablet bed.

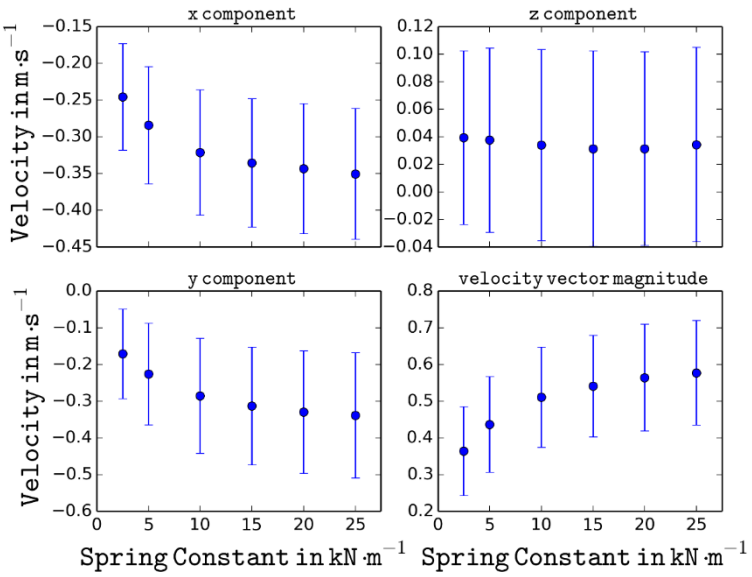

*Figure 10: Velocity vector components and velocity vector magnitude in m/s over various spring constants (coefficient of particle-particle friction = 0.39, coefficient of particle-wall friction = 0.55, time step = 4*10^{-5}s). (BFC 5, 12.6 % fill level, 15rpm).*

In order to understand the impact of time step-size on the simulation performance, it was varied from $5 \cdot 10^{-7}$ up to $4 \cdot 10^{-5}$ seconds for a spring constant of 25,000. Larger time steps were not possible and smaller time steps are not feasible as the time needed for one simulation would increase beyond reasonable limits. As can be seen in Figure 11, the velocity decreases slightly for smaller time steps, yet does not reach a lower limit. Theoretically, the mean velocity should reach a lower limit when using a small enough time step. However, GPUs use single precision when calculating the forces between the tablets (and the forces between the tablets and the coater geometry). Thus, for very small time steps round-off errors may become noticeable, which could explain the decreasing velocity for smaller time steps.

The standard deviation for the simulation results are larger than for the experimental results. This can be explained by the fact that the simulation results include all tablets which can theoretically be seen through the camera, even ones that would be dismissed in the experimental data due to coverage by other tablets. This leads to a wider spread of the tablet velocity, and thus, to a larger standard deviation. To maintain the simulation stability and achieve reasonable tablet velocities, we chose the particle parameters of 0.39 for the PP friction, 25,000 N/m for the spring constant and $4 \cdot 10^{-5}$ for the time step. Using these parameters, a full numerical DoE was performed.

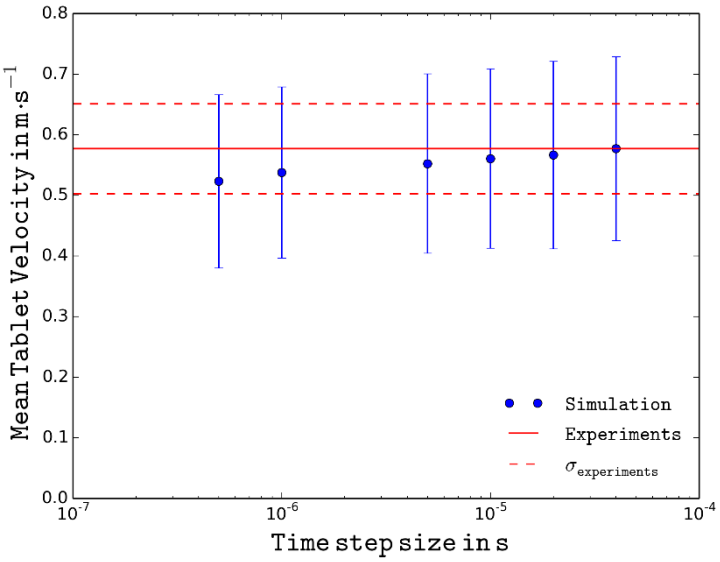

Figure 11: Mean down-bed tablet velocity for various time step sizes and a spring constant of 25,000 N/m (BFC 5, 12.6 % fill level, 15rpm). The red line is the mean tablet velocity and the dashed red line is the standard deviation in the experiments (pp = 0.39, pw = 0.55, spring constant = 25,000 N/m).

B-4.3. Comparison of Simulations with the Experimental Tablet Velocity

After establishing the simulation parameters, simulations were carried out. The mean tablet surface velocities and the standard deviation of the time-averaged velocity (over three seconds) for all cases are shown in Figure 12 and in Table 4. The standard deviation shows the variation of the tablet velocity. The tablets differ in velocity due to several factors, mainly the baffle positions (which in returns influences the bed height) and the influence of other tablets (tablets that impede/push the tablets along in their path down the tablet bed). In the case of BFC 5, experimental and numerical results matched well. In the case of BFC 50, the simulation results were lower than the mean velocity in the experiments. The deviation between the BFC 5 and BFC 50 can be explained by the way the material parameters were adjusted. Material parameters were adjusted to match the experimental results in the BFC 5 at a fill level of 12.6% and a rotation rate of 15 rpm, and thus, may not fit as well the case of the BFC 50. However, a similar dependence on the drum rotation rate was observed on the laboratory (BFC 5) and pilot (BFC 50) scales.

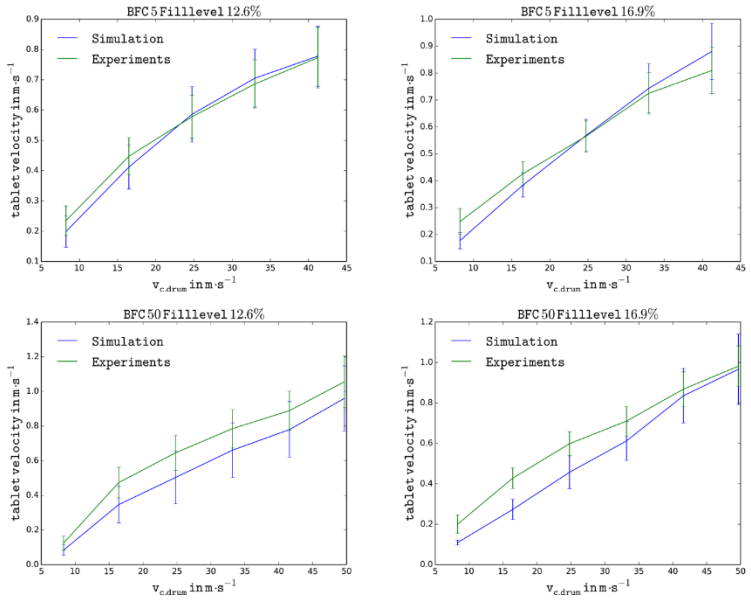

Figure 12: Mean down-bed tablet velocity and standard deviation for the BFC 5 (upper) and BFC50 (under) cases with a fill level of 12.6% (left) and 16.9 % (right).

Table 4: Design of Experiment and experimental/simulation results.

Drum load in kg	Drum Fill level in %	Rotation rate in rpm	circumferential velocity in cm/s	$v_{tablet,exp}$ in cm/s	$v_{tablet,sim}$ in cm/s
3.00	12.6	5.00	8.25	23.5	19.88
3.00	12.6	10.30	16.99	45.0	41.20
3.00	12.6	15.40	25.40	57.7	58.60
3.00	12.6	20.70	34.14	68.6	70.54
3.00	12.6	25.40	41.89	77.2	77.82
4.00	16.9	5.00	8.25	24.7	17.76
4.00	16.9	10.30	16.99	42.6	38.37
4.00	16.9	15.40	25.40	56.5	56.78
4.00	16.9	20.70	34.14	72.4	74.36

4.00	16.9	25.40	41.89	80.9	88.05
16.11	12.6	2.88	8.29	12.5	8.40
16.11	12.6	5.69	16.39	47.4	34.66
16.11	12.6	8.61	24.80	64.4	50.32
16.11	12.6	11.51	33.15	78.8	66.06
16.11	12.6	14.44	41.58	88.9	77.95
16.11	12.6	17.25	49.68	105.6	95.94
21.48	16.9	2.88	8.29	20.0	10.94
21.48	16.9	5.69	16.39	42.7	27.31
21.48	16.9	8.61	24.80	59.9	45.72
21.48	16.9	11.51	33.15	71.0	61.17
21.48	16.9	14.44	41.58	86.9	83.55
21.48	16.9	17.25	49.68	98.2	96.66

Simulation and experimental results agreed well and the trends were well captured. Especially, for the small system (BFC 5) the agreement is very good. For the larger system the agreement is slightly worse, with the velocities being under-predicted by the simulation, for both fill levels. This can be explained by the difference in the measuring methods in the simulation and experiments. In the simulation all tablets which are detected by the ray tracing algorithm are taken into account when calculating the mean tablet velocity. In the experiments only tablets which can be clearly seen are counted when calculating the motion of the tablets between the different frames. Thus, only tablets on top of the tablet bed which are clearly seen are used to determine the tablet bed surface velocity, while tablets in the deeper layers are dismissed. Clearly, top tablets are faster, explaining the slightly higher velocities in the experiments. Thus the tablet velocity is usually faster in the experiments as the experiments include mostly tablets on the tablet bed surface.

To demonstrate that both processes can provide comparable solutions, the spatially averaged velocity of each time step during three seconds is shown for some example cases in Figure 13. As can be seen,

the velocity fluctuates significantly and the frequency and amplitude of the fluctuations is well-captured by the simulation.

The fluctuations are due to the baffle position in the drum, which influences the local tablet bed height and speed by plowing through the tablet bed in the direction opposite to the tablet bed's surface flow. Although the peaks were the same in the simulation and experiments, in all cases the minima were somewhat lower in the simulation, leading to a lower time-averaged tablet mean velocity. Dependency on the baffle passage frequency, which depends on drum rotation rate and number of baffles (Figure 13) can be seen. A similar pattern in the mean velocity fluctuation is observed between simulations and experiments.

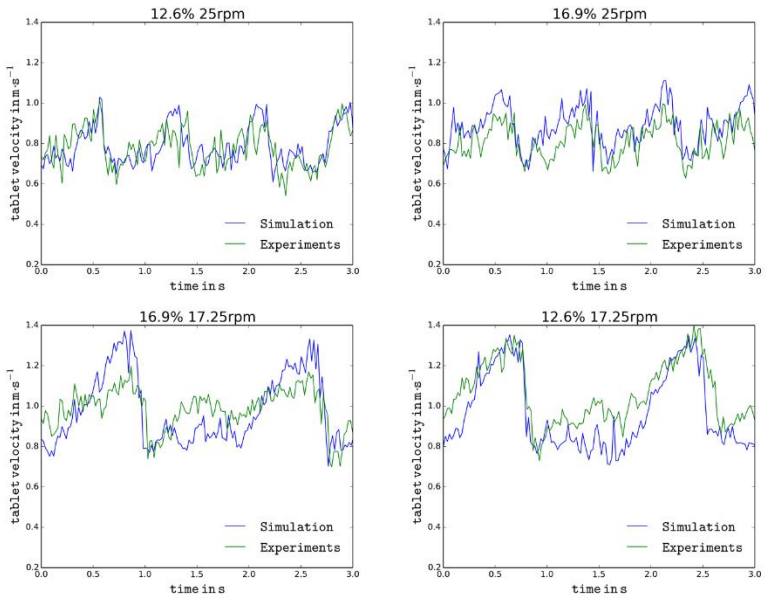

Figure 13: Evolution of the mean down-bed tablet velocity in the experiment and simulation for the 3 seconds of evaluation in the experiment at a drum circumferential speed of 42 cm/s on the laboratory scale, BFC5 (top), and on the pilot scale, BFC 50 (bottom), at 12.6 % and 16.9 % fill levels

A comparison of spatially- and time-averaged tablet velocities in the experiment and simulation is shown in Figure 14. The mean tablet velocity is mostly under-predicted in the simulations. The scatter of the data shows a mean deviation between the simulation and experimental results of 14.66 % and a standard deviation of 12.83%. The largest absolute deviation between simulation and experiments is around 0.1 m/s. significant differences are observed at lower drum rotation rates. At lower rotation rates the influence of the slower tablets which are in the second layer of the tablet bed (seen from the surface) are partially included in the averaging of the simulation data but are excluded by the

experimental investigation due to poor visibility. Additionally, in the image analysis, a lower threshold of the tablet velocity was set as one half of the circumferential drum velocity.

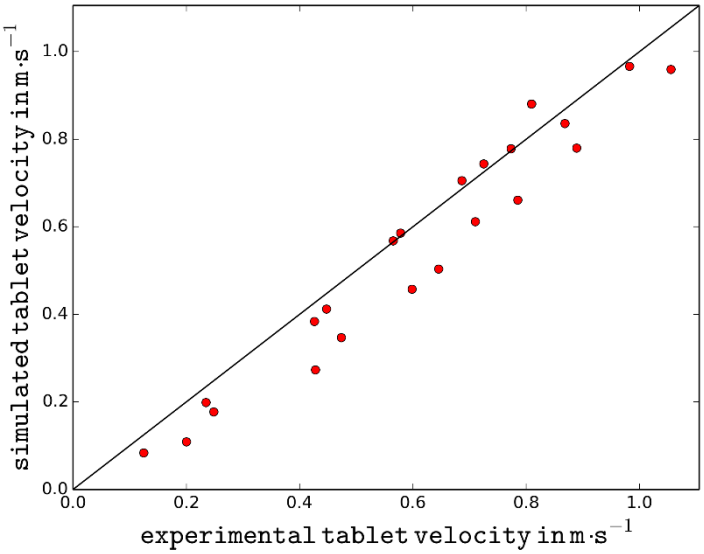

Figure 14: Down-bed tablet velocity in the simulation over the tablet velocity in the experiments.

B-4.4. Changes in the Tablet Bed Behavior and its Relevance for Coating Variation

In reality, material and structure-dependent mechanical properties of the tablet core and, especially, its coating can introduce a change in the tablet spring constant. To that end, we numerically investigated the influence of tablet spring constant on the overall process outcome. First, we studied the influence of an increased spring constant and tablet velocity on the spray residence time (i.e., the time the tablets spend in the spray zone). For measuring the residence time in the spray zone a threshold of 0.4 seconds was chosen. This values was already used in previous work using the same coater geometry and similar rotation rates/ fill level ([20]).

As expected, the mean of the spray residence time distribution decreases with the increasing spring constant due to the increasing tablet velocity. In addition, its distribution becomes narrower (Figure 15). The corresponding tablet velocity distributions for a spring constant of 2,500 and 25,000 N/m are shown in Figure 16. The velocity distribution becomes wider and shifts to higher velocities at a higher spring constant.

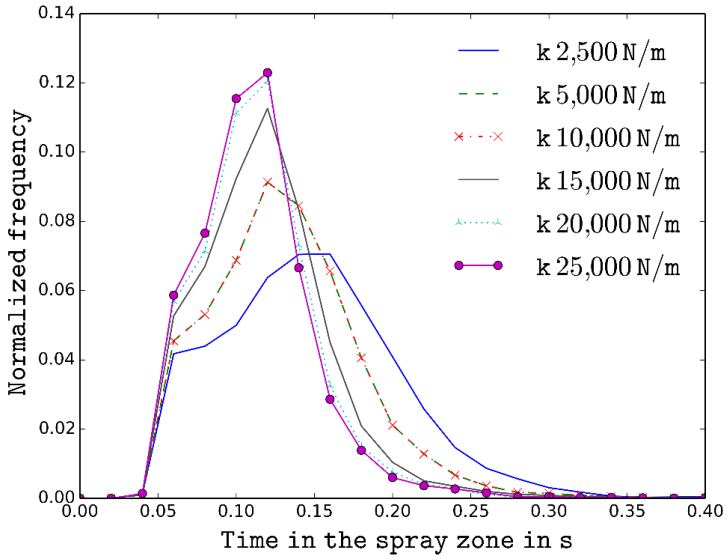

Figure 15: Spray residence time for the various spring constants (left) (BFC 5, 12.6% fill level, 15 rpm).

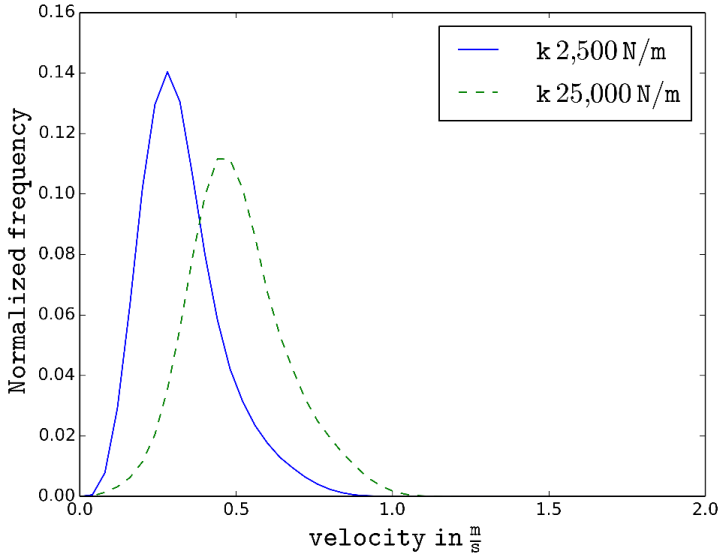

Figure 16: Down-bed velocity distribution for the tablets in the observation zone for spring constants of 2,500 N/m and 25,000 N/m (BFC 5, 12.6% fill level, 15 rpm)

The bed cycle time is the time a tablet spends inside the tablet bed between two distinct spray events. The tablet bed cycle time decreases from around 2/3 to around 1/2 of one drum revolution when the spring constant increases from 2,500 N/m to 25,000 N/m (Figure 17). This is due to higher tablet velocities in the lower bed region, as the upward transport rate should be similar (i.e., the latter is determined by the rotation of the drum). Faster tablets reappear more quickly in the spray zone and have an increased number of spray area passages during a total coating time.

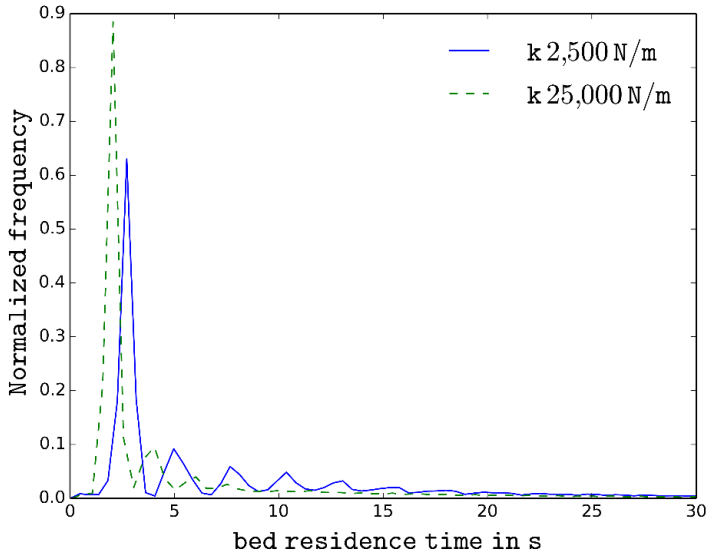

Figure 17: Normalized bed residence time for spring constants of 2,500 N/m and 25,000 N/m (BFC 5, 12.6% fill level, 15 rpm)

B-5. Summary and Conclusions

The proposed approach to measuring the tablet velocity proved to be in good agreement with previous measurements that involved tracer tablets. This opens new ways of directly measuring the tablet velocity during the process. Although tracer tablets are still required for measuring the spray residence and bed cycle times, these values can theoretically be determined based on the tablet velocity.

DEM was used to reproduce the experiments numerically and to improve the understanding of the tablet behavior during the spray coating process. First, we determined the best values of DEM parameters to fit the experiments. To that end, the influence of pp friction, spring constant and time step on the tablet velocity was investigated. It was established that the spring constant has the most significant effect and the pp friction has the smallest one. These results are in agreement with finding from Freireich et al. [31] Next, these parameters were used to reproduce the experiments. The velocities in the simulation matched (or were somewhat below) the velocity in the experiments. However, in both cases the trend was the same and the dependence of tablet velocity on the baffle position was clearly observed in both the experimental and the simulated results.

The simulations could realistically recreate the tablet bed behavior and matched the result in the BFC 5 case. In the case of BFC 50, the simulations were close and matched very well the dependence on the rotation rate. The relative deviation between the simulation and experimental velocity results varied between 45.30% (maximum value) and 0.28% (minimum value) from the experimental results with a

mean deviation of 14.66 % and a standard deviation of 12.83%. The results agreed best at higher rotation rates and least at lower rotation rates.

In summary, this work demonstrates that it is possible to accurately simulate the tablet behavior in a drum coater. The results can be used in the future for even more accurate simulations.

B-6. Bibliography

[1] S. C. Porter, R. P. Verseput, and C. R. Cunningham, "Process Optimization Using Design of Experiments," *Pharm. Technol.*, vol. 1, no. October, 1997.

[2] S. Tobiska and P. Kleinebudde, "Coating uniformity and coating efficiency in a Bohle Lab-Coater using oval tablets," *Eur. J. Pharm. Biopharm.*, vol. 56, pp. 3–9, 2003.

[3] G. W. Smith, G. S. Macleod, and J. T. Fell, "Mixing efficiency in side-vented coating equipment.," *AAPS PharmSciTech*, vol. 4, no. 3, p. E37, 2003.

[4] A. Alexander, T. Shinbrot, and F. J. Muzzio, "Scaling surface velocities in rotating cylinders as a function of vessel radius, rotation rate, and particle size," *Powder Technol.*, vol. 126, no. 2, pp. 174–190, Jul. 2002.

[5] R. Mueller and P. Kleinebudde, "Prediction of tablet velocity in pan coaters for scale-up," *Powder Technol.*, vol. 173, no. 1, pp. 51–58, Apr. 2007.

[6] J. Rantanen and J. Khinast, "The Future of Pharmaceutical Manufacturing Sciences," *J. Pharm. Sci.*, vol. 104, no. 11, pp. 3612–3638, 2015.

[7] W. R. Ketterhagen, M. T. am Ende, and B. C. Hancock, "Process modeling in the pharmaceutical industry using the discrete element method," *J. Pharm. Sci.*, vol. 98, pp. 442–470, 2009.

[8] S. Just, G. Toschkoff, A. Funke, D. Djuric, J. G. Khinast, K. Knop, and P. Kleinebudde, "Optimization of Inter-Tablet Coating Uniformity for an Active Coating Process at the Lab and Pilot Scale," *Int. J. Pharm.*, vol. 30, no. 11, 2013.

[9] A. Kalbag and C. Wassgren, "Inter-tablet coating variability: Tablet residence time variability," *Chem. Eng. Sci.*, vol. 64, no. 11, pp. 2705–2717, 2009.

[10] A. Dubey, R. Hsia, K. Saranteas, D. Brone, T. Misra, and F. J. Muzzio, "Effect of speed, loading and spray pattern on coating variability in a pan coater," *Chem Eng Sci*, vol. 66, no. 21, pp. 5107–5115, Nov. 2011.

[11] G. Toschkoff, S. Just, K. Knop, P. Kleinebudde, A. Funke, D. Djuric, G. Scharrer, and J. G. Khinast, “Modeling of an Active Tablet Coating Process,” *J. Pharm. Sci.*, vol. 104, no. 12, pp. 4082–4092, Sep. 2015.

[12] A. Kalbag, C. Wassgren, S. Sumana Penumetcha, and J. D. Pérez-Ramos, “Inter-tablet coating variability: Residence times in a horizontal pan coater,” *Chem. Eng. Sci.*, vol. 63, no. 11, pp. 2881–2894, Jun. 2008.

[13] B. Freireich, W. R. Ketterhagen, and C. Wassgren, “Intra-tablet coating variability for several pharmaceutical tablet shapes,” *Chem. Eng. Sci.*, vol. 66, no. 12, pp. 2535–2544, Jun. 2011.

[14] D. Suzzi, G. Toschkoff, S. Radl, D. Machold, S. D. Fraser, B. J. Glasser, and J. G. Khinast, “DEM simulation of continuous tablet coating: Effects of tablet shape and fill level on inter-tablet coating variability,” *Chem. Eng. Sci.*, vol. 69, no. 1, pp. 107–121, 2012.

[15] A. O. Favier, J.F., Abbaspour Fard M.H. , Kremmer, M. and Raji, “Shape representation of axi-symmetrical, non-spherical particles in discrete element simulation using multi element model particles,” *Eng. Comput.*, vol. 16, no. 4, pp. 467–480, 1999.

[16] G. Toschkoff, S. Just, A. Funke, D. Djuric, K. Knop, P. Kleinebudde, G. Scharrer, and J. G. Khinast, “Spray Models for Discrete Element Simulations of Particle Coating Processes,” *Chem. Eng. Sci.*, vol. 101, pp. 603–614, 2013.

[17] W. R. Ketterhagen, “Modeling the motion and orientation of various pharmaceutical tablet shapes in a film coating pan using DEM.,” *Int. J. Pharm.*, vol. 409, no. 1–2, pp. 137–49, May 2011.

[18] C. a. Radeke, B. J. Glasser, and J. G. Khinast, “Large-scale powder mixer simulations using massively parallel GPUarchitectures,” *Chem. Eng. Sci.*, vol. 65, no. 24, pp. 6435–6442, Dec. 2010.

[19] D. Jajcevic, E. Siegmann, C. Radeke, and J. G. Khinast, “Large-scale CFD–DEM simulations of fluidized granular systems,” *Chem. Eng. Sci.*, vol. 98, pp. 298–310, Jul. 2013.

[20] P. Boehling, G. Toschkoff, K. Knop, P. Kleinebudde, S. Just, A. Funke, H. Rehbaum, and J. G. Khinast, “Analysis of large-scale tablet coating : Modeling , simulation and experiments,” *Eur. J. Pharm. Sci.*, vol. 90, no. EuPAT 7 Special Issue, pp. 14–24, 2016.

[21] R. Dreu, G. Toschkoff, A. Funke, A. Altmeyer, K. Knop, J. Khinast, and P. Kleinebudde, “Evaluation of the tablets ’ surface flow velocities in pan coaters,” *Eur. J. Pharm. Biopharm.*, vol. 106, pp. 97–106, 2016.

[22] W. Hwu and D. Kirk, “Programming massively parallel processors,” *Comput. Educ. Sci.*, no. Special Edition, pp. 92–104, 2009.

[23] M. Kodam, R. Bharadwaj, J. Curtis, B. Hancock, and C. Wassgren, “Force model considerations for glued-sphere discrete element method simulations,” *Chem. Eng. Sci.*, vol. 64, no. 15, pp. 3466–3475, Aug. 2009.

[24] H. Kruggel-Emden, S. Rickelt, S. Wirtz, and V. Scherer, “A study on the validity of the multi-sphere Discrete Element Method,” *Powder Technol.*, vol. 188, pp. 153–165, 2008.

[25] P. Boehling, G. Toschkoff, K. Knop, P. Kleinebudde, S. Just, A. Funke, H. Rehbaum, and J. G. Khinast, “Analysis of large-scale tablet coating : Modeling , simulation and experiments,” *Eur. J. Pharm. Sci.*, vol. 90, pp. 14–24, 2016.

[26] W. Chen, S.-Y. Chang, S. Kiang, A. Marchut, O. Lyngberg, J. Wang, V. Rao, D. Desai, H. Stamato, and W. Early, “Modeling of pan coating processes: Prediction of tablet content uniformity and determination of critical process parameters,” *J. Pharm. Sci.*, vol. 99, pp. 3213–3225, 2010.

[27] C. O. Sullivan and J. D. Bray, “Selecting a suitable time step for discrete element simulations that use the central difference time integration scheme,” *Eng. Comput.*, vol. 21, no. 2/3/4, pp. 278 – 303, 2003.

[28] R. Dreu, G. Toschkoff, A. Funke, A. Altmeyer, K. Knop, J. Khinast, and P. Kleinebudde, “EVALUATION OF THE TABLET SURFACE FLOW VELOCITIES WITHIN PAN COATERS WITH IMPLICATION TO PROCESS UNDERSTANDING,” *TBA*.

[29] S. Just, G. Toschkoff, A. Funke, D. Djuric, G. Scharrer, J. G. Khinast, K. Knop, and P. Kleinebudde, “Experimental Analysis of Tablet Properties for Discrete Element Modeling of an Active Coating Process,” *AAPS PharmSciTech*, vol. 14, no. 1, pp. 402–411, 2013.

[30] G. Toschkoff, S. Just, K. Knop, P. Kleinebudde, A. Funke, A. Altmeyer, D. Djuric, and G. Scharrer, “Design-of-Experiment based DEM simulation of an active tablet coating process .”

[31] B. Freireich, J. Litster, and C. Wassgren, “Using the discrete element method to predict collision-scale behavior: A sensitivity analysis,” *Chem. Eng. Sci.*, vol. 64, no. 15, pp. 3407–3416, 2009.

C. Simulation of a Tablet Coating Process at Different Scales using DEM

Published as: P. Boehling *et al.*, "Analysis of large-scale tablet coating : Modeling , simulation and experiments," *Eur. J. Pharm. Sci.*, vol. 90, pp. 14–24, 2016.

C-1. Abstract

Spray coating of tablets is an important unit operation in the pharmaceutical industry and is mainly used for modified release, enteric protection, better appearance and brand recognition. It can also be used to apply an additional active pharmaceutical ingredient to the tablet core. Scale-up of such a process is an important step in commercialization. However, scale-up is not trivial and frequently, at manufacturing scales the required coating quality cannot be reached. Thus, we propose a method where laboratory experiments are carried out, yet scale-up is done via computational methods, i.e., by extrapolating results to larger scales.

In the recent years, the Discrete Element Method (DEM) has widely been used to simulate tablet behavior in a laboratory scale drum coater. Due the increasing computational power and more sophisticated DEM algorithms, it has become possible to simulate millions of particles on regular PCs and model industrial scale tablet coating devices. In this work, simulations were performed on the laboratory, pilot and industrial scales and DEM was used to study how different scale-up rules influence the bed behavior on larger scales. The material parameters of the tablets were measured in the laboratory and a glued sphere approach was applied to model the tablet shape.

The results include a vast amount of qualitative and quantitative data at the different scales. In conclusion, the evolution of the inter-tablet coating variation for the different scales and process parameters is presented. The results suggest that keeping the Froude number constant during the scale up process leads to faster processes as the cycle time is shorter and the spray residence time is more uniform when compared to keeping the circumferential velocity constant.

C-2. Introduction

Tablets are one of the most widespread pharmaceutical delivery forms and are frequently coated. The simplest form of coating is color coating, which can be used for branding or for aesthetic or psychological considerations [1]. More complex coating formulations provide a function, e.g., enhanced protection functionality (i.e., low pH in the stomach), modification of the release or, in the case of active coating, introduction of an additional active pharmaceutical ingredient (API). With regard to the second category of functional coating processes, the intra- and inter-tablet coating uniformities are critical

quality parameters. Intra-tablet coating uniformity is the uniformity of coating layer on a single tablet. Inter-tablet coating uniformity is the uniformity of coating mass of all tablets in a batch. Particularly strict limits with regard to the inter-tablet coating uniformity apply to coatings that contains an API, namely the content uniformity requirements of relevant Pharmacopoeia [2], [3].

Experiments can help to optimize these critical quality parameters and to ensure adherence to the limits established by the regulatory agencies. In the lab, behavior of tablets or the influence of operation parameters on the tablet coating quality can be studied [4] and [5] and input data required for modeling can be gathered (e.g., a compartment or Monte Carlo models)[5]–[8]. Also models that use empirical relation between the tablet velocity, spray residence time and bed cycle time to predict the process outcome are developed [9]. Some studies involve pilot-scale drum coaters to investigate the scale-up process and the influence of coater geometries and batch sizes on the process outcome [10]–[12]. Industrial scale drum coaters are rarely used during experimental studies or DoEs due to the high costs [13].

In contrast, simulations make it possible to analyze – in theory at every scale - process properties that cannot be tracked experimentally. Initially, computer simulations were of limited use due to available computational power. As computer technologies have become more sophisticated, simulations of pharmaceutical processes have become more common. They can reduce the cost of experiments: fewer experiments have to be performed and changing parameters is easier. For example, the discrete element method (DEM) is increasingly applied in the pharmaceutical industry. Ketterhagen [14] provides an overview over the various processes for which DEM can be employed.

Investigating the behavior of tablets in a drum coater was one of the first applications of DEM in the pharmaceutical industry [15]. In the simplest cases, tablets can be approximated as spheres [16], [17]. Experiments are performed to ensure the correct material properties [16], [18] and to adapt the specific simulation material parameters (stiffness, coefficient of particle-particle and particle-wall friction etc.) to fit the experiments. With that regard, the shape of simulated particles is important since the bulk and flow characteristics of biconvex tablets differs from that of spheres. Favier et al. [19], [20] proposed using connected spheres, which are allowed to overlap to mimic the shape of real particles. This so-called “glued-sphere approach” was applied in numerous studies [10], [18], [21], [22], e.g., to investigate the tablet shapes and their influence on the tablet bed behavior [23], [24] and to understand the mixing and flow in the tablet bed [25]. For example, Suzzi et al. [26] applied this method

together with a Quality by Design Approach to study the influence of process parameters on the quality of the finial product.

Typically, a few thousand tablets are coated on the lab scale, compared to a few hundred thousand on the pilot scale and 1-2 million tablets on the industrial scale. All of the above referenced studies were performed at the laboratory scale, primarily due to the limited number of tablets that can be simulated with most DEM implementations. To overcome these limitations, a DEM code named 'eXtended Particle System' (XPS) was developed at the RCPE that runs on graphics processors (GPU) and permits a massive parallelization due to its architecture. It is possible to simulate up to 13 million spheres on one gigabyte of GPU RAM using the XPS code, which allows the simulation of industrial-sized tablet coating processes that typically involve 1-2 million tablets. The XPS code has been described by Radeke et al. [27].

A transfer from the laboratory to the industrial scale can be performed using two scale-up rules for drum speed. For drum coaters, these were established by Turton and Chen in [28]. The first method is to scale the rotation rate by keeping the Froude number constant. The Froude number Fr is calculated as:

$$Fr = \frac{\omega^2 \cdot D}{g} \tag{8}$$

which gives a rotation rate of the scaled device:

$$\omega_2 = \omega_1 \cdot \sqrt{\frac{D_1}{D_2}} \tag{9}$$

where ω is the rotation rate, D is the radius of the drum and g is gravity. The subscripts 1 and 2 refer to devices one and two. Circumferential velocity influences the flow regime in the drum [24]. In the case of tablet coating, a flow regime between rolling and cascading is preferable. With a constant Froude number, the flow regime in drum coaters remains constant [17]. However, this scale-up strategy may lead to too high tablet velocities in the bigger drums, and to higher tablet abrasion.

Thus, we also used the second scale-up rule with a constant circumferential speed:

$$\omega_2 = \omega_1 \cdot \frac{D_1}{D_2} \tag{10}$$

For geometrically similar coaters (such as the ones in this study), the fill level ratio is also kept constant:

$$M_2 = M_1 \cdot \frac{D_1^2 \cdot L_1}{D_2^2 \cdot L_2} \quad (11)$$

M is the loading mass and *L* is the length of the drum.

For this study it is assumed that the process settings are given on the lab scale. We then used both scale-up rules 9 and 10 for the rotation rate and for the drum load 11 to calculate settings for pilot- and industrial-scale coaters. With this approach, the pilot- and industrial-scale coaters contain around one hundred thousand and one million tablets, respectively. Moreover, at every scale two rotation rates are obtained, each for every scale-up rule.

Then, a comparison of the lab- and larger-scale coaters was carried out, comparing the bed behavior and velocity of tablets in the spray zones in drums with different rotation rates and with different sizes. Next, spray and bed cycle time at various rotation rate were compared and mixing efficiency of the coaters was evaluated. Finally, the evolution of the coefficient of inter-tablet coating variation ($c_{v,inter}$) was studied on various scales.

C-3. Material and Methods

C-3.1. Coater and Tablets

In this work, we studied an active coating process for the production of tablets. Gastrointestinal therapeutic systems (GITS) were used as a starting material (Bayer Pharma AG, Leverkusen, Germany). GITS are round biconvex two-layer tablets with a diameter of 9 mm and a height of 5 mm.

The coating was performed on the laboratory scale in a Bohle Film Coater 5 (BFC 5, L.B. Bohle Maschinen + Verfahrens GmbH, Ennigerloh, Germany), on the pilot scale in a Bohle Film Coater 50 (BFC 50, L.B. Bohle Maschinen + Verfahrens GmbH, Ennigerloh, Germany) and on the industrial scale in a Bohle Film Coater 400 (BFC 400, L.B. Bohle Maschinen + Verfahrens GmbH, Ennigerloh, Germany). The geometries of coating drums were provided by the manufacturer. The operational settings used for the simulation runs are described in Section C-3.3.

When comparing the geometries of coaters in Figure 18, their similarities in the overall form and the increasing number of baffles with the increasing size of the coater are apparent. The coaters in the Figure are not scaled to size. In reality, they differ by a factor of 5 in diameter and length of the drum between the lab and industrial scales, respectively. The ratio of the length and the drum diameter differ in the various scales.

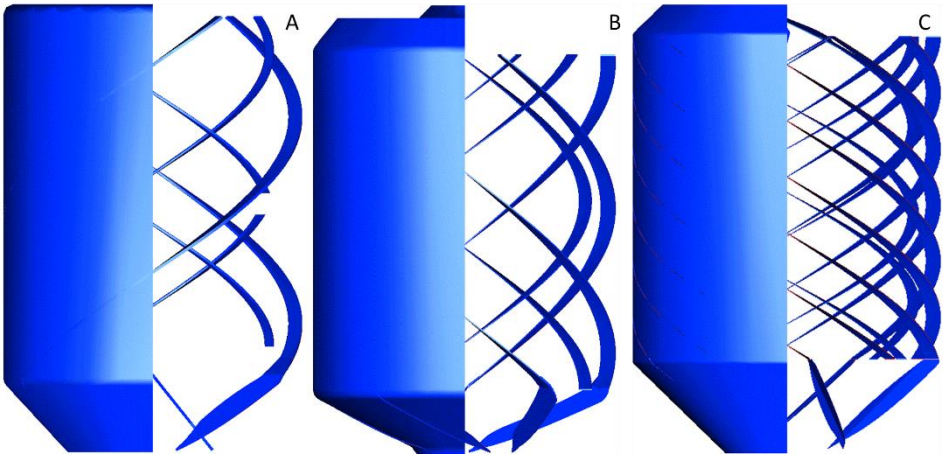

Figure 18: Drum geometries of the BFC 5(A), BFC 50 (B) and BFC 400 (C), not to scale.

The size and volume of the three drums are reported in Table 5.

Table 5: Drum dimensions of the three drums used.

DRUM	RADIUS	LENGTH	VOLUME
	In m	In m	In m^3
BFC 5	0.158	0.45	0.35
BFC 50	0.349	0.82	0.31
BFC 400	0.713	2.24	3.58

C-3.2. Simulation Method

XPS is a DEM code developed at Research Center Pharmaceutical Engineering, which is based on the DEM developed by Cundall and Strack [29]. It uses the CUDA programming language [30], which is a C extension developed by Nvidia for utilizing graphical processing units (GPUs, i.e., graphics cards) to achieve massive speed up of a highly parallelizable algorithm [27].

To simulate the particles, we used a glued sphere approach [31]. The tablet consists of eight overlapping spheres ([32]) and has a mass of 282 mg. The volume and moment of inertia were calculated using a Monte Carlo integration scheme. The position and size of the sub-spheres were adjusted for the modeled tablets to have the same volume and dimensions as the real tablets.

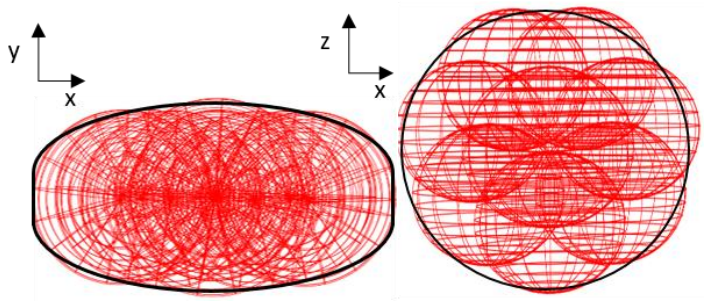

Figure 19: Tablet shape modeled via the glued sphere approach taken from[32].

The coaters' fill level ratios were kept constant to ensure the same relative fill volume in each of them. The resulting fill levels were 3.5 kg (12,411 tablets), 31 kg (110,496 tablets) and 354 kg (1,258,085 tablets) on the lab, pilot and industrial scales, respectively. The tablet properties and the tablet-tablet and tablet-wall interaction parameters were taken from [18]. These properties are reported in Table 6. The material parameters applied in this work were taken from earlier experiments [18].

The material parameters were set to be constant. We did not yet include the influence of the air flow and temperature on the tablet properties, since analyzing friction was not within the scope of this work. The effect of these parameters on the tablet flow behavior was estimated to be low. The forces acting on the tablet rim were modeled in a simplified way using the glued sphere approach. The edges are approximated by the outer spheres of the model tablets and thus behave differently from real tablets.

All simulations have a 6 seconds initialization phase, during which the tablet bed is allowed to reach a quasi steady state. After this, the simulations run for an additional 90 seconds and data are collected. These data are used for the post processing.

Table 6 Simulation parameters

Tablet properties	
Spring constant	2500 N/m
Density	1150 kg/m^3
Interaction Tablet – Wall	
Coefficient of Restitution	0.78
Static friction coefficient	0.45
Rolling friction coefficient	0.01
Interaction tablet – tablet	
Coefficient of Restitution	0.78
Static friction coefficient	0.39
Rolling friction coefficient	0.01
Simulation	
Time step length	4x10^{-5} s
Cell size (X,Y,Z)	(0.0061, 0.0058, 0.0061) m

Position and velocity information of the particles was recorded every 0.02 seconds during the simulations. These data were then analyzed by a post-processing algorithm, which simulated spray coating. For spray coating, a ray-tracing approach was used following a mechanism proposed by Toschkoff et al. [22]. In this approach the spray is simulated as an ensemble of rays that are oriented normal to the tablet-bed surface. At each time step, the algorithm determines the tablets that are hit by a ray. Velocities of the hit tablets were saved independently to obtain the velocity distribution in the spray zone. The spray dimensions were taken from measurements and estimations in the coater. The mean value of the spray zone diameter were used in the post processing. They have an ideal elliptical shape with major and minor axes of 6.5 and 3.2 cm (BFC 5 coater), 10 and 5 cm (BFC 50 coater) and 12 and 6 cm (BFC 400 coater). The spray zone positions with respect to the coater bed are shown in Figure 20.

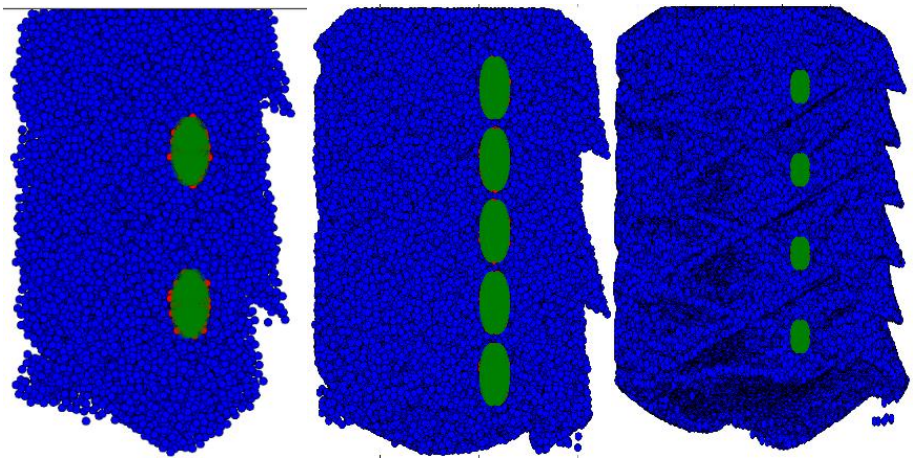

Figure 20: Top view of the spray zones in the BFC5, BFC50 and BFC 400 coaters, tablet bed size not for scale. Note that the tablets in the spray zone are marked as red.

The number of nozzles changed depending on the scale. As can be seen in Figure 20, the ratio between the covered and uncovered areas of the tablet bed increased from the lab scale to the pilot scale and decreased from the pilot to the industrial scale. The ratio of coated tablets to uncoated tablets is important for the initial $c_{v,inter}$ value as was shown in previous already by previous Authors [7][16][17].This may lead to a better coating uniformity on the pilot scale, yet a long processing time on the industrial scale.

C-3.3. Process Parameters

For scale-up purposes, the base case, i.e., the laboratory-scale coater, was chosen to be 3.5 kg and the rotation rates was set to 18 rpm. These data were taken from a previous work [33]. Based on that, the drum loads on the pilot and industrial scales were calculated (via Eq. 11). For the rotation rate, Eqs. 9 10 were used, resulting in 5 DEM simulations. After the simulations were completed, qualitative and quantitative process parameters were investigated.

As a first qualitative check, the shape of the tablet bed was assessed visually for slumping (i.e. the tablet bed moves upward the drum walls and then falls back in one swift movement), which should be avoided. In parallel, the bed angle was calculated. To compare the tablet bed shape, the Python code was used, which reads the saved simulation data and plots via the *matplotlib* module for Python. The script also calculates the bed angle at different time steps by locating the tablets on the surface. Subsequently, a linear regression was used to obtain the slope of the tablet bed. Based on the slope, the bed angle was derived.

Mixing behavior on different scales and for different rotation rates was investigated in two ways. In the first approach, the tablets in the middle of the bed in length-wise direction were marked and the bed was divided into bins along its length (i.e., in axial direction). The ratio between marked and unmarked tablets was calculated for each bin at each time step. Information concerning the evolution of this ratio and standard deviation for the entire coater was generated. The Lacey index was used to determine when the coater was perfectly mixed. In the second approach, the distance travelled by the tablets on the different coating scales and at difference rotation rates was analyzed. The distance travelled by every single tablet in the drum was tracked and normalized by the mean distance travelled.

For further comparison, the mean, 5 and 95 percentile of the distance travelled were evaluated. Finally, spray coating was simulated in the post-processing step, as described by Toschkoff et al [22]. The spray zones were positioned at around 1/3 of the tablet bed top length measured downwards from the top. This algorithm was used to determine the spray residence time, the bed cycle time, the tablet velocity in the spray zone and the evolution of coefficient of inter tablet coating variation ($c_{v,inter}$).

The spray residence time is the time that the tablets spend in the spray zone. The distribution should be as narrow as possible, since it influences the coating efficiency and the $c_{v,inter}$. The bed cycle time is the time that a tablet spends in the total tablet bed between two coating events. Both are important indicators of inter-tablet coating variability. For $c_{v,inter}$ we used the mean coating mass accumulated over all tablets.

$$c_{v,inter} = \frac{\sigma_{mc}}{\mu_{mc}} = \sqrt{\frac{1}{N}\sum_{i=1}^{N}\frac{(m_{c,i}-\bar{m}_c)^2}{\bar{m}_c^2}}, \text{ with } \bar{m}_c = \frac{\sum_{i=1}^{N} m_{c,i}}{N} \quad (12)$$

N is the number of tablets and $m_{c,i}$ is the coating mass of tablet *i*. The aim is to obtain low values of $c_{v,inter}$. While in an experimental investigation, the total variation is estimated from the variation in a sample, in the DEM simulation the coating of all tablets (the entire statistical population) is used for that purpose.

The drum load and rotation rate on various scales are shown in in Table 2 below. It should be noted, that the influence of the spray rate, friction change, temperature of the drying air and the air flow in general are not included in this work. All these parameters (especially the air flow) would lead to unreasonably long simulation times.

Table 7: Drum load, Fill ratio, number of tablets, circumferential velocity and rotation rate

Drum Name	load in kg	Fill ratio In %	Tablets	Circumferential velocity in m/s	Rotation rate in rpm	Froude number
BFC 5	3.5	14.75	12411	0.30	18	0.0029
BFC 50_{Fr}	31.16	14.75	110496	0.44	12.1	0.0029
BFC 50_{vc}	31.13	14.75	110496	0.30	8.14	0.0013
BFC 400_{Fr}	354.78	14.75	1258085	0.63	8.47	0.0029
BFC 400_{vc}	354.78	14.75	1258085	0.30	3.99	0.0006

C-4. Results and Discussion

Simulating the coating process on all scales enables unprecedented insight into the impact of various parameters on the process behavior. For a first comparison, the shape of the tablet bed can be used, as this information reflects what the operator would see in the real-world process. The dynamic bed angle was also investigated since it provides an overview of the flow regimes in the drum coater.

Moreover, tablet velocity in the spray zone on various scales was studied to assess the dependence of the tablet velocity on the rotation rate and drum size. For an in-depth quantitative study of the mixing behavior, the distance the tablets travel during the simulation was investigated. Mixing behavior was analyzed and compared for the various scales as well. Finally, for all five cases the effect of time on the decrease of coefficient of variation was investigated.

C-4.1. Shape of the Tablet Bed

The shape of the tablet bed and, especially, the dynamic bed angle are important characteristics of the tablet coating process. Knowing how the dynamic bed angle changes at different rotation rates is helpful in terms of setting up a consistent process (e.g., positioning of the spray gun). Using the DEM, the dynamic bed angle and the shape of the tablet bed can easily be determined[34][33]. Based on the shape and height of the tablet bed over time it is possible to predict possible slumping behavior.

Figure 21 shows that the overall shape of tablet bed is similar in all cases, from the lab to the industrial scale for both scaling methods. For better comparability, all plots are scaled to the same size. The dynamic bed angle was calculated and averaged for each saved simulation time step. When the circumferential velocity is constant, the dynamic bed angle is lower than when the Froude analogy is used. This effect can be observed in the BFC 50 case and, even more prominently, in the BFC 400 case. This was expected since the dynamic bed angle is directly influenced by the rotation rate. The dynamic

bed angle in Table 8 shows that the bed angle increases slightly with the increasing circumferential velocity (constant Froude number) for the pilot scale and slightly decreases on the large scale. The angle significantly decreases at a constant circumferential velocity with larger scales. This is due to the avalanching behavior of the tablet bed at lower Froude numbers.

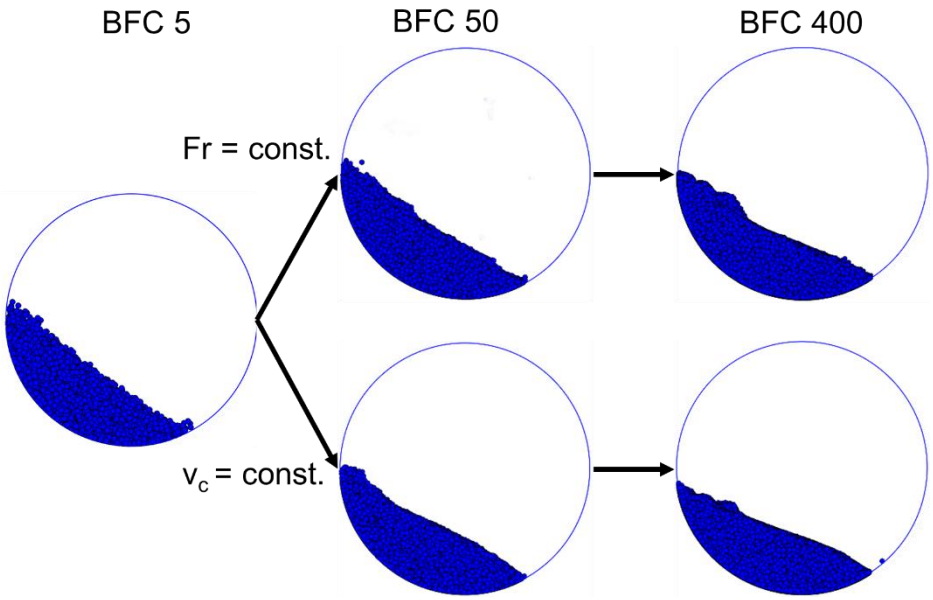

Figure 21: Tablet bed shape observed from the front of the drum in the axial direction. From left to right: BFC5, BFC50 and BFC400; the top row shows a constant Froude number, the bottom row shows a constant circumferential velocity.

Table 8: Dynamic bed angle on various scales and in various cases.

COATER	DYNAMIC BED ANGLE IN °
BFC5	37,2
BFC 50 $_{FR}$	39,9
BFC 50 $_{VC}$	35,2
BFC 400 $_{FR}$	36,4
BFC 400 $_{VC}$	32,7

The results also indicate that adapting the spray nozzle angle/position based on the shape of the bed at various rotation rates can be advantageous for the final product.

C-4.2. Velocity in the Spray Zone

Velocity distribution of the tablets in the spray zone is an important factor for designing the coating process. Most of the time it depends on the circumferential velocity of the rotating drum. Another important factor that influences the tablet velocity is the tablet bed height and the position of spray zone. Typically, tablets will accelerate during the first half of their downwards movement decelerate

during the second half and reach zero speed at the bottom of the tablet bed. After that, they are transported upwards once again alongside the drum walls. Tablets reach their top speed in the area from around the middle to two thirds of the tablet bed [35] [36].

The velocity distribution in the spray zone for constant circumferential velocity and constant Froude number is provided in Figure 22. All tablets inside the spray zone that are hit by at least one ray are counted. Their influence on the velocity distribution is weighted according to the number of rays that hits the tablets, thus tablets on top, which are hit with more rays have a higher impact on the velocity distribution. The velocity distribution for the BFC 400_{FR} appears to be bimodal due to the different velocities on top of the tablet bed. Due to the baffles there tablet bed surface is divided between regions with higher and lower velocity. This effect is even more pronounced for higher circumferential velocities (Froude scaling provides higher circumferential velocities). If the circumferential velocity is constant (subscript vc), the mean tablet velocity across scales is almost constant, i.e., at a constant circumferential velocity, tablet velocities are influenced only slightly by the geometry of the coater and the position of spray zones.

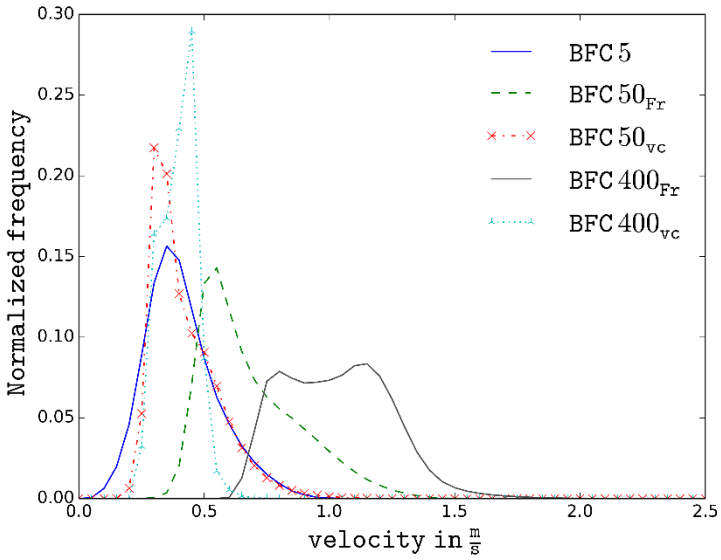

Figure 22: Velocity in the spray zone at a constant circumferential velocity (subscript vc) and with a constant Froude number (subscript Fr).

The mean velocity for the BFC 5 is 0.34 m/s with a standard deviation of 0.15 m/s. when the circumferential velocity is kept constant the mean velocity increases to 0.38 for the BFC 50 (standard deviation of 0.13 m/s) and 0.37 for the BFC 400 (standard deviation of 0.07 m/s). Thus the increase is

negligible and can be explained through the increase in size and the position of the spray zones which allow the tablets to accelerate a little longer than in the smaller scale.

If the Froude number is kept constant and thus the circumferential velocity increases the mean tablet velocity increases as well. For the BFC 50 the mean tablet velocity is 0.62 m/s with a standard deviation of 0.19 m/s and for the BFC 400 the mean tablet velocity is 0.99 m/s with a standard deviation of 0.21 m/s.

The increase of the tablet velocity in the spray zone for a constant Froude number in the BFC 50 is the results of the increased circumferential velocity (~ 50% increase) and results in a nearly 100 % higher tablet velocity and for the case of the BFC 400 the circumferential velocity nearly doubles and the mean tablet velocity increases ~200 %.

C-4.3. Spray Residence Time

Time in the spray zone going from the lab to the industrial scale was investigated. Spray residence time is connected to the tablet velocity in the spray zone. Here it is the time a tablet spends in the spray zone during a single spray event. The distribution for the 5 investigated cases can be seen in Figure 23. Figure 23 indicate that the time in the spray zone is influenced by the rotation rate of the drum. To ensure that each spray event for the tablets in the spray zone is an individual spray event a threshold of 20 store intervals (0.4 sec) was chosen. The store interval is time when the position and velocity of the particles is written out during the simulation. This threshold of 0.4 sec is shorter than the shortest bed cycle time of ~1.5 seconds and is used in all scales. The mean residence spray residence time for the BFC 5 is 0.10 s. For the case of the BFC 50 and a constant circumferential velocity the distribution and mean residence time stays constant (0.095 s). This is due to the time resolution of the ray tracing algorithm (0.02s) that cannot detect differences smaller than 0.02 sec and also due to the slightly increased tablet velocity. For the BFC 400_{vc} the mean residence time increases by around 40 % to 0.14 s and shows an increased tailing which is the result of the previous discussed slumping due to the lower tablet velocity and change tablet bed behavior due to the different Froude number.

With a constant Froude number, on larger scales v_c increases and mean spray residence time decreases. The mean residence time on the lab scale is 0.1 s. With a constant Froude number, it decreases to 0.062 s on the pilot scale and 0.058 s on the industrial scale. This is due to the increases speed of tablets in the spray zone. Again the store interval of 0.02 s does not allow to evaluate if there are bigger differences in the spray residence time distribution but one can assume that there are some fast tablets that receive coating but are not counted in this evaluation.

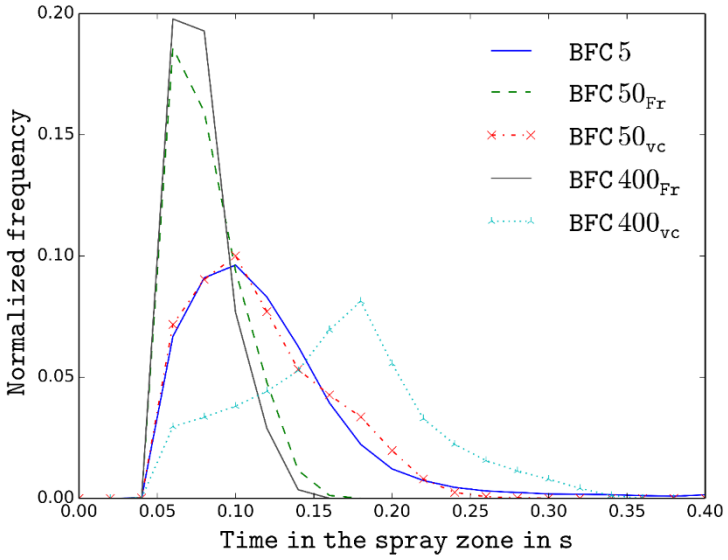

Figure 23: Time in the spray zone for various drum sizes and at various rotation rates. (vc = constant circumferential velocity, Fr = constant Froude number)

In Figure 24 the spray residence time is shown for all cases over the number of revolutions. All cases except for the BFC 5 have a similar distribution of the spray residence time when plotted over the number of revolution with a mean value of around 0.01 revolutions per pass. Mean residence time for the BFC 5 is 0.03. This can be explained by the faster rotation rate in the BFC 5. This effect should be considered when planning or scaling up a process from the laboratory scale.

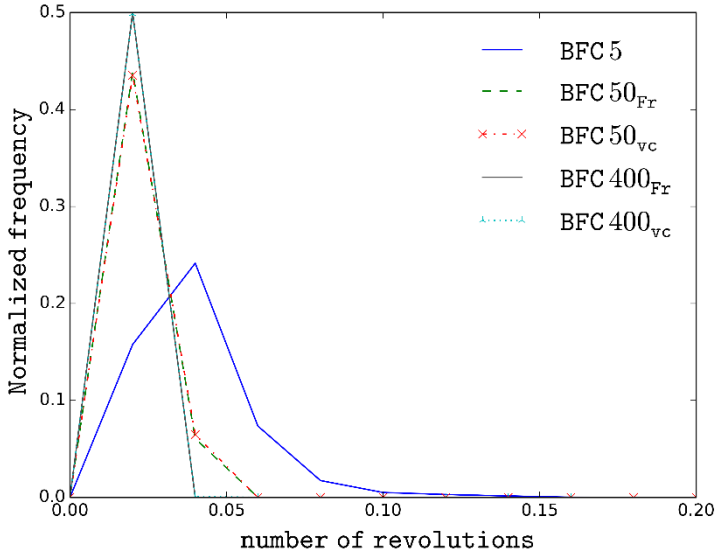

Figure 24: Time in the spray zone for various drum sizes and at various rotation rates over the number of revolutions. (vc = constant circumferential velocity, Fr = constant Froude number)

A narrow distribution of time in the spray zone is advantageous: the spray amount that each tablet receives is more uniform and the risk of over-wetting is reduced. In contrast, a wide distribution may mean that some tablets (especially at the tail towards high residence times) are exposed to the spray for too long. This can cause defects, such as sticking of tablets to each other or to the wall. Knowing the quantitative dependence of residence time on process conditions (e.g., Figure 23) may prevent tablet damage through a knowledge-based, targeted increase of rotation rate. The time in the spray zone also affects the development of the $c_{v,inter}$ as a narrower distribution of the spray residence time effects the coefficient of inter tablet variation as it decreases the standard variation of the tablet coating mass to the mean coating mass as shown by Freireich [7] up to a point where the variation in the spray residence time is far lower than in the bed residence time. After this point decreasing the variation of the spray residence time has no effect on the coefficient of inter tablet coating variation.

C-4.4. Bed Residence Time

Bed residence time is the time a tablet spends in the tablet bed during two distinct spray events. It is shown two folds here, first over time (Figure 25) and second over the number of revolutions (Figure 26). Figure 25 shows that the bed cycle time is dependent on the drum size and rotation rate. The BFC 5 has the shortest bed cycle time, due to the smallest drum radius and highest rotation rate), while the BFC 400_{vc} has the longest bed cycle time. For all cases the probability that a tablets enters again the spray zone after one cycle is the highest.

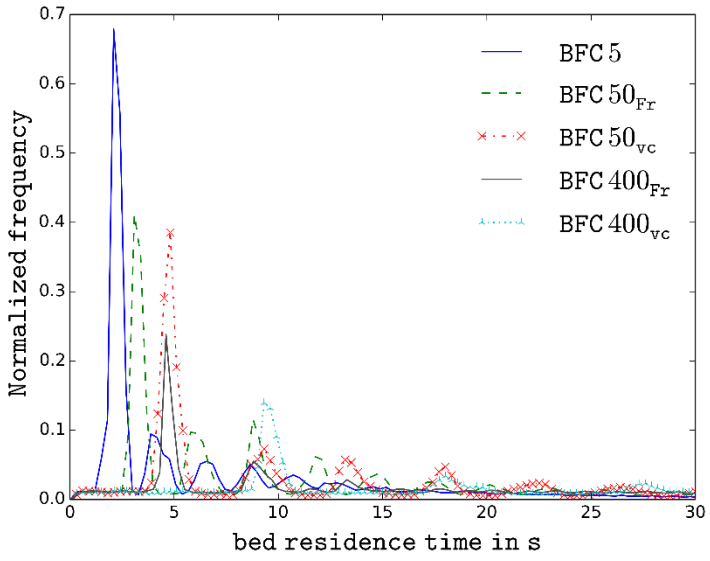

Figure 25: Bed cycle time for different cases.

When the bed residence time is plotted over the number of revolution all plots nearly collapse and lay on top of each other independent from the drum size and rotation velocity (Figure 26). The difference can be explained by the difference on how the tablet bed is covered with spray zones and the distance the tablets travel in the tablet bed. The closer the spray zones are to each other the higher is the likeliness that a tablet will be spray again in the next cycle. This was already shown to be true in smaller scales [33], and is here shown that it is also true for larger scales. The bed cycle times is around 0.6 revolutions, thus the tablet bed cycle time is less than one drum rotation cycle. This is true for all cases except for the BFC 5 where only the mean of the first peak is identical with the peaks of the other cases. This behavior can be explained by the wider distribution of the individual cycles and the longer time per rotation in the spray zone (see Figure 24) which skews the cycle bed cycle time to longer cycles especially for later cycles. This is explained by the shape of the tablet bed which is approximately around 1/3 of the drum wall and a nearly equal long distance on top of the tablet bed.

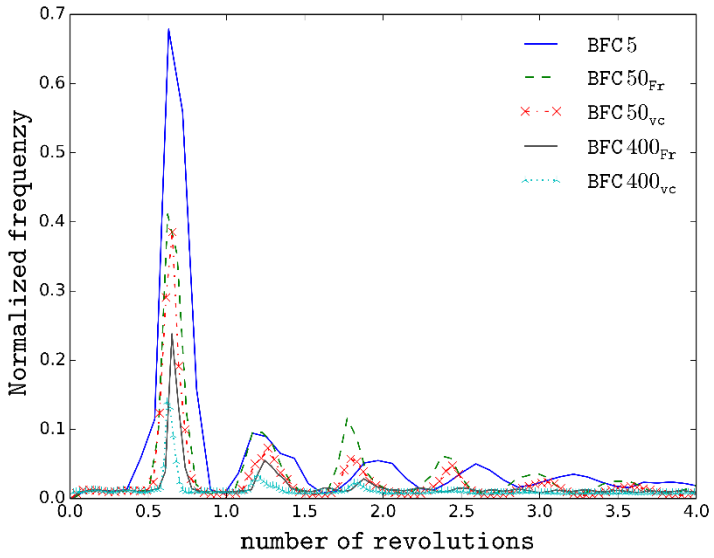

Figure 26: Bed cycle time over the number of revolutions for different cases.

C-4.5. Mixing Efficiency

The Lacey index is used to determine the mixing quality in a granular material. It compares the two most extreme cases of the total segregation and random mixing with the current state of the granular material. The Lacey index can have the values of 0 (total segregation) or 1 (random mixing).

$$M_L = \frac{\sigma_0^2 - \sigma(t)^2}{\sigma_0^2 - \sigma_r^2} \quad (13)$$

where $\sigma(t)$ is the standard deviation, σ_0 is the total segregated state and σ_r is the standard deviation in a totally randomly mixed state.

To measure M_L, the tablet bed is divided into bins along the axial direction. Each bin had the width of one tablet diameter. Thus there are 47 bins in the BFC 5, 83 bins in the BFC 50 and 226 bins in the BFC 400. The tablets in the center of the tablet bed are marked in the beginning of the evaluation. Thus 282 tablets in the BFC 5 (2.27 %) ~2400 tablets in the BFC 50 (2.15 % and 2.14 %) and ~28000 tablets in the BFC 400 (2.22 % and 2.27 %). Thus, nearly the same ratio of tablets is marked in each case. The marked tablets together with example bins (bins are not shown in real size) are shown in Figure 27. The ratio between marked to unmarked tablets in every bin and the standard deviation for the tablet bed per time step are calculated. The standard deviation per time step is than used to calculate the Lacey index. Where the standard deviation at time step 0 was used as σ_0. σ_r is the standard deviation after the value of the standard deviation is constant.

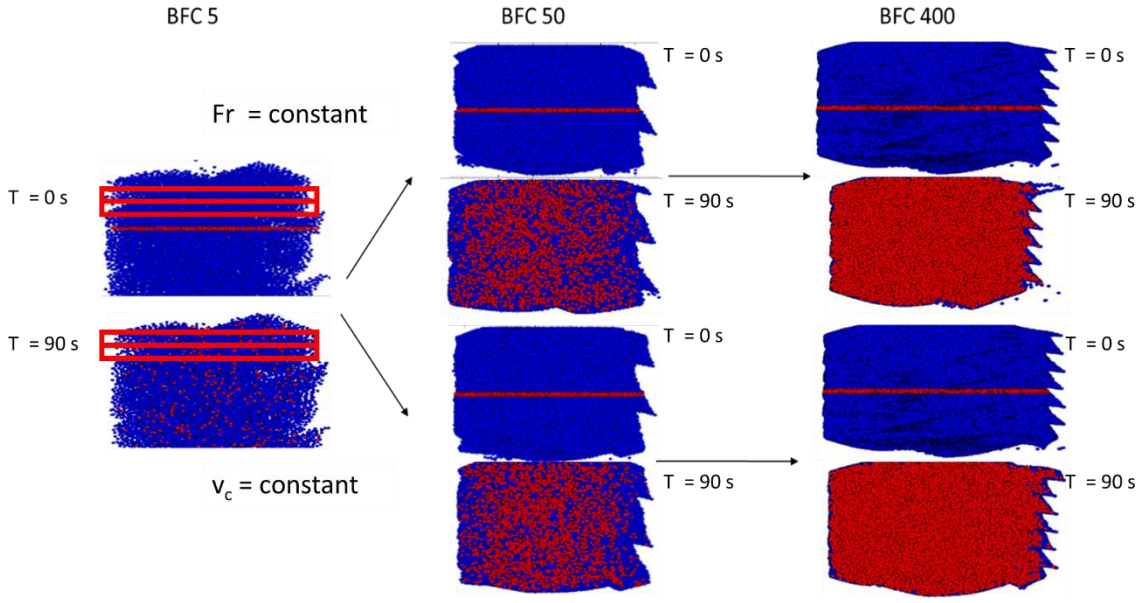

Figure 27: Start (0 seconds) and end mixture (90 seconds) for BFC5, 50 and 400 with a constant Froude number and at a constant circumferential velocity (top and bottom rows). Please note that the marked tablets are plotted after the unmarked in this graph and thus seem to be on top of the other tablets. Actually the tablets are mixed in the tablet bed.

M_L is plotted as a function of the number of rotations in Figure 28. The Figures indicates that the tablet bed mixing shows very similar behavior in all 5 cases. The Lacey index depends similar to the bed residence time on the number of rotations. In the BFC 5 and BFC 50_{vc} a short reduction in ML between

0.4 and 0.5 rotation can be explained by a back mixing of the marked tablets into the bins in which already other marked tablets are sitting.

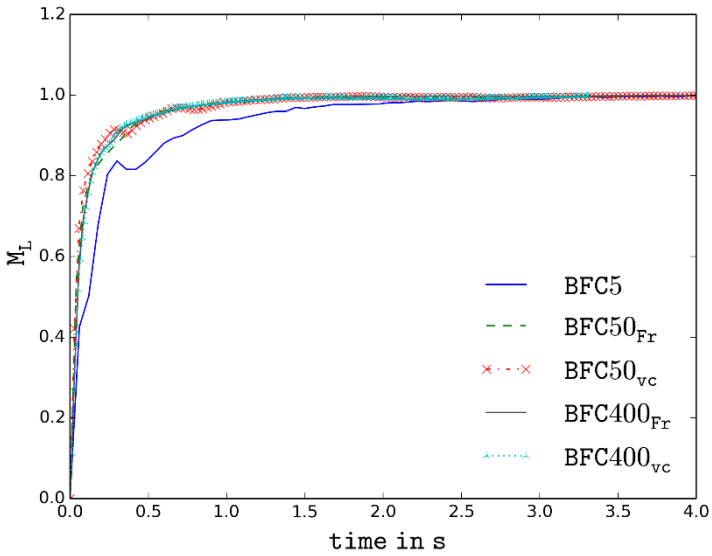

Figure 28: Lacey index M_L over the number of rotations at constant circumferential velocity and Froude number

C-4.6. Distance Traveled

The distribution of distance traveled by the tablets in the drum should be as uniform as possible. It is an indicator of good mixing in the axial and radial directions. Significant variations in the tablet movement can be a sign of dead zones that should be avoided during the coating process.

One of the main advantages of the DEM is that, since the position and velocity of every particle are known at all times, it is easy to establish were dead zones occur. For better comparability, the traveled distance was normalized by the mean distance traveled are shown in Table 9**.** Figure 29 shows that the overall normalized distance traveled in all cases (except $BFC400_{vc}$) is similar to the base case in the small drum.

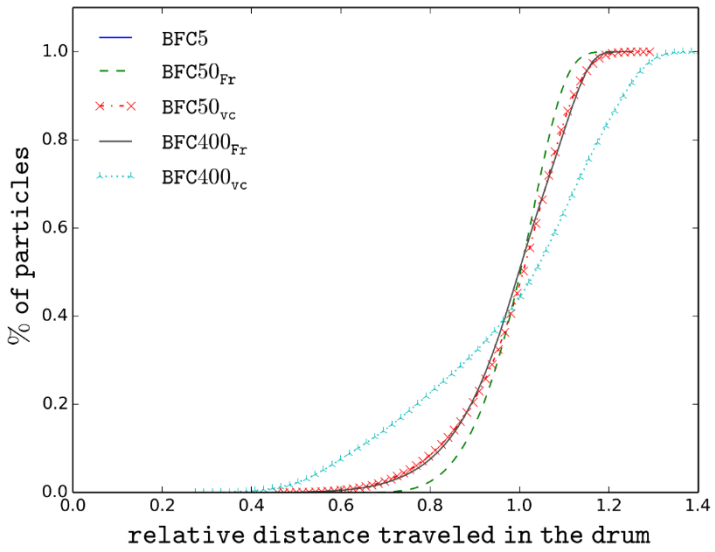

Figure 29: Relative distance traveled in the coating drum. The total distance is standardized by the mean distance traveled.

A narrow distribution of the traveled distance is an indicator for good mixing in the drum. On the industrial scale, a wider distribution at constant circumferential velocity scaling indicates that mixing is more challenging. With a constant Froude number scaling, this can be counter-acted by an increased tablet velocity. Table 9 shows the minimal, maximal and mean distances traveled, as well as the ratio of the 5 and 95 percentile values. The ratio is a good indicator of how narrow the distribution of traveled distance is. It has values from around 1.2 in the lab-scale case to 1.87 in case 4, indicating a very wide distribution, which can also be seen in Figure 29.

Table 9: Minimal and maximal distances traveled in the five investigated cases during the 90 s simulated process time

Coater	*5 % distance traveled*	*95 % distance traveled*	*Mean distance traveled*	*Ratio*
	in m	in m	in m	
BFC 5	13.42	16.07	14.74	1.20
BFC 50 Fr	20.48	25.17	23.05	1.23
BFC 50 vc	12.50	16.59	14.82	1.33
BFC 400 Fr	33.48	44.01	39.20	1.31
BFC 400 vc	11.33	21.22	17.27	1.87

Clearly, the ratio of the shortest and longest distance travelled increases at lower rotation rates, which implies that the rotation rates should be above a certain minimum. This was not expected since the M_L suggests that mixing does not depend on the rotation rates. The higher the rotation rate, the better mixing becomes, especially in bigger drums. This should be considered when choosing the process parameters.

C-4.7. Time Dependence of Uniformity

According to the literature[33], the coefficient of variation should decrease with the inverse square root of time.

$$c_{v,inter} \approx \frac{1}{\sqrt{t}} \tag{14}$$

In this work, we tested if this is true on various scales. In Figure 30, $c_{v,inter}$ is shown over the process time (double logarithmic scale). Although $c_{v,inter}$ does, to some degree, depend on the drum speed, the drum scale has a more significant effect on it. The initial $c_{v,inter}$ value at the different scale sizes is constant for the individual scales, because the same amount of tablets is coated at the first time step. This effect is explained in the literature in various works ([7],[16],[17]) because the initial $c_{v,inter}$ can be calculated from the following observation:

$$c_{v,inter} = \sqrt{\frac{1-x}{x}} \tag{15}$$

Where x is the ratio of the tablets in the spray zone to the total amount of tablets. The decrease in $c_{v,inter}$ is slower at slower rotation rates as a lesser number of individual tablets are inside the spray zone for the same amount of time as less tablets are pass through the spray zone in the same amount of time. As expected, $c_{v,inter}$ is the highest on the industrial scale in $BFC400_{vc}$ as the cycle time highest and initial ratio of coated to uncoated tablets is the lowest.

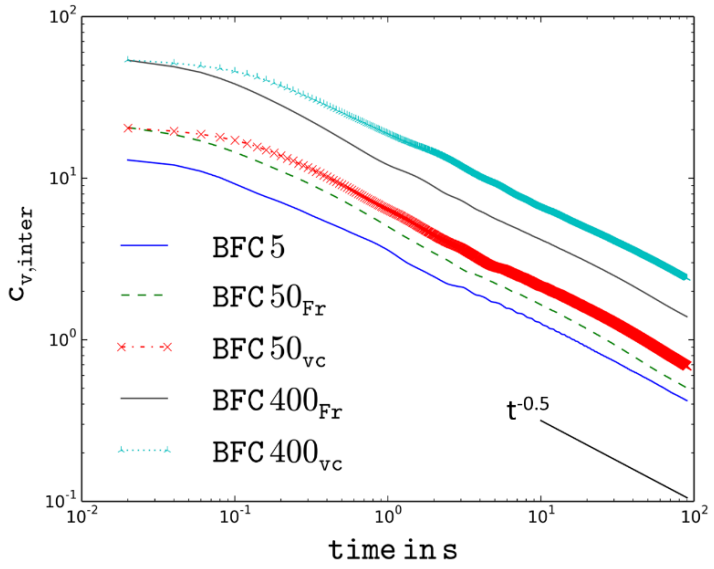

Figure 30: Coefficient of variation over the total simulated time at a constant circumferential velocity and with a constant Froude number with the spray zones defined beforehand

For the first few tablets travelling through the spray zone, $c_{v,inter}$ changes slowly. After around 1 second, the curve of $c_{v,inter}$ nearly reaches the expected slope in the double logarithmic plot of -1/2, as reported in the literature for spherical tablets [16], [37] and non-spherical tablets using the glued sphere approach [33]. After around 60 seconds the slope of the decrease is constant for all cases. In an ideal coating process, the tablets are coated independent of the previous coating event (i.e., a Markovian process). However, in reality the tablets that are coated have a higher chance of travelling along the coater wall to the top of the tablet bed and being sprayed again. This was confirmed by the bed cycle times, where the possibility is the highest that a tablet passes again through the spray zone after one cycle. The slope of the decline is -0.51 for the BFC 5 -0.53 for the $BFC50_{Fr}$ -0.57 for the $BFC50_{vc}$ -0.52 for the $BFC400_{Fr}$ and $BFC400_{vc}$.

A higher rotation rate shortens the process time and provides a lower $c_{v,inter}$ after a given time. At a constant rotation rate, $c_{v,inter}$ decreases at a constant rate with the increasing process time, when plotted over a double logarithmic axes. A higher rotation rate is favorable due to the shorter process time. $c_{v,inter}$ after 90 seconds (Figure 31) confirms that a higher rotation rate is favorable since it reduces the process time significantly.

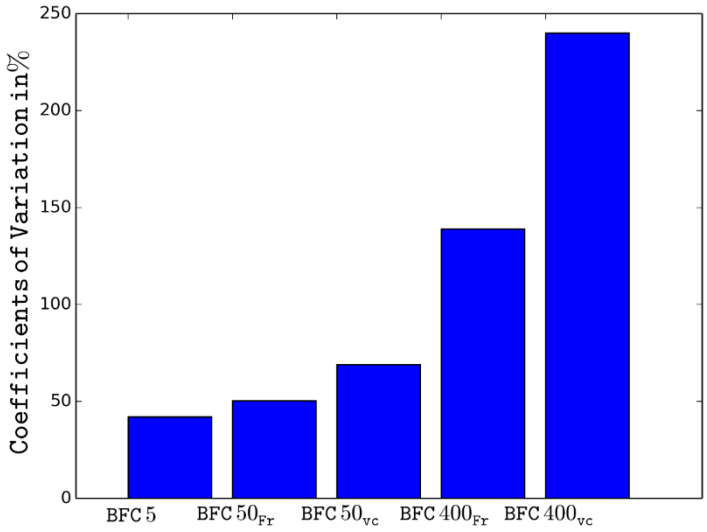

Figure 31: $c_{v,inter}$ in % after 90 seconds on various scales and at various rotation rates.

C-5. Conclusion

This work demonstrates the possibilities that DEM offers with regard to scale-up of a tablet coating process. The particle range in this work is between 10,000 and 1.5 million tablets, which can easily be simulated using a modern DEM algorithm [38]. To measure tablet properties, experimental and real shapes of the tablet were considered for the purposes of simulation process.

The tablet coating process was scaled-up from the laboratory coater to the pilot and industrial scales. The two most commonly used scale-up rules were tested and the difference in the tablet bed behavior was documented. The first rule is to keep the Froude number constant and regulate the rotation rate of the drum accordingly. The other rule is to keep the circumferential velocity constant.

The tablet velocity influences the spray and bed cycle times. By keeping the Froude number constant the circumferential velocity of the coating drum increases with increasing drum diameter, which increases the overall tablet velocity and especially the tablet velocity on top of the tablet bed. Keeping the circumferential velocity constant shows that the tablet velocity stays constant. When the spray and bed cycle time is compared between the different scales it shows that keeping the Froude number constant the time in the spray zone is constant or decreases (especially prominent in the industrial scale) and the bed cycle time is shorter when compared to the results of a constant circumferential velocity. These effects are more prominent in the industrial scale than in the pilot scale. Moreover, mixing is influenced by the rotation rate and the uniformity of the distance travelled distribution.

Mixing is enhanced when scaling up using a constant Froude number compared to a constant circumferential velocity. The better the mixing efficiency is, the faster $c_{v,inter}$ decreases. At low rotation rates, due to poorer mixing, $c_{v,inter}$ decreases slower than at faster rotation rates, and the tablet coating process takes a shorter time with a constant Froude number than at a constant v_c. Thus, keeping the Froude number constant is preferable to keeping the circumferential velocity constant as it allows a lower the necessary process time in the larger scales. Keeping the Froude number constant also ensures that the tablet bed are in the same state (rolling cascading) in the bigger scales. Thus higher rotation rates can be used but should be tested in the laboratory scale (or the simulation) first to ensure that the tablet bed flow regime stays the same. Assuming that the tablets withstand the mechanical stress due to the higher velocities and impact forces, higher rotation rates can be used.

The results from simulation can also be used as input parameters for simplified models e.g. Chen et al. [9] describing the drum tablet coating process to help identify the process parameters needed for the models. Simulations can be used to confirm the simplified model predictions before testing them in experiments which would save time and money as more process setting points can be tested in parallel. (e.g. the number of tablets in the spray zone, tablet velocity, tablet spray residence and bed cycle time.)

This work demonstrates that it is possible to predict the tablet bed behavior using the common scale-up rules. Overall, we confirmed that the DEM can help to improve the mechanistic understanding of and optimize the tablet coating process. The scale-up using simulations can be faster and at reduced costs (prototype construction, faulty batches etc.).

Nevertheless, it must be emphasized that the scale-up study presented here exclusively focused on mixing, bed dynamics and spray interaction. Thermal effects were not included. Typically, during scale-up the bed temperature or the exhaust air temperature are kept constant, in order to have the same film formation process (film-forming temperature). In addition, the mass-flow ratio between coating solution sprayed and process air should be kept similar, in order to have the same energy input per kg of tablets.

C-6. Bibliography

[1] E. C. Program, “June 24-26, 2009 St. Hugh’s College, Oxford University, Oxford, UK 1,” no. 91, pp. 1–21, 2009.

[2] E. Pharmacopoeia, “European Pharmacopoeia (PhEur) chapter 2.9.40 Uniformity of dosage units,” *Eur. Pharmacop.*, vol. 8.8, pp. 3117–3120.

[3] The United States Pharmacopeial Convention, “United States Pharmacopoeia (USP) 38 general chapter <905> Uniformity of dosage units,” *United States Pharmacopoeia*, no. <905> Uniformity of dosage units, 2011.

[4] D. Brock, J. A. Zeitler, A. Funke, K. Knop, and P. Kleinebudde, “A comparison of quality control methods for active coating processes.,” *Int J Pharm*, vol. 439, no. 1–2, pp. 289–95, Dec. 2012.

[5] D. M. Koller, G. Hannesschläger, M. Leitner, and J. G. Khinast, “Non-destructive analysis of tablet coatings with optical coherence tomography.,” *Eur. J. Pharm. Sci.*, vol. 44, no. 1–2, pp. 142–8, Sep. 2011.

[6] C. Denis, M. Hemati, D. Chulia, J.-Y. Lanne, B. Buisson, G. Daste, and F. Elbaz, “A model of surface renewal with application to the coating of pharmaceutical tablets in rotary drums,” *Powder Technol.*, vol. 130, no. 1–3, pp. 174–180, Feb. 2003.

[7] B. Freireich and J. Li, “A renewal theory approach to understanding interparticle coating variability,” *Powder Technol.*, vol. 249, pp. 330–338, 2013.

[8] P. Pandey and R. Turton, “Movement of different-shaped particles in a pan-coating device using novel video-imaging techniques.,” *AAPS PharmSciTech*, vol. 6, no. 2, pp. E237–44, Jan. 2005.

[9] W. Chen, S.-Y. Chang, S. Kiang, A. Marchut, O. Lyngberg, J. Wang, V. Rao, D. Desai, H. Stamato, and W. Early, “Modeling of pan coating processes: Prediction of tablet content uniformity and determination of critical process parameters,” *J. Pharm. Sci.*, vol. 99, pp. 3213–3225, 2010.

[10] S. Just, G. Toschkoff, A. Funke, D. Djuric, J. G. Khinast, K. Knop, and P. Kleinebudde, “Optimization of Inter-Tablet Coating Uniformity for an Active Coating Process at the Lab and Pilot Scale,” *Int. J. Pharm.*, vol. 30, no. 11, 2013.

[11] R. Mueller and P. Kleinebudde, “Influence of scale-up on the abrasion of tablets in a pan coater.,” *Eur. J. Pharm. Biopharm.*, vol. 64, no. 3, pp. 388–92, Nov. 2006.

[12] R. Mueller and P. Kleinebudde, “Prediction of tablet velocity in pan coaters for scale-up,” *Powder Technol.*, vol. 173, no. 1, pp. 51–58, Apr. 2007.

[13] J. Wang, J. Hemenway, W. Chen, D. Desai, W. Early, S. Paruchuri, S.-Y. Chang, H. Stamato, and S. Varia, “An evaluation of process parameters to improve coating efficiency of an active tablet film-coating process.,” *Int. J. Pharm.*, vol. 427, no. 2, pp. 163–9, May 2012.

[14] W. R. Ketterhagen, M. T. am Ende, and B. C. Hancock, “Process modeling in the pharmaceutical industry using the discrete element method,” *J. Pharm. Sci.*, vol. 98, pp. 442–470, 2009.

[15] K. Yamane, T. Sato, T. Tanaka, and Y. Tsuji, “Computer Simulation of Tablet Motion in Coating Drum,” *Pharm. Res.*, vol. 12, no. 9, pp. 1264–1268, 1995.

[16] A. Kalbag and C. Wassgren, “Inter-tablet coating variability: Tablet residence time variability,” *Chem. Eng. Sci.*, vol. 64, no. 11, pp. 2705–2717, 2009.

[17] A. Kalbag, C. Wassgren, S. Sumana Penumetcha, and J. D. Pérez-Ramos, “Inter-tablet coating variability: Residence times in a horizontal pan coater,” *Chem. Eng. Sci.*, vol. 63, no. 11, pp. 2881–2894, Jun. 2008.

[18] S. Just, G. Toschkoff, A. Funke, D. Djuric, G. Scharrer, J. G. Khinast, K. Knop, and P. Kleinebudde, “Experimental Analysis of Tablet Properties for Discrete Element Modeling of an Active Coating Process,” *AAPS PharmSciTech*, vol. 14, no. 1, pp. 402–411, 2013.

[19] A. O. Favier, J.F., Abbaspour Fard M.H. , Kremmer, M. and Raji, “Modelling nonspherical particles using multisphere discrete elements,” *Eng. Mech.*, no. October, pp. 971–977, 2001.

[20] M. H. Abbaspour-fard, “discrete element modelling of the dynamic behaviour of non-spherical particulate materials,” no. September, 2000.

[21] D. Suzzi, G. Toschkoff, S. Radl, D. Machold, S. D. Fraser, B. J. Glasser, and J. G. Khinast, “DEM simulation of continuous tablet coating: Effects of tablet shape and fill level on inter-tablet coating variability,” *Chem. Eng. Sci.*, vol. 69, no. 1, pp. 107–121, 2012.

[22] G. Toschkoff, S. Just, A. Funke, D. Djuric, K. Knop, P. Kleinebudde, G. Scharrer, and J. G. Khinast, “Spray Models for Discrete Element Simulations of Particle Coating Processes,” *Submitt. to Chem. Eng. Sci.*, 2013.

[23] B. Freireich, W. R. Ketterhagen, and C. Wassgren, “Intra-tablet coating variability for several pharmaceutical tablet shapes,” *Chem. Eng. Sci.*, vol. 66, no. 12, pp. 2535–2544, Jun. 2011.

[24] W. R. Ketterhagen, “Modeling the motion and orientation of various pharmaceutical tablet shapes in a film coating pan using DEM.,” *Int. J. Pharm.*, vol. 409, no. 1–2, pp. 137–49, May 2011.

[25] E. Sahni, R. Yau, and B. Chaudhuri, “Understanding granular mixing to enhance coating performance in a pan coater: Experiments and simulations,” *Powder Technol.*, vol. 205, pp. 231–241, 2011.

[26] S. Adam, D. Suzzi, C. Radeke, and J. G. Khinast, “An integrated Quality by Design (QbD) approach towards design space definition of a blending unit operation by Discrete Element Method (DEM) simulation.,” *Eur. J. Pharm. Sci.*, vol. 42, no. 1–2, pp. 106–15, Jan. 2011.

[27] C. a. Radeke, B. J. Glasser, and J. G. Khinast, “Large-scale powder mixer simulations using massively parallel GPUarchitectures,” *Chem. Eng. Sci.*, vol. 65, no. 24, pp. 6435–6442, Dec. 2010.

[28] R. Turton and X. X. Cheng, “The scale-up of spray coating processes for granular solids and tablets,” *Powder Technol.*, vol. 150, no. 2, pp. 78–85, Feb. 2005.

[29] C. P. A. and O. D. L. Strack, “A discrete numerical model for granular assemblies,” *Géotechnique*, vol. 29, no. 1, pp. 47–65, Jan. 1979.

[30] Nvidia, “Nvidia CUDA C Programming Guide Version 4.2,” p. 173, 2012.

[31] A. O. Favier, J.F., Abbaspour Fard M.H. , Kremmer, M. and Raji, “Shape representation of axi-symmetrical, non-spherical particles in discrete element simulation using multi element model particles,” *Eng. Comput.*, vol. 16, no. 4, pp. 467–480, 1999.

[32] P. Boehling, G. Toschkoff, K. Knop, P. Kleinebudde, S. Just, A. Funke, H. Rehbaum, and J. G. Khinast, “Analysis of large-scale tablet coating : Modeling , simulation and experiments,” *Eur. J. Pharm. Sci.*, 2015.

[33] G. Toschkoff, S. Just, K. Knop, P. Kleinebudde, A. Funke, D. Djuric, G. Scharrer, and J. G. Khinast, “Modeling of an Active Tablet Coating Process,” *J. Pharm. Sci.*, p. n/a–n/a, Sep. 2015.

[34] E. Sahni and B. Chaudhuri, “Experiments and numerical modeling to estimate the coating variability in a pan coater.,” *Int. J. Pharm.*, vol. 418, no. 2, pp. 286–96, Oct. 2011.

[35] D. Suzzi, S. Radl, and J. G. Khinast, “Local analysis of the tablet coating process: Impact of operation conditions on film quality,” *Chem. Eng. Sci.*, vol. 65, no. 21, pp. 5699–5715, Nov. 2010.

[36] A. Alexander, T. Shinbrot, and F. J. Muzzio, “Scaling surface velocities in rotating cylinders as a function of vessel radius, rotation rate, and particle size,” *Powder Technol.*, vol. 126, no. 2, pp. 174–190, Jul. 2002.

[37] A. Dubey, R. Hsia, K. Saranteas, D. Brone, T. Misra, and F. J. Muzzio, “Effect of speed, loading and spray pattern on coating variability in a pan coater,” *Chem Eng Sci*, vol. 66, no. 21, pp. 5107–5115, Nov. 2011.

[38] D. Jajcevic, E. Siegmann, C. Radeke, and J. G. Khinast, “Large-scale CFD–DEM simulations of fluidized granular systems,” *Chem. Eng. Sci.*, vol. 98, pp. 298–310, Jul. 2013.

D. Analysis of Large-Scale Tablet Coating: Modeling, Simulation and Experiments

Published as: P. Boehling *et al.*, "Analysis of large-scale tablet coating : Modeling , simulation and experiments," *Eur. J. Pharm. Sci.*, vol. 90, pp. 14–24, 2016.

D-1. Abstract

This work concerns a tablet coating process in an industrial-scale drum coater. We set up a full-scale Design of Simulation Experiment (DoSE) using the Discrete Element Method (DEM) to investigate the influence of various process parameters (the spray rate, the number of nozzles, the rotation rate and the drum load) on the coefficient of inter-tablet coating variation ($c_{v,inter}$). The coater was filled with up to 290 kg of material, which is equivalent to 1,028,369 tablets. To mimic the tablet shape, the glued sphere approach was followed, and each modelled tablet consisted of eight spheres. We simulated the process via the eXtended Particle System (XPS), proving that it is possible to accurately simulate the tablet coating process on the industrial scale. The process time required to reach a uniform tablet coating was extrapolated based on the simulated data and was in good agreement with experimental results.

The results are provided at various levels of details, from thorough investigation of the influence that the process parameters have on the $c_{v,inter}$ and the amount of tablets that visit the spray zone during the simulated 90 seconds to the velocity in the spray zone and the spray and bed cycle time. It was found that increasing the number of nozzles and decreasing the spray rate had the highest influence on the $c_{v,inter}$. Although increasing the drum load and the rotation rate increased the tablet velocity, it did not have a relevant influence on the $c_{v,inter}$ and the process time.

D-2. Introduction

Tablets are the most common form of drug products and they are often coated to mask the API's taste, to add protection functionality, to provide a modified release of an active pharmaceutical ingredient (API) or to add a second API (active coating). Especially, with respect to active coating, ensuring content uniformity - and thus coating uniformity - is a challenging task. Consequently, intra-tablet and inter-tablet coating variability are critical quality attributes (CQAs). Intra-tablet coating variability is the variability in the coating mass on a single tablet, with the edges and the bands being especially critical. In contrast, inter-tablet coating variability refers to the variance between all tablets in one batch. For

the case of active coating, inter-tablet variability is even more critical and is regulated by the corresponding guidelines and pharmacopoeias.

One of the main goals of designing a coating process is to ensure that it reliably delivers a low inter-tablet coating variability. Thus, mixing of the tablet bed and the spraying process are often studied experimentally, typically in a small-scale drum coater [1], [2], [3]. Since extensive experimentation on the pilot or, even more demanding, on the production scale typically is prohibitively expensive, experimental studies are mainly performed on the laboratory scale. Scale-up rules and the experience of the process engineer are used to calculate/estimate the correct loads and rotation rates on larger scales[4], [5], [6], [7]. Verification of the process parameters is carried out via test runs on the industrial scale, which are also used for obtaining the approval of the regulatory agencies. Results of experiments on the industrial scale are rarely published[8].

One way to reduce the amount of experiments and the associated costs is to perform simulations in addition to experiments. In this context, the Discrete Element Method (DEM), developed by Cundall and Strack in 1979 [9], has proven to be an effective simulation methodology. In this method, Newton's second law of motion and a momentum balance are solved for each particle in three dimensions. All forces, including normal and tangential contact forces are included and the detail of modeling distinguishes the different implementations of DEM. DEM has successfully been applied in the pharmaceutical industry [10]. Tablet coating is particularly suitable for DEM simulations as the number of particles (i.e., tablets) is relatively low compared to other processes involving granular material, where particle numbers easily reach many billions [11]. In the past, simulations reported in the literature focused mainly on small- scale systems, with the number of tablets being in the order of 10^4-10^5 [12]–[14]. Early simulations used spheres [15] to approximate the tablet's shape: the glued sphere approach was developed to model non-spherical particles [16] through multiple spheres [13], [14], [17],[18]. However, due to an increasing computational power available and sophisticated parallelization efforts, it is now possible to simulate many millions of particles on a single graphical processing unit (GPU)[19], [20]. In combination with the glued sphere approach, current models can simulate the tablet coating process on the pilot and even on production scales with up to 2 million tablets within a reasonable amount of time. Based upon these new approaches, it is possible to create a full factorial Design of Simulation Experiment (DoSE) with multiple factors on every scale.

In the current study, we modeled the coating process and simulated the flow of tablets in a production-scale drum tablet coater to determine the optimal process parameters. A full DoSE on the production

scale was carried out, which so far was not possible due to the limited computational resources. The Coefficient of Variation in the coating drum was calculated for various process settings. Moreover, the influence of the drum load, the rotation rate, the spray rate and the number of nozzles on the $c_{v,inter}$ were studied. The end-point of the process (i.e., the time needed to complete the process with the desired coating thickness and quality) could be predicted based on the simulation data. The predicted end point was then compared to experimental results. The spray residence time, the bed cycle time and the tablet velocity in the spray zone and their effect on the $c_{v,inter}$ were investigated.

D-3. Material and methods

D-3.1. Tablet coating process, tablet and drum design

In this study an active coating process was considered for the production of tablets that contain two APIs: one in the coating and the other in the core. Gastrointestinal therapeutic systems (GITS, see Figure 32) were used as a starting material (Bayer Pharma AG, Leverkusen, Germany). These are biconvex round tablets with a diameter of 9 mm and a height of 5 mm. During the coating process, a coating solution containing the API candesartan (Cilexetil) was sprayed on the tablets.

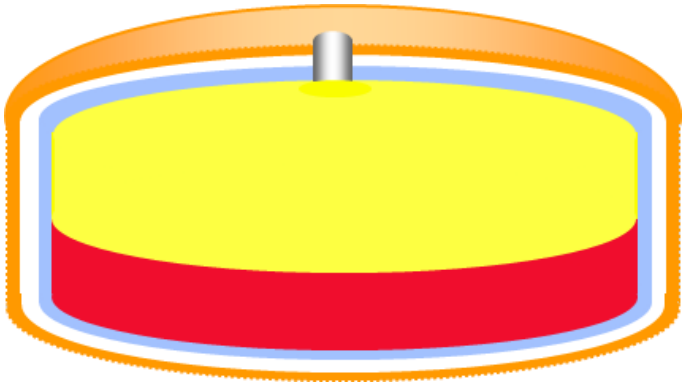

Figure 32: GITS tablet schema, orange is an outer tablet color coating, white the active coating layer discussed in this paper, blue a semipermeable membrane with an orifice surrounding the inner drug layer (yellow) and the polymeric push compartment (red).

During the coating process, the tablet bed is flowing in the drum coater due to the drum rotation [21]. Integrated baffles in the coater enhance axial and radial mixing and ensure that no dead zones are formed. Individual tablets are transported upwards in the bed. After reaching the top of the tablet bed, the tablets slide down and pass through the spray zone where the coating mass is applied. The spray droplets impact on the tablet surface, spread and the solvent is removed (dried) by the drying air. The remaining polymer particles of the coating suspension form first a tightly packed bed and then a film.

This occurs only above the minimum film forming temperature (MFFT). Thus, a minimum temperature in the bed needs to be maintained.

The coating mass applied to an individual tablet mostly depends on the time a tablet stays in the spray zones. The results of a DEM simulation of the tablet bed during the coating process and the spray zone position are shown in Figure 33. The tablet velocities are represented by color variations: the fastest tablets are on the top of the tablet bed.

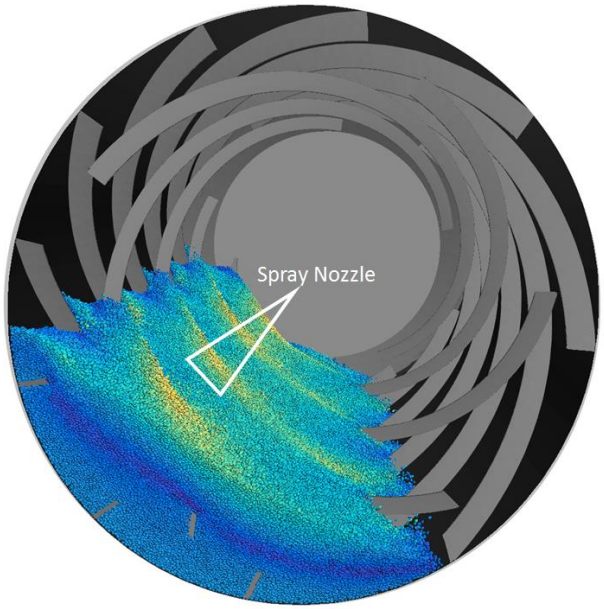

Figure 33: Filled drum coater and the position of the spray nozzles. The drum is filled with 290 kg (1,028,369 tablets) of material and is rotating with 8 rpm. The tablets are colored according to their velocity.

D-3.2. Experimental investigation

Experimental investigations were performed at the Bayer site to investigate the necessary process time for achieving a desired coating quality. The tablets were coated in a production-size coater (BFC 400, L.B Bohle Maschinen + Verfahren GmbH, Ennigerloh, Germany). The geometry of the coating apparatus was provided by the manufacturer (Figure 34). During the experiments, the drum load was varied between 240 and 260 kg. The rotation rate was set to 9 rpm and the spray rate was varied between 160 g/min to 360 g/min. The tablets were coated between 172 up to 522 min. The set of experiments can be seen in Table 10.

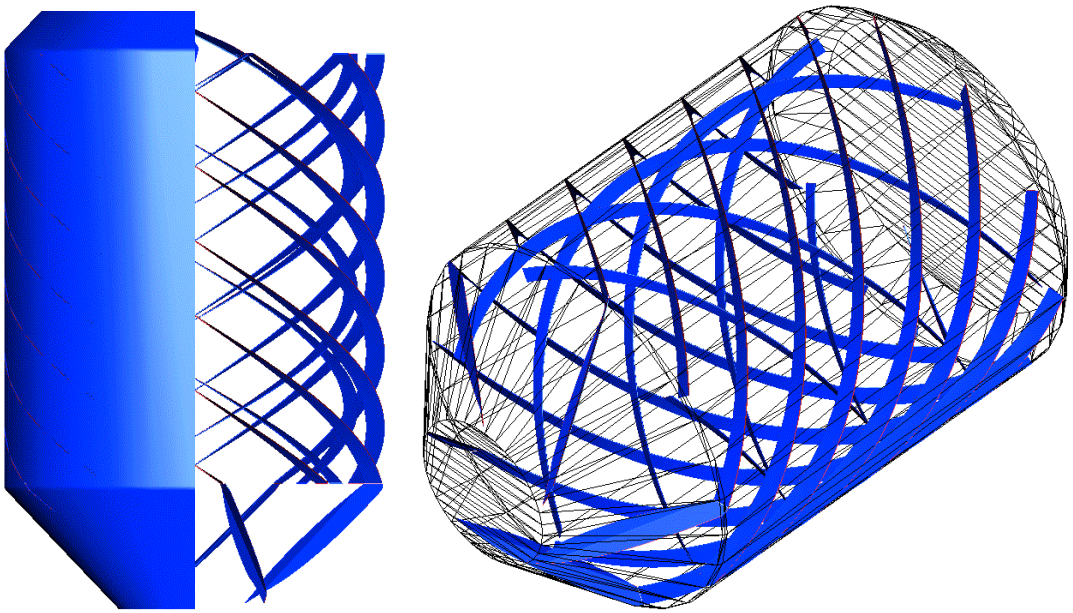

Figure 34: Mesh of the BFC 400 drum used in the simulation.

Table 10: Study design of the experimental part

Case	*Load* *In kg*	*Rotation Rate* *In rpm*	*Spray Rate* *In g/min*	*Duration* *In min*
A	260	9	360	172
B	240	9	240	248
C	250	9	160	368
D	250	9	360	345
E	250	9	240	522

D-3.3. Simulation model

XPS is a DEM algorithm written in CUDA, which is a C-extension developed by Nvidia and is designed for GPU computing. While a modern CPU typically has about 24 cores, CUDA allows for parallel computing with over 2000 CUDA cores. Parallelization of the DEM algorithm allows the simulation of up to 130 million spheres in a single GPU, applying a linear spring dashpot model to calculate the forces acting on the particles upon collision (see [19], equations 1-11).

To compute the interaction between non-spherical particles (e.g., tablets), a glued sphere approach was applied. Each simulated particle was represented via several primitive shapes. XPS currently uses overlapping spheres to mimic the real shape of a complex-shaped particle. The material properties

(Table 11) were taken from [22] and adapted accordingly. The modeled tablets were represented via eight spheres (Figure 4), which had the same volume as the real tablet. This approach allows simulating the process within a reasonable amount of time.

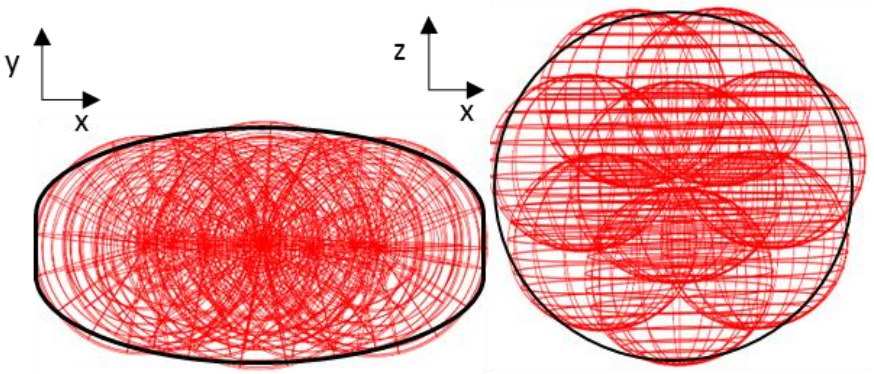

Figure 35: Tablet shape as modelled with the glued sphere approach

Table 11: Simulation and material parameters

Tablet properties	
Spring constant	2500 N/m
Density	1150 kg/m^3
Interaction Tablet – Wall	
Coefficient of Restitution	0.78
Static friction coefficient	0.45
Rolling friction coefficient	0.01
Interaction tablet – tablet	
Coefficient of Restitution	0.78
Static friction coefficient	0.39
Rolling friction coefficient	0.01
Simulation	
Time step length	$4 \cdot 10^{-5}$ s
Cell size (X,Y,Z)	(0.0061, 0.0058, 0.0061) m

D-3.4. Simulation setup

One tablet weight is 282 mg. The total number of tablets depends on the fill level, and was between 815,602 (230 kg) and 1,028,368 (290 kg) tablets. Tablets were allowed to settle during the first six seconds of simulation, the tablet bed reached a steady state and the created data were discarded. The simulation continued for additional 90 seconds (in true process time) and information on the position, velocity and orientation of the particles was analyzed every 0.02 seconds. Finally, the simulation continued for one additional second with a storage interval of 0.002 seconds to obtain a highly temporal resolution for the investigation of the spray residence time. The stored files were then analyzed using the post-processing algorithms written in Python.

D-3.4.1. Design of simulation experiments

The simulation runs were chosen following a statistical design, commonly known as Design of Experiments (DoE). Derived from this terminology, we refer to this approach as *Design of Simulation Experiments* (DoSE). Upper and lower limits were defined for each parameter. The goal was to mimic the real process and find the optimal process parameters. The rotation rate and the fill level varied between 8 to 10 rpm and 230 to 290 kg, respectively. For each load and rotation rate, a DEM simulation was performed (i.e., a total of 7 simulations). The impact of the spray was determined after the DEM simulation, i.e., during post-processing: Here, the number of nozzles was four, six and eight and the center spray rate was 240 g/min, with changes to 160 and 360 g/min. This resulted in 9 different post-processing parameters and a total of 7×9 (63) simulated cases (Table 12).

D-3.4.2. Spray modeling

There are several methods for modeling the spray via DEM. One method includes the spray coating process in the simulation where spray droplets are considered DEM particles. Other approaches account for the spray during post processing using a ray tracing algorithm [23]. In this work, a ray tracing algorithm was used similar to the one proposed by Toschkoff et al. [23]. For details of the method refer to [23]. The position and dimension of the spray zones were obtained from the real process. In this method, the spray is simulated as a bundle of rays. The spray zones are oriented as shown in Figure 5, i.e., at 1/3 of the distance down from the top of the tablet bed. With the ray tracing algorithm it is possible to determine which tablets are currently in the spray zone. Additionally, the velocity of these tablets, and their spray-residence and bed-cycle time can be determined exactly. For every single tablet, the amount of coating mass is determined which depends on the number of rays that hit the tablet. The mass is computed according to

$$m_{ray} = \frac{\dot{m}_{spray}}{n_{rays}} \cdot \Delta t \tag{16}$$

m_{ray} is the mass that gets added during one storage interval (0.02 s) to the tablet if it is hit inside the spray zone by one single ray. $\dot{m}_{spray}$ is the spray rate in g/s, n_{rays} is the number of rays used in the post processing and Δt is the store interval. The more rays hit the tablet the more coating mass the tablet receives. Thus, the time and the exposure of the tablet in the spray zone is taken into account. The more rays (n_{rays}) are used in the post processing the more accurate the calculation becomes. Realistic spray cones with varying density and shape can be modeled as well with this approach. With this information the coefficient of variation can be calculated *a posteriori*. Thus, using this approach varying spray gun configurations can be studied rapidly.

In our case, the spray regions are elliptically shaped. Spray zone dimensions are 6 x 12 mm. In total three nozzle set-ups were investigated with 4, 6 and 8 nozzles each (Figure 36).

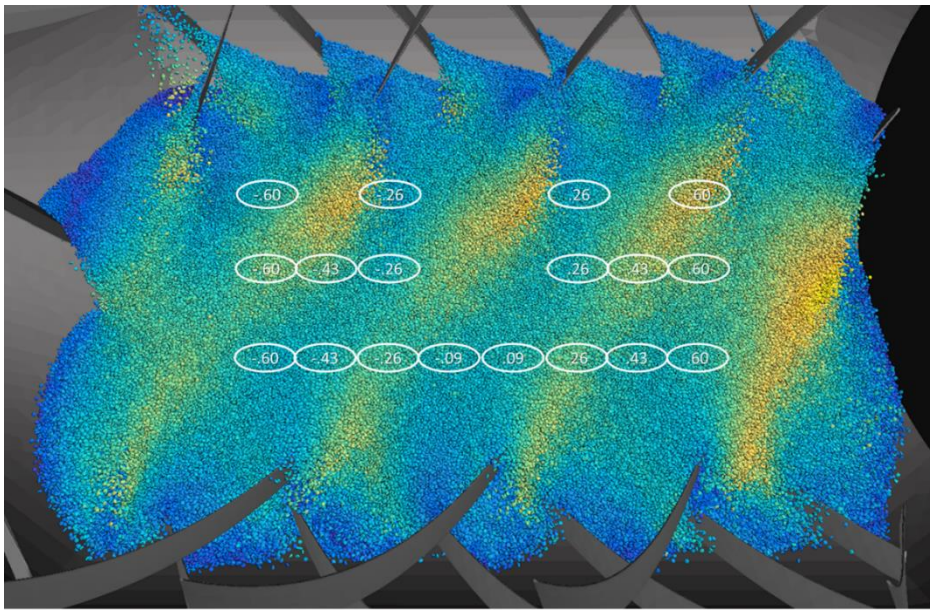

Figure 36: Spray zones (white ellipses). The number inside the ellipse is the distance from the middle of the coater in the BFC 400 (view from the top, normal to the tablet bed surface). The set up with four nozzles represents the true position. The configuration with six and eight nozzle is shifted down for the purpose of clarity.

D-3.4.3. Critical quality attributes

Inter-tablet coating variability was chosen as the relevant quality criterion of the coating process. It is defined as the $c_{v,inter}$,which is the standard deviation σ_{mc} of the coating mass distributed over all tablets divided by the mean of the coating mass μ_{mc}:

$$c_{v,inter} = \frac{\sigma_{mc}}{\mu_{mc}} = \frac{\sqrt{\frac{1}{N}\sum_{i=1}^{N}\left(m_{c,i} - \overline{m}_c\right)^2}}{\overline{m}_c}, with\ \overline{m}_c = \frac{1}{N}\sum_{i=1}^{N} m_{c,i} \quad (17)$$

Here, N is the number of tablets, $m_{c,i}$ is the coating mass of tablet *i* and $\overline{m}_c$ is the mean coating mass. The goal of the optimization of the tablet coating process is to obtain a consistently low $c_{v,inter}$. Typically, in experimental investigations the total variation is estimated based on the variation in a sample. In contrast, in a DEM simulation the coating of all tablets (the entire statistical population) is used for this calculation. The associated limit set by regulations is 6.25 % [24].

The simulations were run using varying parameter settings to investigate their influence on the process outcome. The parameters were chosen based on the ability to adjust the parameters in realistic coating

operations, i.e., the rotation rate, the fill level, the number of spray nozzles and the spray rate. Other parameters, such as the tablet-tablet friction, were excluded as these parameters cannot be controlled.

For each variation in the rotation rate and fill level, a DEM simulation was performed for 90s of real processing time. The spray analysis was done as post processing (described above). The total spray rate was given and, depending on the number of nozzles, each nozzle sprayed a fraction of the total spray rate (i.e., for 2 nozzles each nozzles sprays 50 % of the total spray rate). We extrapolated the spray results (i.e., the coefficient of variation $c_{v,inter}$) to 300 min for a base spray rate of 240 g/min in two ways: First, we calculated the exponent of decay of $c_{v,inter}$ for the last 30 seconds of DEM simulation time. Next, we used literature data [25]–[28] that report that the $c_{v,inter}$ is inversely proportional to the square time:

$$c_{v,inter} \propto \frac{1}{\sqrt{t}} = t^{-0.5} \tag{18}$$

Finally, we used this equation to extrapolate the $c_{v,inter}$ after 300 min and to the process durations given in the experimental study Table 10. Thus, two differently predicted $c_{v,inter}$ are available and reported below.

Varying the number of nozzles and the spray rate was done during the post processing. The base case of the spray rate was 240 g/min for a total coating time of 300 min, yielding a total amount of coating solution of 72 kg. In the simulations the spray was varied (160 g/min and 360 g/min). Thus, also the coating time had to be adapted to 450 min and 200 min, respectively. The coefficient of variation $c_{v,inter}$ does not depend on the absolute spray rate (see Eq. 17), yet strongly depends on the spraying time as mentioned above (Eq. 18). Thus, $c_{v,inter}$ for the spray rate settings 160 g/min and 360 g/min was computed based on Eq. 19:

$$c_{v,inter,2} = c_{v,inter,1}\sqrt{\frac{\dot{V}_2}{\dot{V}_1}} \tag{19}$$

D-4. Results

The results of the designed simulation experiments (DoSE) are shown in Table 12. Table 3 also contains the final result for the $c_{v,inter}$ after 90 s of computation. Moreover, Table 2 presents the final $c_{v,inter}$ extrapolated to the end of the process, i.e., after 300 min at a spray rate of 240 g/min and shorter/longer times depending on the selected spray rate. 240 g/min was set as the base value for the spray rates. For different spray rates the $c_{v,inter}$ was calculated using Eq. 19 For different nozzle numbers the API concentration in the spray was assumed to change accordingly. Two different extrapolated

numbers are given: First, with the exponent calculated based on the time decay during the last 30 s of the simulated first 90s, and, second, with an exponent of -0.5 as given in the literature (Eq. 18)

Table 12: Design of Simulation Experiment in the BFC 400 and the corresponding values of $c_{v,inter}$ after 90 s (extrapolated to 135 s and 60 s), 300 min (450 min and 200 min)with an ideal decay and with a fitted decay. The $c_{v,inter}$ values for a spray rate of 160 and 360 g/min were adapted according to Eq. 19

Case	Load	Rotation rate	Number of	Spray Rate	$c_{v,inter}$	$c_{v,inter}$	$c_{v,inter}$
	in kg	in rpm	Nozzles	in g/min	after 90 s	final exponent 0.5	final fitted exponent
1	230	8	4	160	82.32%	5.62%	4.98%
2	230	8	4	240	100.82%	6.89%	6.10%
3	230	8	4	360	123.47%	8.43%	7.48%
4	230	8	6	160	67.07%	4.59%	3.79%
5	230	8	6	240	82.15%	5.63%	4.64%
6	230	8	6	360	100.61%	6.89%	5.68%
7	230	8	8	160	59.26%	4.20%	2.97%
8	230	8	8	240	72.58%	4.99%	3.63%
9	230	8	8	360	88.89%	6.11%	4.45%
10	230	10	4	160	73.74%	5.04%	4.37%
11	230	10	4	240	90.31%	6.17%	5.35%
12	230	10	4	360	110.61%	7.56%	6.55%
13	230	10	6	160	61.08%	4.20%	3.38%
14	230	10	6	240	74.81%	5.12%	4.13%

15	230	10	6	360	91.63%	6.28%	5.06%
16	230	10	8	160	54.70%	4.20%	2.76%
17	230	10	8	240	66.99%	4.61%	3.38%
18	230	10	8	360	82.05%	5.64%	4.14%
19	240	9	4	160	78.56%	5.37%	4.57%
20	240	9	4	240	96.22%	6.58%	5.60%
21	240	9	4	360	117.85%	8.06%	6.85%
22	240	9	6	160	64.57%	4.43%	3.45%
23	240	9	6	240	79.08%	5.43%	4.22%
24	240	9	6	360	96.85%	6.65%	5.17%
25	240	9	8	160	57.54%	4.20%	2.77%
26	240	9	8	240	70.47%	4.85%	3.39%
27	240	9	8	360	86.31%	5.94%	4.15%
28	250	9	4	160	79.49%	5.44%	4.59%
29	250	9	4	240	97.35%	6.66%	5.63%
30	250	9	4	360	119.23%	8.16%	6.89%
31	250	9	6	160	65.32%	4.48%	3.43%
32	250	9	6	240	80.00%	5.49%	4.20%
33	250	9	6	360	97.98%	6.73%	5.14%
34	250	9	8	160	58.01%	4.20%	2.70%
35	250	9	8	240	71.04%	4.90%	3.31%
36	250	9	8	360	87.01%	6.00%	4.05%

37	260	9	4	160	80.37%	5.50%	4.62%
38	260	9	4	240	98.43%	6.73%	5.66%
39	260	9	4	360	120.55%	8.25%	6.93%
40	260	9	6	160	66.12%	4.54%	3.50%
41	260	9	6	240	80.98%	5.56%	4.29%
42	260	9	6	360	99.18%	6.80%	5.25%
43	260	9	8	160	58.55%	4.20%	2.69%
44	260	9	8	240	71.71%	4.94%	3.30%
45	260	9	8	360	87.83%	6.05%	4.04%
46	290	8	4	160	88.81%	6.09%	4.82%
47	290	8	4	240	108.78%	7.45%	5.91%
48	290	8	4	360	133.22%	9.13%	7.23%
49	290	8	6	160	72.30%	4.98%	3.40%
50	290	8	6	240	88.55%	6.10%	4.17%
51	290	8	6	360	108.45%	7.47%	5.10%
52	290	8	8	160	63.59%	4.41%	2.43%
53	290	8	8	240	77.88%	5.40%	2.98%
54	290	8	8	360	95.38%	6.62%	3.65%
55	290	10	4	160	79.60%	5.43%	4.98%
56	290	10	4	240	97.49%	6.65%	6.10%
57	290	10	4	360	119.40%	8.14%	7.47%
58	290	10	6	160	65.55%	4.48%	3.89%

59	290	10	6	240	80.29%	5.48%	4.77%
60	290	10	6	360	98.33%	6.72%	5.84%
61	290	10	8	160	58.31%	4.20%	3.21%
62	290	10	8	240	71.42%	4.89%	3.93%
63	290	10	8	360	87.47%	5.99%	4.81%

D-4.1. Coefficient of inter-tablet coating variation

In Figure 37 the evolution of $c_{v,inter}$ is shown for spray rate of 240 g/min. For clarity, only the best (230 kg, 10 rpm, 8 nozzles) and worst case (290 kg, 8rpm, 4 nozzles) are shown. The results for $c_{v,inter}$ in the other cases are in between these two extremes. The exponent of decay during the last 30 seconds was calculated and was the basis for extrapolating the values to a total process time of 300 min. Since $c_{v,inter}$ is plotted over a double logarithmic scale, it appears to be linear. Note that for lower (higher) spraying rates and thus longer (shorter) coating times better (worse) results are achieved.

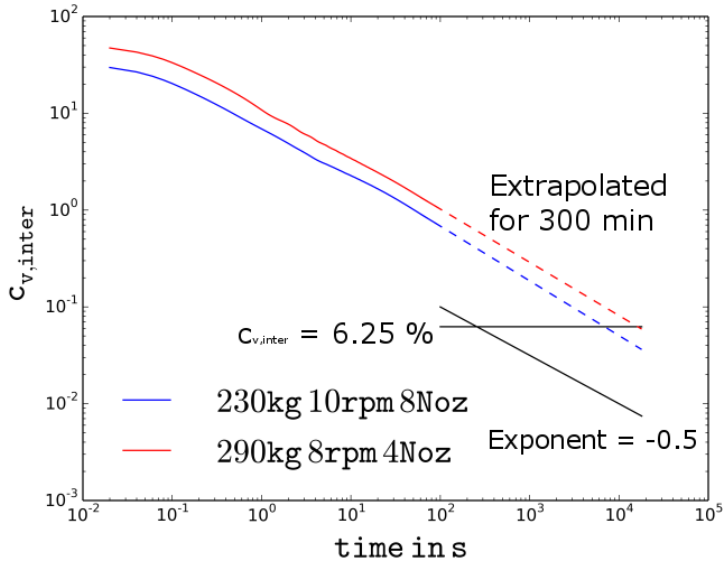

Figure 37: $c_{v,inter}$ over the simulated time and estimated values for a process time of 300 min for the best and worst cases. The dashed line is extrapolated from the last 30 seconds with the calculated exponent.

In literature (e.g., [25], [29], [30] ,[31]) it was reported that the exponent of decay for $c_{v,inter}$ evolution is -0.5, based on the assumption that the coating process is random. In our simulations, initially the decay was flatter than the literature value. This is expected during the initialization phase of the coating process. However, the exponent steadily increased and reached a value slightly above -0.5 in all cases.

A linear fit in the double-logarithmic diagram was used during the last 30 s to compute the exponent. The exponent did not change, even when fewer data points (the last 20, 10 or 5 seconds of simulated time) were used, indicating that the process reached a quasi-steady state in terms of mixing after 60s. The fitted values are shown in Table 13.

Table 13: Exponent of the decrease in $c_{v,inter}$ as a function of time

Load	**Rotation rate**	**Number of Nozzles**	**Number of Nozzles**	**Number of Nozzles**
in kg	in rpm	4	6	8
230	8	-0.530	-0.543	-0.565
230	10	-0.534	-0.547	-0.564
240	9	-0.537	-0.553	-0.573
250	9	-0.538	-0.557	-0.579
260	9	-0.539	-0.555	-0.581
290	8	-0.550	-0.577	-0.616
290	10	-0.523	-0.533	-0.548

As can be seen these values are all significantly above the value for a random coating event reported in the literature and increase with an increasing number of nozzles. This shows that the coating process is not purely random and is faster than predicted by Eq18 in this specific coater.

Based on these results the minimum process time was computed to reach a $c_{v,inter}$ of 6.25% (Table 14) which is independent of the spray rate. The strongest effect is the number of nozzles. Clearly, a higher nozzle number leads to a significantly shorter process time. Moreover, it can be seen that increasing the rotation ratedecreases the necessary process time, while increasing the drum load increases the process time. This is true in all cases, except for 290 kg and 8 rpm, where – in this case -possibly not enough bed cycles were simulated to reach a steady state.

For comparison, in Table 15 the required coating times are presented using a constant exponent of k=-0.5. In all cases, the process took significantly longer. Thus, the results indicate that with proper design of the tablet mixing system in the drum a faster coating process can be achieved in order to reach a required $c_{v,inter}$.

Table 14: Process time in [min] until $c_{v,inter}$ of 6.25 % is reached at a spray rate of 240 g/min, extrapolated using the fitted exponent from Table 13

Drum Load	**Rotation rate**	**Number of Nozzles**	**Number of Nozzles**	**Number of Nozzles**
in kg	in rpm	4	6	8
230	8	265	160	106
230	10	207	130	93
240	9	226	136.	95
250	9	228	136	93
260	9	231	141	92
290	8	251	138	84
290	10	264	167	119

Table 15: Process time in [min] until $c_{v,inter}$ of 6.25 % is reached at a spray rate of 240 g/min extrapolated using a constant exponent of -0.5.

Drum Load	**Rotation rate**	**Number of Nozzles**	**Number of Nozzles**	**Number of Nozzles**
in kg	in rpm	4	6	8
230	8	335	223	176
230	10	269	185	150
240	9	306	208	166
250	9	313	213	169
260	9	320	218	172
290	8	393	263	206
290	10	312	212	169

D-4.2. Comparison of experimental and simulation results

Experimental investigations were performed on the industrial scale to determine the minimal necessary process time to achieve consistently a $c_{v,inter}$ below 6.25 %. The experiments were performed at the Bayer production facility. The process time, of these experiments, varied between 172 and 522 min. Thus the results of the simulations were extrapolated for the same period, using the same exponents used as for the 300 min extrapolation. The load was between 240 to 260 kg, the rotation rate was 9 rpm in every case, the spray rate was varied between 160 and 360 g/min and 4 spray nozzles. A total of 5 experiments were performed, and the results were compared with the values extrapolated

from the 90 seconds simulated process time. The results were extrapolated using, first, the fitted exponents from Table 13 and, second, a fixed exponent of -0.5. The results are shown in Figure 38.

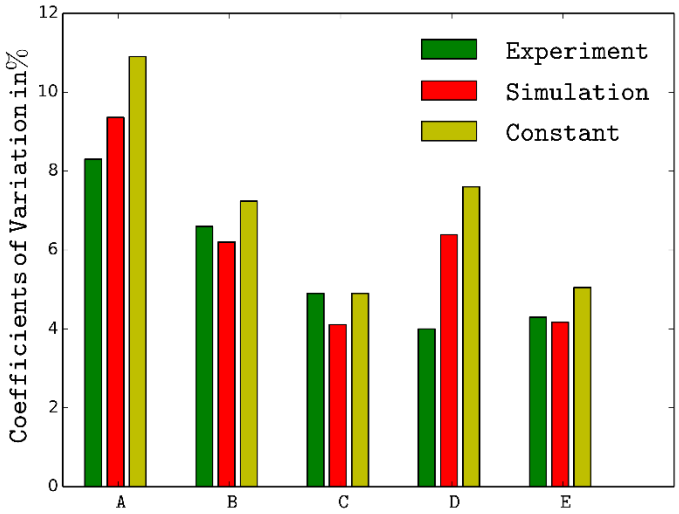

Figure 38: $c_{v,inter}$ for experiments and simulations as a bar chart. A (drum load: 260 kg, rotation rate: 9 rpm, process time: 172 min, spray rate: 360 g/min), B (drum load: 240 kg, rotation rate: 9 rpm, process time: 248 min, spray rate: 240 g/min), C (drum load: 250 kg, rotation rate: 9 rpm, process time: 368 min, spray rate: 160 g/min), D (drum load: 250 kg, rotation rate: 9 rpm, process time: 345 min, spray rate: 360 g/min), A (drum load: 250 kg, rotation rate: 9 rpm, process time: 522 min, spray rate: 240 g/min)

As can be seen, all extrapolated results closely match the experimental ones. The fitted exponent had a mean deviation of 0.51 %, which gives a relative deviation of 10 %. For the constant exponent, the mean deviation was 1.02 % and the mean relative deviation was 22 %. For the fitted exponent, the results were either over- or under-predicted. For a constant exponent, all results were under-predicted. The smaller error when using the fitted exponent confirms that the exponent is indeed higher than -0.5, indicating good mixing in the coating drum. The difference in the results may be due to the way the $c_{v,inter}$ is measured in experiments and simulations. In experiments, 10-30 tablets are typically chosen and with the aid of statistical methods they allow to draw conclusions of the $c_{v,inter}$ of the whole batch. In simulations, it is extrapolated from the $c_{v,inter}$ of the entire batch after 90 s. The deviation can also be caused by the simplification of the simulation due to omitting several factors that influence the process outcome, including the change of tablet-tablet friction through the spray coating, the moisture content in the drum, the drying process air and possible spray losses. However, the influence of these parameters seems to be small.

In summary, the results also show that DEM simulations can predict reliably the process time without performing experiments on the production scale, and can thus reduce the required number of experiments on the production scale.

D-4.3. Inter-tablet coating uniformity as a function of process parameters

As described in the DoSE the $c_{v,inter}$, was calculated for 63 cases after 90 seconds and extrapolated for a total process time of 300 min for a spray rate of 240 g/min and for other processing times depending on the spray rate. The results were analyzed via Umetrics Modde®, which is a widely used tool for design of experiments, multi-variate data analysis (MVDA) and model generation in the pharmaceutical industry. A first order-model in Eq. 20 was used to calculate the dependence and influence of various process parameters on $c_{v,inter}$. Furthermore, a second order-model Eq. 21 was applied as well:

$$c_{v,inter} = a_1 x_R + a_2 x_L + a_3 x_S + a_4 x_N \quad (20)$$

$$c_{v,inter} = a_1 x_R + a_2 x_L + a_3 x_S + a_4 x_N + b_1 x_R^2 + b_2 x_L^2 + b_3 x_S^2 + b_4 x_N^2 \quad (21)$$

Here x_R denotes rotation ate, x_L denotes drum load, x_S denotes the spray rate and x_N denotes the number of nozzles. The corresponding coefficients a_i (b_i) were determined by fitting the known data points. The model after 90s (135 s and 60 s) shows a good fit (R^2 = 0.906) and good predictive capability (Q^2 = 0.893). The results for the extrapolated values after 300 min (450 min and 200 min) using the calculated exponent show a good fit as well (R^2 = 0.895) and predictive capability (Q^2 = 0.875). The centered and scaled coefficients are shown in Figure 39 to illustrate the effect of the process parameters after 90s (135 s and 60 s) and 300 min (450 min and 200 min). The second order model had nearly the same fit (R^2 = 0.910) and predictive capability (Q^2 = 0.900). Thus, the simpler model was chosen.

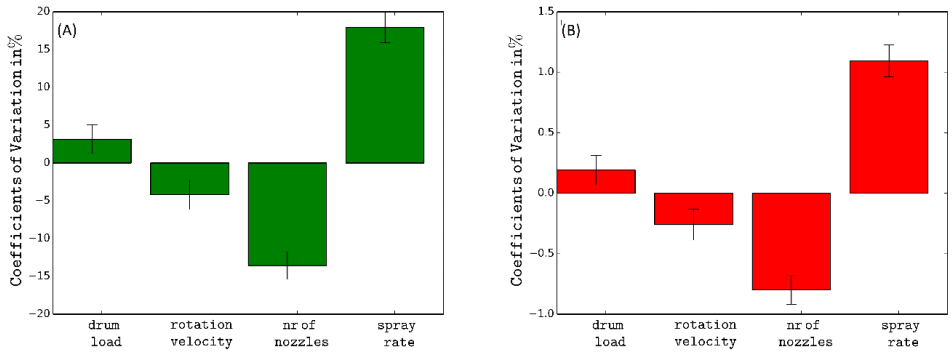

Figure 39: Effect of the various parameters on the $c_{v,inter}$ after 90 s (A) and 300 (B) min (Considering different spray rates using Eq. 19 using the linear model in Eq. (5). The relative relationship is constant going from 90 s to 300 min.

A high absolute value in the coefficient Plot Figure 39 indicates that a factor has a significant influence on $c_{v,inter}$. A negative value means that by increasing this value $c_{v,inter}$ can be decreased, and a high positive value means that by decreasing the factor $c_{v,inter}$ can also be decreased. As can be seen from Figure 39 the number of nozzles and the spray rate have the greatest influence. An increased number of nozzles allow for more tablets sprayed at the same time which reduces the minimal necessary process time and increases drastically the $c_{v,inter}$ for the same process time.

Using the established model, we investigated how changing the process parameters changed the process outcome. The results of this multi-variate data analysis (MVDA) are shown as a 4D contour plot in Figure 40. $c_{v,inter}$ was calculated for 300 mins and a spray rate of 240 g/min and adjusted the $c_{v,inter}$ according to Eq. 19 for a spray rate of 160 and 360 g/min (i.e. 450 min and 200 min). Since the scale is the same for all plots, one can quickly determine which settings are more suitable to reach a certain desired $c_{v,inter}$. Overall, the best results were achieved with eight nozzles and a spray rate of 160 g/min (upper left part), and the worst results were achieved with 4 nozzles and the highest spray rate (lower right).

In Figure 40 it can be seen that conditions in the lower-right sub-plot (for 300 min) do not achieve a required $c_{v,inter}$ value ≤ 6.25%. The cases with 4 nozzles and a spray rate of 240 g/min and 6 nozzles and 360 g/min are on the edge of the desired limit, with some settings (rotation rate and drum load) over the limit and some exactly at the limit. Another advantage of the plot is that multiple scenarios that fulfill the requirements can be weighed against each other. For example, one could increase the number of nozzles, and thus, decrease processing time and/or increase overall efficiency.

Finally, it can be seen that higher nozzle numbers give consistently a lower $c_{v,inter}$, thus providing a consistently higher product quality. Alternatively, one could lower the loading or increase speed for intermediate nozzle numbers and medium to high spray rates. However, this is of less importance. In general, this figures show again, that increasing the number of spray guns has the most significant benefit and allows operation in a wide range of operating conditions.

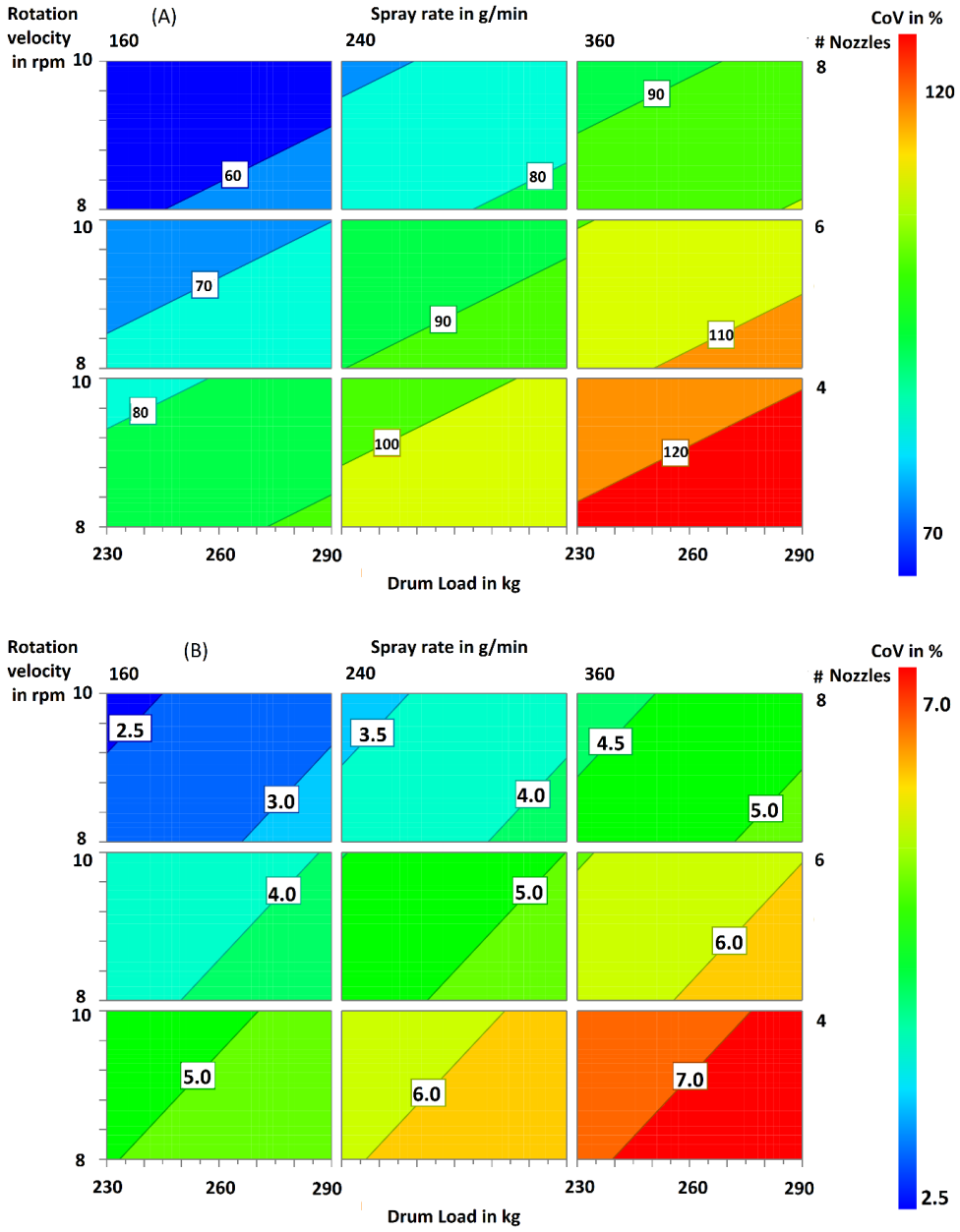

Figure 40: 4D contour plot showing the effect of the four investigated process parameter on the $c_{v,inter,}$ after 90 s (A) and extrapolated for a process time of 300 min (B) (with a spray rate of 240 g/min and adapted for lower/higher spray rates using Eq. 19 with a decay calculated based on the last 30 seconds of the simulation (lower).

D-4.4. Number of sprayed tablets

The number of tablets that visited the spray zones at least once during the simulated 90 seconds of process time is an important indicator of the coater's mixing efficiency and the reliability of the extrapolation with regard to the total coating time. The amount of coated tablets per time is shown in Figure 41. Only the best and worst results for four and eight nozzles are shown. The results for all other cases are between these extreme values.

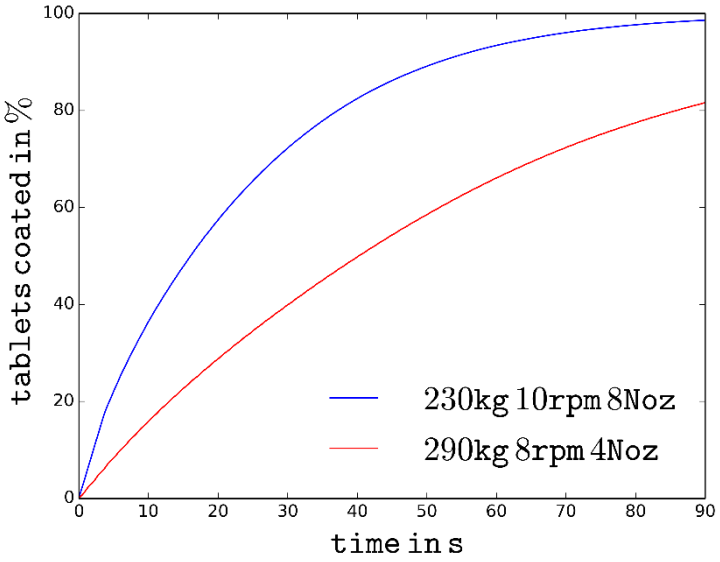

Figure 41: Percentage of tablets that were sprayed at least once. For clarity reasons, only the best and worst cases (see above) are shown.

As expected, the best results are achieved with a load of 230 kg and 10 rpm and 8 nozzles, with 98.6% of the tablets appearing in the spray zone at least once during the simulation. The worst case is the case with 290 kg and 8 rpm and 4 nozzles, with only 81.6% of the tablets visiting the spray zone. The difference is due to the varying number of tablets and rotation rate. Faster rotation rates promote better mixing of the tablet bed, resulting in more tablets coated within a shorter time and reducing the risk of dead zones due to poor mixing. This clearly demonstrates that a low fill level and a high rotation rate leads to relatively more tablets coated within the same time period.

D-4.5. Velocity distribution in the spray zone

The velocity distribution in the spray zone is important for the process performance. A uniform distribution of the velocity in the spray zone results in a uniform spray residence time distribution and a good coating quality due to a homogenous distribution of coating mass per pass. Higher velocities lead to shorter single-visit residence times, better mixing in the spray zone and an increased probability of tablet and coating defects due to abrasion. In contrast, low tablet velocities increase the risk of over-wetting the tablet, which is the main cause for tablets sticking together and other defects.

Figure 42 demonstrates that the velocity distribution is quite similar and rather narrow in all seven cases with different loading and rotation rates. Moreover, the results reflect data from the literature, i.e., that the tablet velocity increases with the increasing drum load and rotation rate. The mean

velocity was between 1.035 m/s for 230 kg and 8 rpm and 1.377 m/s for 290 kg and 10 rpm, being 33% higher.

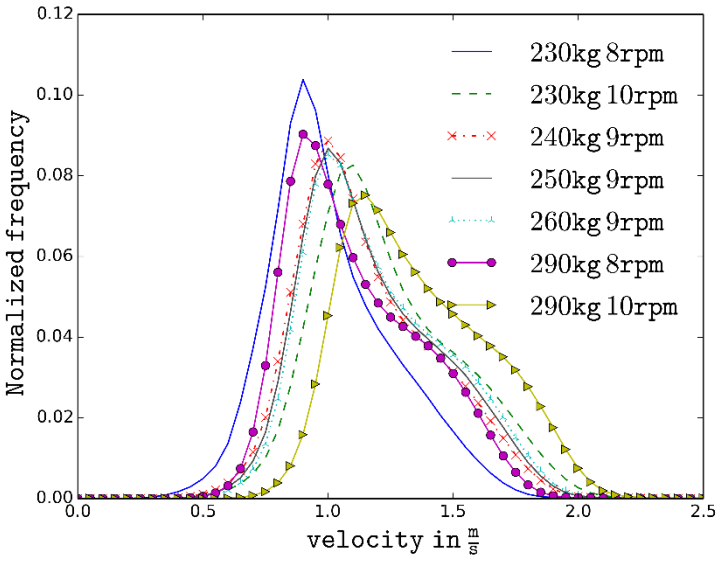

Figure 42: Velocity distribution in the BFC 400 at the various process settings.

D-4.6. Spray residence time

The spray residence time is defined as the time span tablets spend in the spray zones during one coating event. It is directly influenced by the tablets velocity. It affects the process outcome: a narrow distribution in the spray residence time also results in a uniform spray coating since each tablet receives the same amount of coating mass per pass through the spray zone. The spray residence time distribution is shown in Figure 43. In this case, the simulation was performed for an additional 1 second and the storage interval was set to 0.002 seconds, in contrast to the 0.02 seconds during the previous 90 seconds. This was done to capture tablets in the spray zone that would not be captured otherwise.

Due to the similar velocity distributions, the spray residence time distributions are similar in all cases. When the velocity is slower, the tablets spend longer time in the spray zone but the difference is small. Large variations of the rotation rate would potentially lead to more significant changes in the distribution.

The longest mean residence time of around 0.047 seconds was in the case of 290 kg and 8 rpm and shortest one was in the case of 0.036 seconds for 290 kg and 10 rpm With regard to the mean time value, the difference was 25%, which is less than the mean velocity difference of 33%. No tablet was

inside the spray zone for longer than 0.16 seconds, and since the results for six or eight nozzles were the same as for four nozzles, they are not shown.

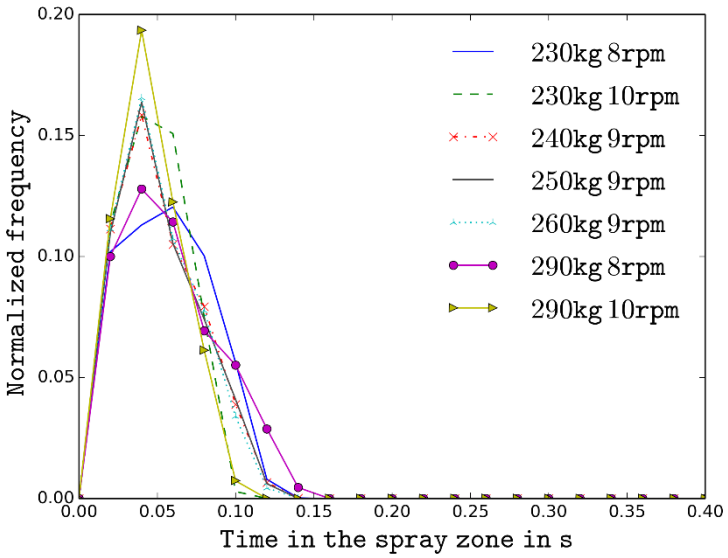

Figure 43: Spray residence time in the BFC 400 for different process settings and a store data interval of 0.002 (four nozzles)

D-4.7. Bed cycle time

Bed cycle time is the time that a tablet spends outside the spray zone between two individual spray events. The normalized distribution of the bed cycle time is shown in Figure 44 and Figure 45 for all loads and rotation rate and 4 spray nozzles. Figure 44 shows a high first peak after approximately 4.5 seconds followed by smaller peaks at regular intervals. Higher rotation rate shifted the peaks to shorter times and vice versa. The decreasing chance of a tablet to reenter the spray zone after one missed cycle can be explained by the way the tablets move inside the drum. When a tablet passes through the spray zone, the re-entry probability is high. When a tablet misses the spray zone, the re-entry probability is only half as high to enter the spray zone. But the time for one cycle is constant (second peak). This is true for all subsequent cycles and can explain why all subsequent peaks are smaller than the first one and approximately only half as high as the previous peak. After a certain amount of cycles the probability that the tablet enter the spray zone again reaches one hundred percent.

If the distribution of the bed cycle time is plotted vs. the number of revolutions the curves for different rotation rates collapse, as shown in Figure 45, which plots bed cycle time as a function of the number of revolutions. The logarithmic y-axis also highlights the period peaks more clearly. Here, the bed cycle time is approximately 2/3 of the time needed for one rotation. This plot also shows that the bed cycle

time is nearly independent of the drum load in the range of parameters studied. This behavior was already shown for smaller coaters in the laboratory scale and is confirmed by Toschkoff et. al. [30].

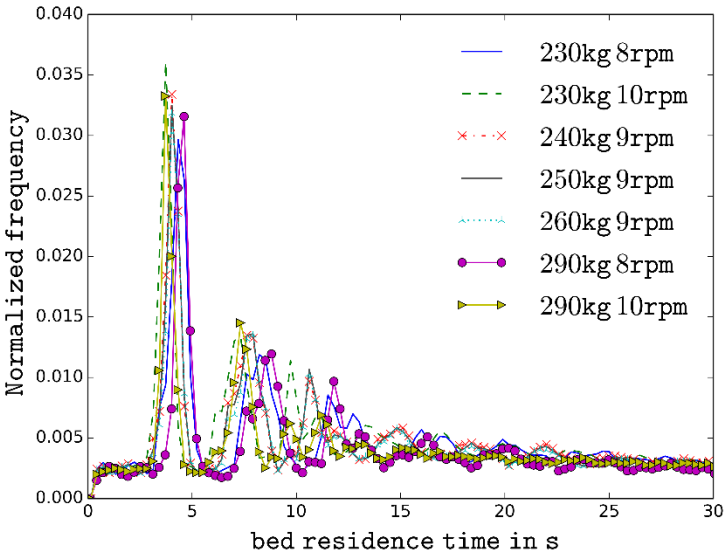

Figure 44: Normalized bed cycle time during thirty seconds of process time.

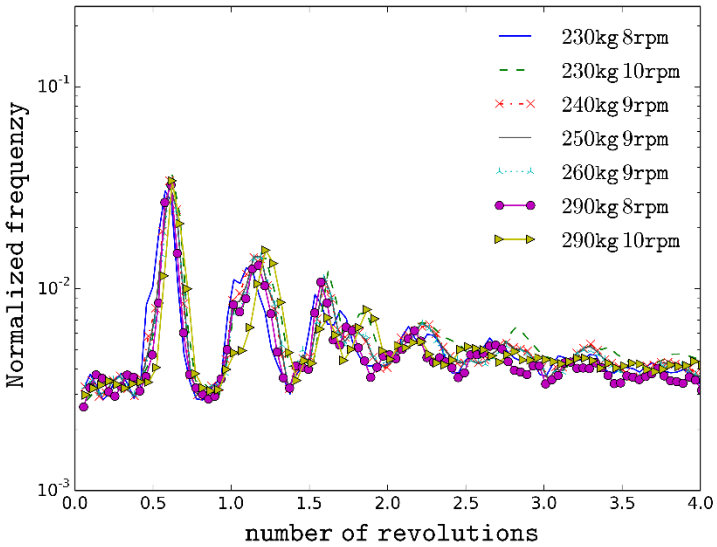

Figure 45: Normalized bed cycle time for the different process settings in the BFC 400 vs. the number of revolutions.

D-5. Summary and Conclusion

The objective of this work was to simulate the tablet coating process in a production-scale drum coater filled with up to 290 kg (1,028,369 tablets) of material using the Discrete Element Method. To that end, a full factorial 2^2+3 Design of Simulation Experiments was executed to investigate the impact of the

various process parameters: the drum load (ranging from 230 kg to 290 kg) and the rotation rate(ranging from 8 to 10 rpm). Moreover, the spray rate and the number of nozzles were varied.

First, the influence of process parameters on the coefficient of inter-tablet variation, $c_{v,inter}$, was investigated. The simulations indicate that the number of nozzles and the spray rate have the highest impact on $c_{v,inter}$, while the drum load and the rotation rate have a much lower impact. The last 30 seconds of the simulation were used to calculate the exponent of the $c_{v,inter}$ decrease as function of time. The calculated exponent in all cases was larger than the value reported in the literature for a randomly mixed process (-0.5), indicating that the coating process is not completely random but is influenced by the optimized mixing in the drum. The number of nozzles also influences the decrease of the $c_{v,inter}$: increasing the number of nozzles increases the exponent, i.e., leading to faster reduction of the $c_{v,inter}$ compared to a purely random process.

The computed exponents were used to predict the $c_{v,inter}$ value for a 300 min process. Experimental results confirmed the computational results. The computed exponents offered a better predictions and resulted in a mean deviation of only 0.51 % between measured and predicted coefficient of variation $c_{v,inter}$. The mean deviation of the fixed exponent (-0.5) was 1.02 %. Thus, it is possible to predict the process outcome accurately based on only 90 seconds of simulation time and with particle parameters obtained from the laboratory experiments.

The data were used in a MVDA to determine the optimal process parameters via a 4d plot. The best strategy was to decrease the drum load and the spray rate and increase the rotation rateand the number of nozzles. The best $c_{v,inter}$ value of 54.7 % after 90 seconds was achieved for a load of 230 kg, a rotation rate of 10 rpm, eight nozzles and a spray rate of 160 g/min. After extrapolation to 300 min, these settings give a $c_{v,inter}$ of 2.73% with the fitted exponent, which is significantly below the 6.25 % required by regulations.

The velocity distribution and the spray residence time varied little for different process settings. The difference between the minimal and maximal values was 33 % and 25 %, respectively. The bed cycle time showed an even smaller difference.

Our study was intended to demonstrate that DEM simulations can be a useful tool for studying large-scale industrial coating process with >1 Mio tablets. Thus, the number of experiments on the industrial scale can be reduced and the influence of various process parameters on the process can be studied *in silico*. Consequently, design, scale-up, transfer and control of coaters can now be done via well-

documented and experimental confirmed computational tools. Moreover, DEM can improve the mechanistic understanding of the tablet coating processes and can help in optimizing the process, i.e., computations can help to determine the shortest process time, to minimize the number of experiments and to significantly reduce the process development costs and process failures, leading to the need to discard a batch. It can be especially advantageous on the production scale, with one batch often containing over 1 million tablets.

D-6. Bibliography

[1] B. D. Rege, J. Gawel, and J. H. Kou, “Identification of critical process variables for coating actives onto tablets via statistically designed experiments,” vol. 237, pp. 87–94, 2002.

[2] D. Suzzi, S. Radl, and J. G. Khinast, “Local analysis of the tablet coating process: Impact of operation conditions on film quality,” *Chem. Eng. Sci.*, vol. 65, no. 21, pp. 5699–5715, Nov. 2010.

[3] S. Tobiska and P. Kleinebudde, “Coating uniformity and coating efficiency in a Bohle Lab-Coater using oval tablets,” *Eur. J. Pharm. Biopharm.*, vol. 56, pp. 3–9, 2003.

[4] R. Mueller and P. Kleinebudde, “Prediction of tablet velocity in pan coaters for scale-up,” *Powder Technol.*, vol. 173, no. 1, pp. 51–58, Apr. 2007.

[5] R. Turton and X. X. Cheng, “The scale-up of spray coating processes for granular solids and tablets,” *Powder Technol.*, vol. 150, no. 2, pp. 78–85, Feb. 2005.

[6] S. Just, G. Toschkoff, A. Funke, D. Djuric, J. G. Khinast, K. Knop, and P. Kleinebudde, “Optimization of Inter-Tablet Coating Uniformity for an Active Coating Process at the Lab and Pilot Scale,” *Int. J. Pharm.*, vol. 30, no. 11, 2013.

[7] D. M. Koller, G. Hannesschläger, M. Leitner, and J. G. Khinast, “Non-destructive analysis of tablet coatings with optical coherence tomography.,” *Eur. J. Pharm. Sci.*, vol. 44, no. 1–2, pp. 142–8, Sep. 2011.

[8] W. Chen, S.-Y. Chang, S. Kiang, A. Marchut, O. Lyngberg, J. Wang, V. Rao, D. Desai, H. Stamato, and W. Early, “Modeling of pan coating processes: Prediction of tablet content uniformity and determination of critical process parameters,” *J. Pharm. Sci.*, vol. 99, pp. 3213–3225, 2010.

[9] C. P. A. and O. D. L. Strack, “A discrete numerical model for granular assemblies,” *Géotechnique*, vol. 29, no. 1, pp. 47–65, Jan. 1979.

[10] K. Yamane, T. Sato, T. Tanaka, and Y. Tsuji, “Computer Simulation of Tablet Motion in Coating Drum,” *Pharm. Res.*, vol. 12, no. 9, pp. 1264–1268, 1995.

[11] W. R. Ketterhagen, M. T. am Ende, and B. C. Hancock, “Process modeling in the pharmaceutical industry using the discrete element method,” *J. Pharm. Sci.*, vol. 98, pp. 442–470, 2009.

[12] G. Toschkoff, S. Just, K. Knop, P. Kleinebudde, A. Funke, D. Djuric, G. Scharrer, and J. G. Khinast, “Modeling of an Active Tablet Coating Process,” *J. Pharm. Sci.*, p. n/a–n/a, Sep. 2015.

[13] D. Suzzi, G. Toschkoff, S. Radl, D. Machold, S. D. Fraser, B. J. Glasser, and J. G. Khinast, “DEM simulation of continuous tablet coating: Effects of tablet shape and fill level on inter-tablet coating variability,” *Chem. Eng. Sci.*, vol. 69, no. 1, pp. 107–121, 2012.

[14] W. R. Ketterhagen, “Modeling the motion and orientation of various pharmaceutical tablet shapes in a film coating pan using DEM.,” *Int. J. Pharm.*, vol. 409, no. 1–2, pp. 137–49, May 2011.

[15] W. R. Ketterhagen, R. Bharadwaj, and B. C. Hancock, “The coefficient of rolling resistance (CoRR) of some pharmaceutical tablets,” *Int. J. Pharm.*, vol. 392, no. 1–2, pp. 107–110, 2010.

[16] A. O. Favier, J.F., Abbaspour Fard M.H. , Kremmer, M. and Raji, “Shape representation of axi-symmetrical, non-spherical particles in discrete element simulation using multi element model particles,” *Eng. Comput.*, vol. 16, no. 4, pp. 467–480, 1999.

[17] G. Toschkoff and J. G. Khinast, “Mathematical modeling of the coating process.,” *Int J Pharm*, Aug. 2013.

[18] G. Toschkoff, D. Suzzi, W. Tritthart, F. Reiter, M. Schlingmann, and J. G. Khinast, “Detailed Analysis of Air Flow and Spray Loss in a Pharmaceutical Coating Process,” *Aiche J.*, vol. 58, pp. 399–411, 2012.

[19] C. a. Radeke, B. J. Glasser, and J. G. Khinast, “Large-scale powder mixer simulations using massively parallel GPUarchitectures,” *Chem. Eng. Sci.*, vol. 65, no. 24, pp. 6435–6442, Dec. 2010.

[20] D. Jajcevic, E. Siegmann, C. Radeke, and J. G. Khinast, “Large-scale CFD–DEM simulations of fluidized granular systems,” *Chem. Eng. Sci.*, vol. 98, pp. 298–310, Jul. 2013.

[21] R. Y. Yang, a. B. Yu, L. McElroy, and J. Bao, “Numerical simulation of particle dynamics in different flow regimes in a rotating drum,” *Powder Technol.*, vol. 188, no. 2, pp. 170–177, Dec. 2008.

[22] S. Just, G. Toschkoff, A. Funke, D. Djuric, G. Scharrer, J. G. Khinast, K. Knop, and P. Kleinebudde, "Experimental Analysis of Tablet Properties for Discrete Element Modeling of an Active Coating Process," *AAPS PharmSciTech*, vol. 14, no. 1, pp. 402–411, 2013.

[23] G. Toschkoff, S. Just, A. Funke, D. Djuric, K. Knop, P. Kleinebudde, G. Scharrer, and J. G. Khinast, "Spray Models for Discrete Element Simulations of Particle Coating Processes," *Submitt. to Chem. Eng. Sci.*, 2013.

[24] E. Pharmacopoeia, "Technical Guide," 2011.

[25] A. Kalbag and C. Wassgren, "Inter-tablet coating variability: Tablet residence time variability," *Chem. Eng. Sci.*, vol. 64, no. 11, pp. 2705–2717, 2009.

[26] B. Kandela, U. Sheorey, A. Banerjee, and J. Bellare, "Study of tablet-coating parameters for a pan coater through video imaging and Monte Carlo simulation," *Powder Technol.*, vol. 204, pp. 103–112, 2010.

[27] P. Pandey, Y. Song, F. Kayihan, and R. Turton, "Simulation of particle movement in a pan coating device using discrete element modeling and its comparison with video-imaging experiments," *Powder Technol.*, vol. 161, no. 2, pp. 79–88, 2006.

[28] D. Shi and J. J. McCarthy, "Numerical simulation of liquid transfer between particles," *Powder Technol.*, vol. 184, no. 1, pp. 64–75, May 2008.

[29] A. Dubey, R. Hsia, K. Saranteas, D. Brone, T. Misra, and F. J. Muzzio, "Effect of speed, loading and spray pattern on coating variability in a pan coater," *Chem Eng Sci*, vol. 66, no. 21, pp. 5107–5115, Nov. 2011.

[30] G. Toschkoff, S. Just, K. Knop, P. Kleinebudde, A. Funke, A. Altmeyer, D. Djuric, and G. Scharrer, "Design-of-Experiment based DEM simulation of an active tablet coating process ."

[31] A. Kalbag, C. Wassgren, S. Sumana Penumetcha, and J. D. Pérez-Ramos, "Inter-tablet coating variability: Residence times in a horizontal pan coater," *Chem. Eng. Sci.*, vol. 63, no. 11, pp. 2881–2894, Jun. 2008.

E. Computational Fluid Dynamics-Discrete Element Method Modeling of an Industrial-Scale Wurster Coater

Published as: . Böhling *et al.*, "Computational Fluid Dynamics-Discrete Element Method Modeling of an Industrial-Scale Wurster Coater," *J. Pharm. Sci.*, vol. 108, pp. 538–550, 2018.

E-1. Abstract

Large-scale fluid-bed coating operations using Wurster coaters are common in the pharmaceutical industry. Experimental measurements of the coating thickness are usually analyzed for just few particles. To better predict the coating uniformity of the entire batch, computational techniques can be applied for process understanding of the key process parameters that influence the quality attributes. Recent advances in computational hardware, such as graphics card (GPU), has enabled simulations of large industrial-scale systems. In this work, we perform coupled CFD-DEM simulations of a large-scale coater that model the actual particle sizes. The influence of process parameters, the inlet-air flow rate, atomizing-air flow rate, bead-size distribution, and Wurster-gap height, are studied. The focus of this study is to characterize the flow inside the coater; eventually, this information will be used to predict the coating uniformity of the beads. We report the residence time distribution of the beads inside the Wurster column, i.e., the active coating zone, which serves as a proxy for the amount of coating received by the beads per pass. The residence time provides qualitative and quantitative measurements of the particles-coating uniformity. We find that inlet air-flow rate has the largest impact on the flow behavior and, hence, the coating uniformity.

E-2. Introduction

Fluid-bed coating is widely used in the food, chemical, and pharmaceutical industry to apply one or more coating layers onto smaller particles (e.g., mini-tablets, pellets, agglomerated granules, etc.)—these coatings can be aesthetic or functional. The latter may be required, for example, to protect from environmental influences, modify the release behavior, add an active drug coating, or for taste-masking. Several types of fluidized bed coaters exist, which are differentiated by the way the coating solution (or suspension) and fluidization air are introduced. The main classes are the top-, bottom- and side-spray fluidized-bed coaters [1]. The Wurster coater is a special type of bottom-spray fluidized bed coaters [2], in which a riser tube is placed in the middle of the coater geometry to channel the air flow ('chimney effect') to provide a more uniform exposure of particles to the spray, leading to a more uniform coating.

Experiments involving Wurster coaters have mostly been conducted at the laboratory-scale [1], thereby providing insights into the minimal fluidization air velocity of particles and fluidization behavior. For example, positron emission particle tracking (PEPT)[3] [4] can be used to follow individual particles through a Wurster coating process. Using PEPT, the residence time distribution (RTD) in different region of the coater [5][6][7] can be mapped as a function of the operating parameters. However, it is difficult to extract meaningful data from experiments on larger scales, since it is prohibitively expensive to set up PEPT measurements at industrial scales. In-depth experimental investigations of industrial-scale coaters with hundreds of millions of particles are therefore rare; often, experiments at larger scales are conducted to perform a pass/fail assessment of process settings without a thorough analysis of operating ranges.

In contrast, computer simulations may be used to understand complex coating processes in greater detail, including tracking the movement of every particle in the fluidized bed. For modeling a fluid bed, the air flow has to be modeled in conjunction with particle trajectories. Particle-particle interactions (collisions) become especially important for dense-phase systems. Computer simulations based on computational fluid dynamics (CFD) coupled with the discrete element method (DEM) is an appropriate technique to model fluidized beds; the CFD portion is used to model air flow while the DEM tracks particle trajectories and collisions. An overview of CFD-DEM simulation for fluidized bed systems was reported by Deen [8].

In CFD, the simulation volume is resolved in finite volumes (cells) and the Navier-Stokes equations describing the fluid flow are solved for each cell. All variables are considered to be locally volume-averaged quantities over the cell control volume V, which has to be at least one order of magnitude larger than the particle volume V_p[9]. DEM was developed to simulate the behavior of granular (particulate) materials [10]. Initially, DEM was limited to a few hundreds to a few thousand particles, but eventually simulations of laboratory-scale devices became possible [11][12]–[14], [15]. Simple two-dimensional geometries were considered in coupled simulations [16]–[18]. New algorithms have allowed the simulation of increasingly complex systems, including physical property changes of particles during coating [19]–[21] and heating of particles in a fluid [22], [23]. Moreover, advances in the computational speed and the development of better algorithms enabled the simulation of many millions [24], [25] of particles in industrial-scale devices [26], [27] using a graphics processing unit (GPU) ([28] [29]). Moreover, non-spherical particle models are becoming increasingly versatile [30][31]. These studies provide a better understanding of particle dynamics, since each individual collision can be

calculated and investigated separately. This even makes it possible to model particle breakage or similar effects [32]. Experimental validation of DEM simulation results continues to be an area of research [33].

In the present work, the commercial DEM code XPS (eXtended Particle Systems) is coupled with CFD code AVL-Fire® to simulate an industrial-scale Wurster coater process (Glatt GPCG 15/30). The DEM portion of the simulation is executed on the GPU and the CFD portion runs on the central processing unit (CPU) [34]. Due to the efficient coupling algorithm, a coupled simulation containing millions of particles can be executed on a relatively inexpensive, local workstation, allowing rapid testing of various process settings[26], [27].

In previous investigation, XPS was validated for single, double, and triple pseudo-2D fluidized system [34]. Because wall effects are less pronounced in real 3-D applications (such as Wurster coaters) compared to pseudo-2D beds, we performed an additional validation of the CFD-DEM method using a 3-D system. The test data for validation was obtained from a lab-scale Wurster coater study published by Li et al. [15], where particle residence times in different zones, particle velocity profiles, and particle cycle times were reported from PEPT experiments.

The primary goal of this work was to provide insights into the performance of an industrial-size Glatt GPCG 15/30 Wurster coater, operating with a batch size of 40 kg, as a function of different processing conditions. The coating process contains approximately 200 million particles. However, our GPU-based DEM code can currently model up to 20 million of particles. Therefore, in this work, we exploited the azimuthal symmetry of the Wurster geometry to our advantage to successfully simulate a smaller, 3-D sector (pie-slice) of the full unit.

Altogether, four process parameters were varied: the fluidization air flow rate, the atomization air flow rate, the Wurster gap height and the particle size distribution. Variations in the particle size distribution were intended to reflect the difference between the various coating stages. The first three parameters were studied to elucidate their influence on the single-visit spray-zone RTD and the cycle time distributions (CTD). Moreover, aspects of the flow profile, such as the transverse velocity profile, the mass of beads inside the Wurster tube, and the mass flow through the Wurster tube were compared for various process settings.

E-3. CFD-DEM Method

The CFD-DEM computational approach treats the fluid flow (gas phase) as a continuum (Eulerian approach) and models every particle (solid phase) as a discrete element (Lagrangian approach). In DEM,

the motion of discrete particles is tracked by solving Newton's second law of motion. Since particle-particle and particle-wall collisions occur frequently in Wurster coaters, describing these interactions is critical for predicting the particle-bed dynamics. For scalability and accuracy reasons [8], [34], the soft-sphere method was used in this work.

For the motion of each particle, a linear force balance is solved,

$$m_p \frac{d\mathbf{v_p}}{dt} = -V_i \nabla \mathrm{p} + \beta\left(\mathbf{v}_\mathrm{f} - \mathbf{v}_\mathrm{p}\right) + \sum_0^{N_P} \mathbf{F}_{P\to P} + \sum_0^{N_W} \mathbf{F}_{P\to W} + m_p \mathbf{g} \tag{22}$$

where m_p is the particle mass, $\mathbf{v}_\mathrm{p}$ is the particle velocity, $\mathbf{v}_\mathrm{f}$ is the gas velocity, $-V_i \nabla p$ is the pressure gradient force, β is the inter-phase momentum transfer coefficient, $\mathbf{F}_{\mathrm{P->P}}$ is the particle-particle force and $\mathbf{F}_{\mathrm{P->W}}$ is the particle-wall force. The three-dimensional angular momentum of the particle is calculated as

$$\mathbf{I}_p \frac{d\boldsymbol{\omega}_\mathrm{p}}{dt} = \sum_0^{N_P} \mathbf{M}_P \tag{23}$$

where $\boldsymbol{\omega}_\mathrm{p}$ is the angular velocity, $\mathbf{M}_\mathrm{P}$ is the torque and $\mathbf{I}_\mathrm{p}$ is the moment of inertia. The detailed DEM algorithm can be found in [28].

Coupling between the air and particles, i.e., the CFD and DEM, occurs via the interphase fluid-particle drag model. In the literature, several drag force models are reported [35],[29],[36]. All of them describe the inter-phase momentum transfer coefficient as a function of particle volume fraction ε_p, gas volume fraction ε_g, particle Reynolds number Re_p, particle diameter d_p and particle density ρ_p. In our work, the model proposed by Gidaspow [35] is used, which combines the Ergun [37] equation for dense regimes and a correlation for more dilute regimes proposed by Wen and Yu [38]. Detailed information about the used coupling mechanism can be found in Jajcevic et al. [34].

The gas phase was modeled by solving the volume-averaged Navier-Stokes equations. All variables are considered to be locally volume-averaged quantities over the cell control volume V, which was chosen to be at least one order of magnitude larger than the particle volume V_P [34]. The conservation of mass can be written as follows:

$$\frac{\partial}{\partial t}\left(\varepsilon_f \cdot \rho_f\right) + \nabla \cdot \left(\varepsilon_f \cdot \rho_f \cdot \mathbf{v}_\mathrm{f}\right) = 0 \tag{24}$$

where ρ_f is the fluid density, ε_f is the local volume fraction of the fluid, $\mathbf{v}_\mathrm{f}$ is the fluid velocity vector and t is the time. Similarly, the conservation of the momentum is

$$\frac{\partial}{\partial t}\left(\varepsilon_f \cdot \rho_f \cdot \mathbf{v}_\mathrm{f}\right) + \nabla\left(\varepsilon_f \cdot \rho_f \cdot \mathbf{v}_\mathrm{f} \cdot \mathbf{v}_\mathrm{f}\right) = -\varepsilon_f \cdot \nabla \mathrm{p} - \nabla \cdot \left(\varepsilon_f \cdot \boldsymbol{\tau}_f\right) + \varepsilon_f \cdot \rho_f \cdot \mathbf{g} - \mathbf{S}_M \quad (25)$$

Here p is the hydrodynamic pressure, τ_f is the stress tensor, g is the gravitational acceleration and $\mathbf{S}_M$ is the inter-phase momentum transfer between particles and fluid. The stress tensor is defined as

$$\boldsymbol{\tau} = -p \cdot \mathbf{I} + \sigma \quad (26)$$

I is the unit matrix and **σ** is the viscous stress tensor,

$$\sigma = \mu_f \cdot \left(\nabla \mathbf{v}_f + \nabla \mathbf{v}_f^{\tau}\right) - \frac{2}{3} \cdot \mu_f \cdot \nabla \cdot \mathbf{v}_f \cdot \mathbf{I} \quad (27)$$

with μ_f being the dynamic viscosity. The turbulence was modeled using standard k-zeta-f turbulence model in the steady state as well as coupled simulation.

E-4. Validation of particle flow and verification of "pie-slice" approach for a large scale Wurster coater simulation

Our CFD-DEM coupling method for momentum exchange between the gas and solid phase has already been validated for single-, double-, and triple-spouted pseudo-2D beds by Jajcevic et al. [34]. The simulation results were in good agreement with the measurement and simulation data of Van Buijtenen et al. [39] . In a pseudo-2D spouted bed, the distances between the front and back walls are typically equal to a few particle diameters (i.e., 5 times the particle diameter), causing significant wall effects that damp particle-velocity fluctuations and dominate the flow dynamics of the system. Since in real applications, such as in Wurster coaters, wall effects are clearly less pronounced than that in pseudo-2D beds (the volume to surface-area ratio is much larger for 3-D fluidized beds), we performed an additional validation of the CFD-DEM coupling method to reconfirm the modeling method's validity. The test case for the validation was a lab-scale Wurster coater described by Li et al. [7]. The authors experimentally estimated the residence time, cycle time, and time-averaged vertical particle velocities via PEPT. In a follow-up study, they utilized their previously-generated experimental data to validate new CFD-DEM simulations and demonstrated that predictions were in good agreement with the experiments. In the present work, our CFD-DEM code was used to model the lab-scale fluidized bed described by Li et al. with identical simulation input parameters and process settings.

The domain of the Wurster coater was divided into four different zones (Figure 1), in which the residence times were evaluated. Li et al. [15] report the time-averaged particle velocity at a distance of 90 mm from the bottom plate and the cycle time distribution.

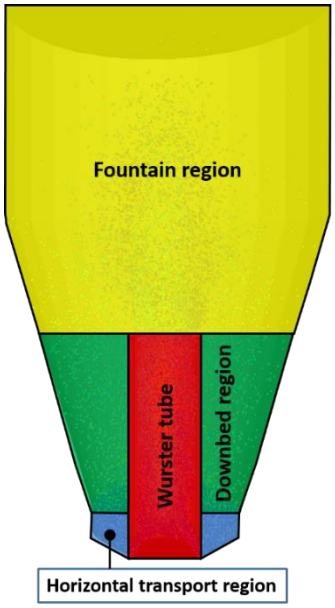

Figure 46: Wurster coater zones according to Li et al. [6] and [13].

Particle flows inside a Wurster coater can be characterized as primarily axial; flow in circumferential direction is less prominent. Thus, “pie-slice” simulations (where only a slice is simulated) may be performed without any significant loss of accuracy. This reduces the amount of particles that need to be considered and accelerates the simulations. In our work the full system (360°) and a 90° “pie-slice” segment (quarter) were considered. In the model, two vertical walls are defined as symmetry planes and the number of particles and the inlet air flow rate (including atomization air flow rate) are reduced by a factor of 4.

Figure 47 shows the time-averaged vertical particle velocity at a height of 90 mm above the air distributor plate; comparisons are shown between the PEPT measurements from Li et al. [7], the reference CFD-DEM simulation data from Li et al. [15], and our present CFD-DEM simulation predictions. For both Li et al. [13] and our present case, the simulations over-predict the particle velocity close to the Wurster tube axis (in the radial zone spanning from 0 mm to about 10 mm from the central axis). Nevertheless, our results show better agreement with the PEPT measurements compared to Li et al. [13]. Inside the Wurster tube and close to the cylinder wall, both simulations predict negative vertical particle velocity, identifying recirculation close to the Wurster tube wall. Outside of the Wurster tube, the results of our simulations and the PEPT data are very similar. Comparing the full and the quarter models, it can be seen that both simulations predict almost identical particle velocities.

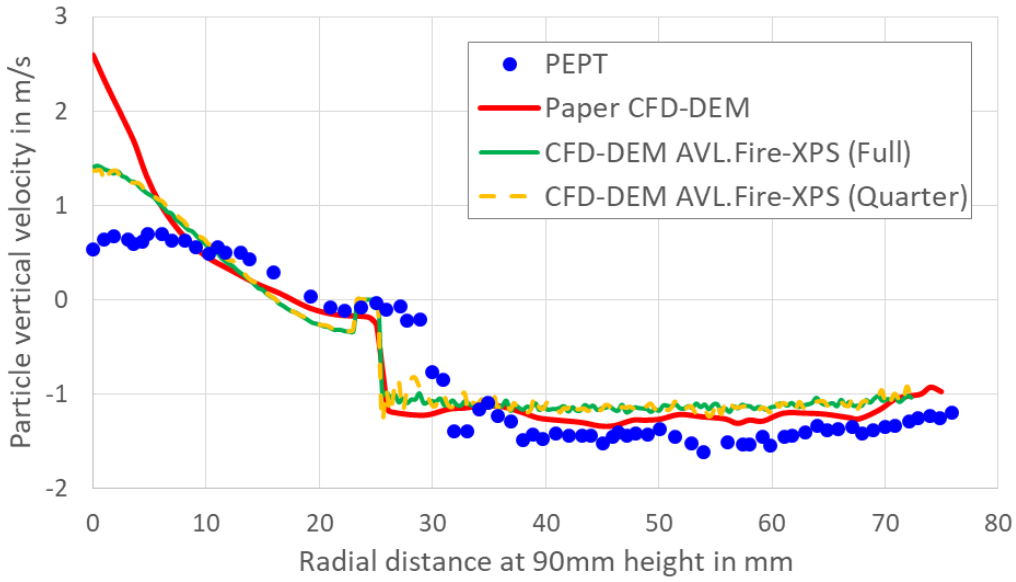

Figure 47: Time-averaged particle velocity at 90mm from the bottom plate. Comparison between experimental data, reference simulation results and obtained results during this project.

Figure 3 shows the time-averaged residence time inside the four Wurster zones. Inside the Wurster tube and the fountain zones, the results of both our simulations (full and quarter models) are very close to the PEPT measurements and reference simulation data from Li et al. [13]. Nevertheless, in the horizontal region, the reference CFD-DEM data of Li et al. [13] and our results somewhat under-predict the experimental residence time. Again, when comparing full and the quarter models, very minor differences between the full and the quarter models can be seen. Within the Wurster tube, the quarter model over-predicts particle residence time by 0.18 seconds in comparison to full-model results. In the horizontal transport region, the residence time is under-predicted by 0.16 seconds. Notwithstanding, these differences are small.

Figure 4 shows the cycle time distribution and a comparison between our results and both reference data sets from Li et al. Our results slightly under-predict the percentage of the particles with a cycle time longer than 5 seconds and over-predict the percentage of particles with a cycle time shorter than 5 seconds. Since our simulation results are very close to the reference data, it can be concluded that our CFD-DEM approaches (both full and quarter models) can predict particle dynamics in the Wurster coater with the desired level of accuracy. Henceforth, the pie-slice model can be used for the large-scale simulations because the deviation compared to the full model is small.

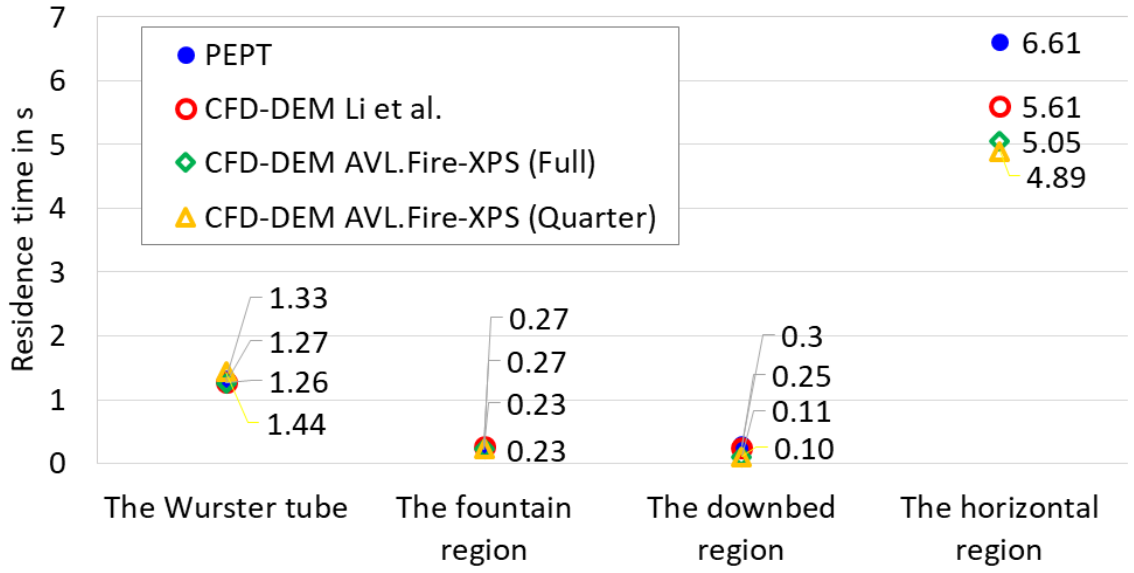

Figure 48: Time-averaged residence time in the various Wurster coater zones. Comparison between experimental data, reference simulation results and obtained results during this project.

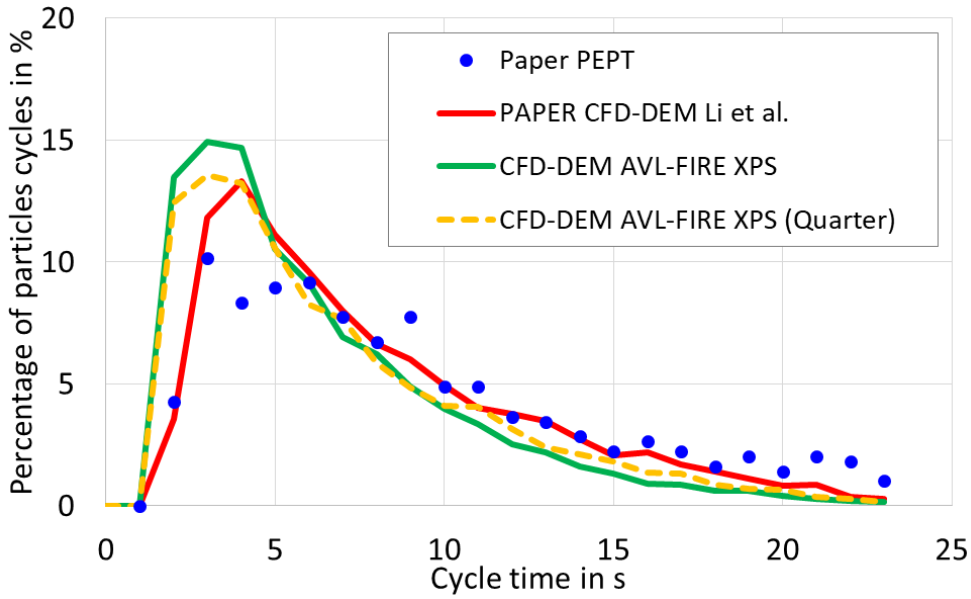

Figure 49: Cycle time distribution. Comparison between experimental data, reference simulation results and obtained results during this project.

E-5. Glatt 15/30 Wurster coater: Materials and process conditions

A schematic snapshot of the Glatt-15/30 Wurster coater is shown in Fig. 5a. The height of the unit, measured from the distributor plate (air inlet) to the top filters is approximately 1.9 m. The height is comprised of two main sections: a lower conical portion and an upper, cylindrical expansion chamber

leading up to the air outlet. The Wurster-column insert has a height of 0.6 m and a diameter of approximately 0.2 m. The spray nozzle is situated at the center of the bottom distributor plate, and is surrounded by a short collar. The distributor plate contains a series of holes of varying diameters that help divert the airflow as desired (Fig. 5b). Holes in the central core region are larger than those in the outer annular region, resulting in a greater inlet air velocity at the center under the Wurster tube.

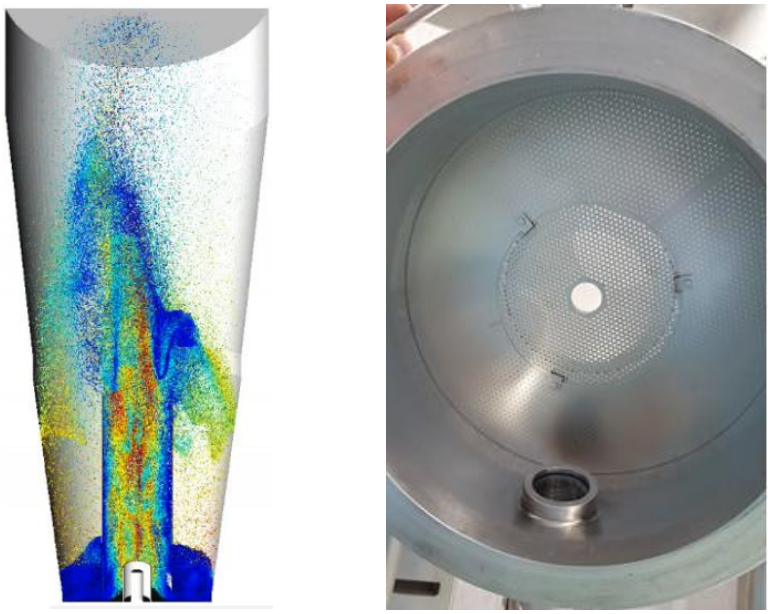

(a) (b)

Figure 50: A schematic snapshot of the Glatt-15/30 Wurster coater (a) and distributor plate (b).

The bead cores to be coated are composed of microcrystalline cellulose (MCC). The particle-size distribution of the beads (PSD) was determine experimentally using a shape analyzer (Sympatec QicPic). These experimentally-measured PSDs, shown in Figure 51, were used as direct inputs to the CFD-DEM simulations. The density was measured using gas pycnometry (AccuPyc II 1340 Pycnometer) and also used as an input to the simulations. In Figure 51, three different particle size distributions are shown, corresponding to uncoated particles (blue: PSD 0), PSD after the first coating stage (green: PSD 1), and after the second and final coating stage (red: PSD 2).

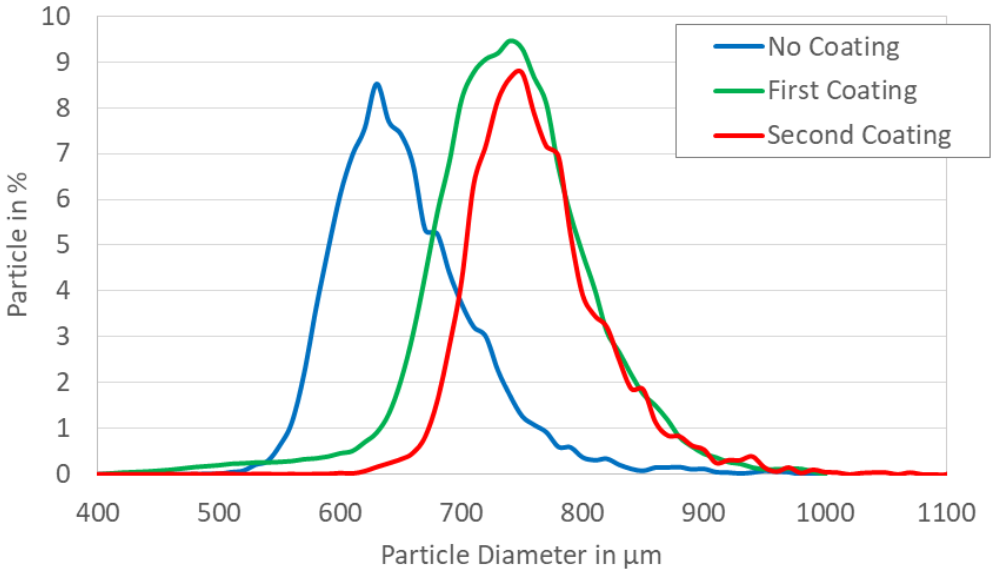

Figure 51: QicPic analysis of the particle size distribution of the three coating stages.

The particle properties used in the CFD-DEM simulations are summarized in Table 16. The friction coefficients are taken from the values reported by Li et al. [2] for MCC particles. The coefficient of restitution and static friction was taken from the literature, viz., Li et al. [15]. The spring constant for the spring dashpot model was chosen to allow a relatively large time step, while keeping the simulation computational stable. This is an adequate particle-particle force model as these beads are not cohesive and particle collision events are secondary to the air-driven fluidization behavior [19]. Density and viscosity of air was taken from standard engineering reference tables.

Table 16: Particle parameters used in the CFD-DEM simulation

Particle properties	
Spring constant	1000 N/m
Density (PSD 0, PSD 1, PSD 2)	1497 kg/m^3, 1420 kg/m^3, 1386 kg/m^3
Mean particle sauter diameter (PSD0, PSD1, PSD2)	639.97 µm, 719.86 µm, 749.74 µm
Standard deviation of particle diameter	49.2 µm 56.8 µm, 60.2 µm
Interaction Particle – Wall	
Coefficient of Restitution	0.83
Static friction coefficient	0.53
Rolling friction coefficient	0.01
Interaction Particle – Particle	
Coefficient of Restitution	0.80
Static friction coefficient	0.33
Rolling friction coefficient	0.01
Simulation	
DEM Time step length	$1 \cdot 10^{-5}$ s
CFD	
CFD time step length	$1 \cdot 10^{-3}$ s
Air Density	1.204 kg/m³
Air Viscosity	18.37 µPas

To recap, in this study, we varied four parameters which we believe influences the coating process: atomization air-flow rate, fluidization air-flow rate, Wurster=gap height, and particle size distribution.

These parameters are marked in Figure 52. The ranges of the various process parameters are shown in Table 17. The case with a batch load of 40 kg, fluidization air-flow rate of 850 m^3/h, atomization air-flow rate of 45 m^3/h, Wurster gap height of 30 mm, PSD corresponding to those for uncoated particles (PSD 0) was chosen as the base case (reference case). The baseline values are denoted by blue-colored font in Table 2. In total, 10 simulations were performed as part of our parametric investigation.

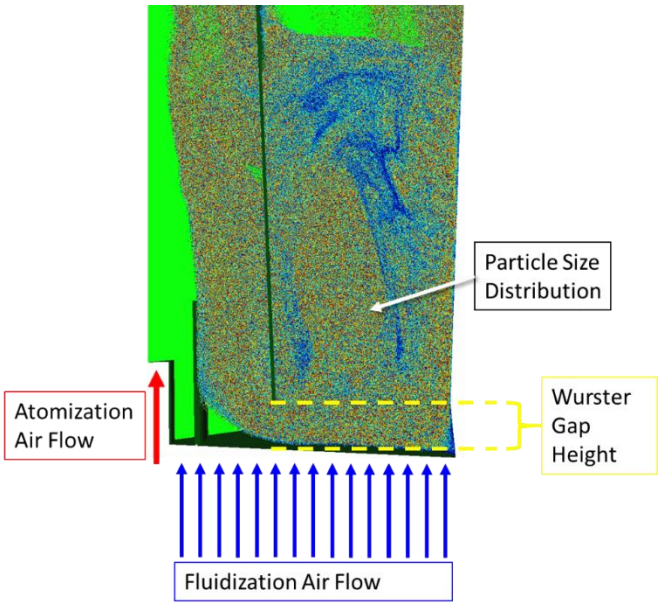

Figure 52: Process parameters considered in the parameter study.

Table 17: Parameters varied in the simulations (the base case simulation is marked blue)

Air flow (Gap: 30mm, Atomization rate: 45m^3/h)	**700 m^3/h**	**850m^3/h**	**1100m^3/h**	
Atomization air rate (Air flow rate: 850m^3/h, Gap 30mm)	**45m^3/h**	**52m^3/h**	**61m^3/h**	
Wurster gap height (Air flow rate: 850m^3/h, Atomization rate: 45m^3/h)	**20mm**	**30mm**	**40mm**	**50mm**
PSD and particle density (Air flow rate: 850m^3/h, Gap: 30mm, Atomization rate: 45m^3/h)	**PSD 0** **1497 kg/m^3**	**PSD 1** **1411 kg/m^3**	**PSD 2** **1386 kg/m^3**	

The results of interest from our CFD-DEM simulations, as these quantities strongly influence the coating variability, are the single-visit residence time distribution (RTD) in the spray zone and the cycle time

distribution (CTD). The single-visit residence time is defined as the time a particles spends in the Wurster tube. The cycle time is the time a particle spends between two distinct visits to the Wurster region. Other flow properties that are measured and reported are the mass of particles in the Wurster tube (i.e., the number of particles that receive coating at any given instant) and the mass-flow rate through the Wurster tube.

E-6. Results

E-6.1. Estimation of air-flow distribution through the distributor plate

As shown in Figure 50b, the distributor plate includes a large number of small holes. To include these details in the full-scale CFD-DEM model would result in a very large number of computational cells and, as a consequence, very long computational times. However, the distributor plate is may be simplified as a series of annular mass-flow-inlet boundary conditions. However, the inlet air mass-flow distribution through each annular region is not known. To determine the air flow distribution through the core and outer annular regions, a highly-resolved, steady-state CFD-only simulation of the perforated distributor plate was executed wherein all holes in the plate were explicitly resolved. The particles inside the Wurster coater were simulated as a static porous zone. The solid void fraction was set to 0.6 in the particle bed and 0.1 inside the Wurster tube. The values for the solid fraction in the particle bed and Wurster tube were later checked against the coupled CFD–DEM simulations and found to be roughly comparable. The steady state mesh had about 9 million computational cells when modeling a 90° segment (Fig. 9).

Figure 53 shows the velocity distribution for the base-case, air-flow rate of 850 m^3/h. The velocity is the largest close to the center of the Wurster coater; the air flow is diverted to this central regions not only due to the larger holes available, but also due to the lower permeability through the densely-packed particle bed above the outer annular region.

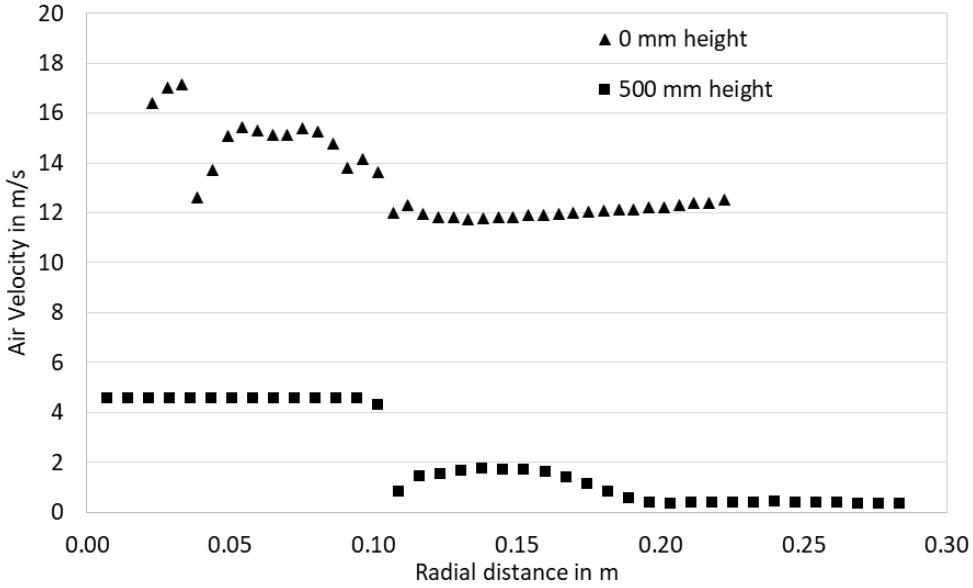

Figure 53: Air flow velocity at 0mm and 500mm height from the bottom plate. Steady-state simulation including resolved plate.

The distribution of the air flow among the various distributor-plate regions is shown in Figure 54. The values are: 51% in the central core region, 36% in the outer annular region of the distributor plate, and 13% in narrow zone in between. Although the air flow distribution may change with the net air-flow rate, any such changes were assumed to be negligible and the same distribution was used in all cases.

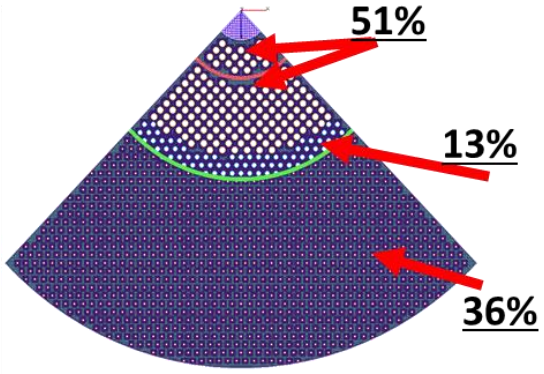

Figure 54: Mass flow distribution on the distributor plate in the steady-state simulation (fluidization air flow rate of 850 m^3/h).

For the coupled CFD-DEM simulations, a mesh with about 90,000 CFD cells was created. The inlet region was divided into 4 area regions: a jet region, core region (with 51% air flow), outer annular region (36% air flow), and the narrow in-between region (13% air flow). Each region was prescribed its own inlet air velocity, computed from the previously-described steady-state CFD simulations. The area includes a thin layer of cells which is representing the distributor plate. To account for the volume excluded by

the solid portions (steel) of the distributor plates, a thin layer of cells was defined with appropriate porosity. Using this strategy, it is possible to replace the distributor plate and to closely match both the mass-flow rate and inlet velocity with those in an actual system.

E-6.2. Time-Averaged Particle Velocity at 500 mm Height

Now that the inlet airflow distribution has been estimated all the simulation conditions described in Table 2 can be executed. The time-averaged radial particle velocity profile was evaluated at a height of 500 mm above the distributor plate. This location was chosen because it is a location above the free surface of the particle bed, yet still below the upper rim of the Wurster tube. Figure 55 shows the results of (a) three different fluidization air flow rates, (b) three atomization air flow rates, (c) four Wurster gap heights and (d) finally three different particle size distributions (which represent different coating stages). The vertical solid black line in all four graphs marks the radial location of the Wurster-tube wall. The first number in the legend description represents air flow rate in m^3/h, the second one the atomization air flow rate in m^3/h, the third one the particle size distribution (see Figure 51), and the last one the Wurster gap height in mm.

It can be seen that the particle velocity inside the Wurster tube increases with increasing fluidization air flow rate (Figure 55 (a)). Near the center line of the Wurster tube, the particle velocity is not significantly affected by an increasing fluidization air flow rate. This is probably due to the central spray nozzle position and the fact that the atomization air-flow rate is not changed for the three runs reported in Fig. 10a. However, in the regions farther away from the spray nozzle, the vertical particle velocities are larger as the fluidization air-flow rate increases.

Increasing the atomization air flow rate slightly increases the particle velocity along the Wurster coater axis, (Figure 55 (b)). This effect is, however, small compared to the other parameters examined and the region of influence is small—realize that radial distances near the center constitute a smaller volume. As we near the inner wall of the Wurster-tube, the particle velocities are unaffected by an increase in the atomization air flow.

The influence of the Wurster-gap height (Fig. 10c) is more complex since the particle velocity in the center increases with increasing Wurster-gap height, but decreases close to the inner Wurster wall. The Wurster-gap height controls the particle mass-flow rate entering the tube as well as the mass inside the tube, thus directly influencing the particle fraction in the spray zone and resulting in different coating performances.

For larger particle sizes (Figure 55 (d)), a higher particle velocity along the inner Wurster wall is observed. This can be explained by the fact that larger particles have a larger projected area and thus a larger acting drag force. Additionally, the density of the particles decreases with increasing coating layers, and thus, the mass of the coated particles does not increases as fast as the projected area. The velocity close to the central axis of the Wurster tube is slightly decreased by increasing the particle size.

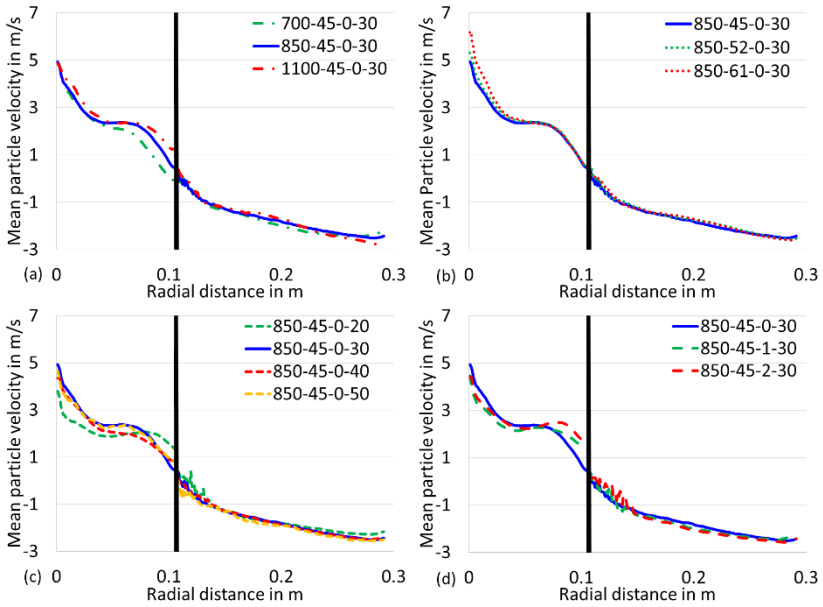

Figure 55: Time averaged vertical particle velocity at 500 mm height for (a) three fluidization air flow rates, (b) atomization air flow rate, (c) Wurster gap heights and (d) coating stages. The solid black lines in all four graphs symbolizes the Wurster tube wall. The first number in the legend description represents air flow rate in m³/h, the second one the atomization air flow rate in m³/h, the third one the particle size distribution (see Figure 6), and the last one the Wurster gap height in mm.

The effect of increasing particle velocity with increasing particle size can be seen in Figure 56, which plots a contour map of particle velocities. A cluster of particles with negative velocity can be seen for the uncoated particles, i.e., PSD 0 (Fig. 11a) but not for the coated particles with larger particle diameters (PSD 1 and PSD 2) (Figure 56 b and c). This is valid for the total simulated time span. This explains the lower time-averaged particle velocity close to the Wurster tube of the uncoated particles (PSD 0), see Figure 55(d).

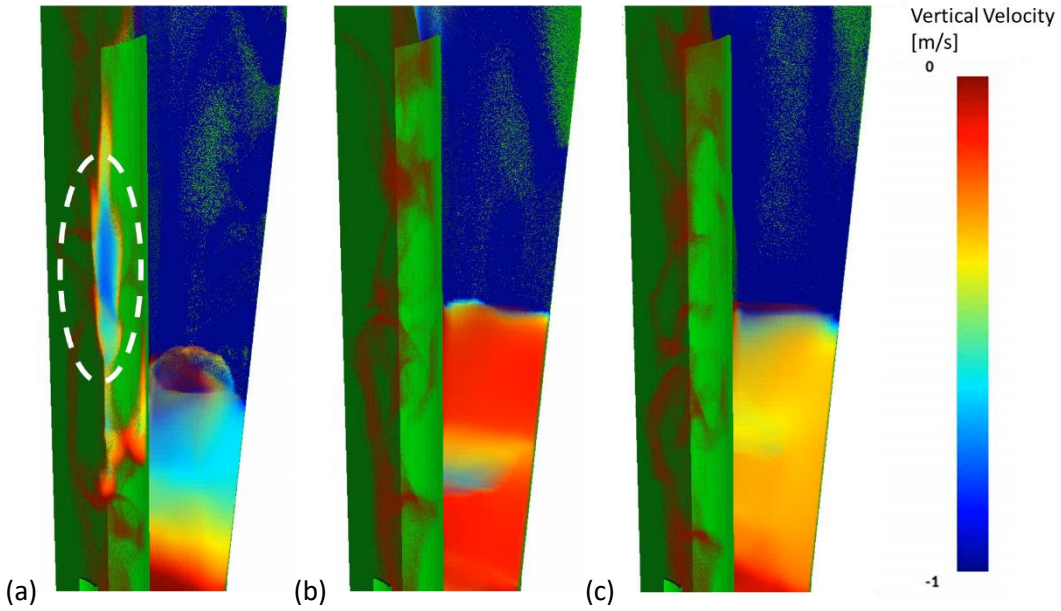

Figure 56: Vertical particle velocity close to the Wurster wall: a) uncoated particle and PSD0, and coated particles (b and c). The particle cluster with negative vertical velocity is marked in the dashed circle. The particle with higher velocities are made transparent.

E-6.3. Evaluation of Residence Time Distribution (RTD) inside the Wurster Tube

The Wurster tube residence time is the time that an individual particle spends in the tube during a single visit. Since a DEM simulation can track millions of particles, it is possible to obtain RTD statistics after 40 s of simulated process time, even though the real process time may span several hours.

Figure 57a shows the RTD for varying inlet air-flow rates. Figure 12b shows the average residence time computed from the curves in Fig. 12a. In Fig. 12b, the size range of beads is further subdivided into five size classes and the mean residence time is calculated for each size class. The purpose of this subdivision is to evaluate whether there is any systematic variation in the spray-zone, i.e., Wurster tube, residence time as a function of particle size. The fluidization air flow rate clearly has a noticeable impact on the RTD and the mean residence time. The mean RT reduces from ~0.69 s for 700 m^3/h inlet flow rate to ~0.32 s for 1100 m^3/h. Moreover, the width of the RTD decreases with the increasing fluidization air-flow rates. It can be also seen that the mean residence within the Wurster tube does not depend on the particle-size class, i.e., smaller and larger beads in the coater have almost-identical behavior and follow similar trajectories. These results demonstrate that the particles are well mixed within the Wurster tube and no size-based segregation occurs.

Although the modes of the RTD curves in Figure 12 (left-hand figure) are similar for all fluidizing air-flow rates, a large difference between the mean residence times can be observed (right-hand figure).

Upon closer examination, differences in the distributions for longer residence times, between 1 s to 2 s, can be seen. For the lowest fluidization air flow rate (green curve), some particles have long residence times within the Wurster tube. By examining the simulation animations, we find that these longer residence times are caused by recirculation of some particles near the inner wall of the Wurster tube. These longer-residing particles, although few in number, influence the mean residence time approximately by a factor of 2 between air-flow rates of 700 m^3/h and 1100 m^3/h.

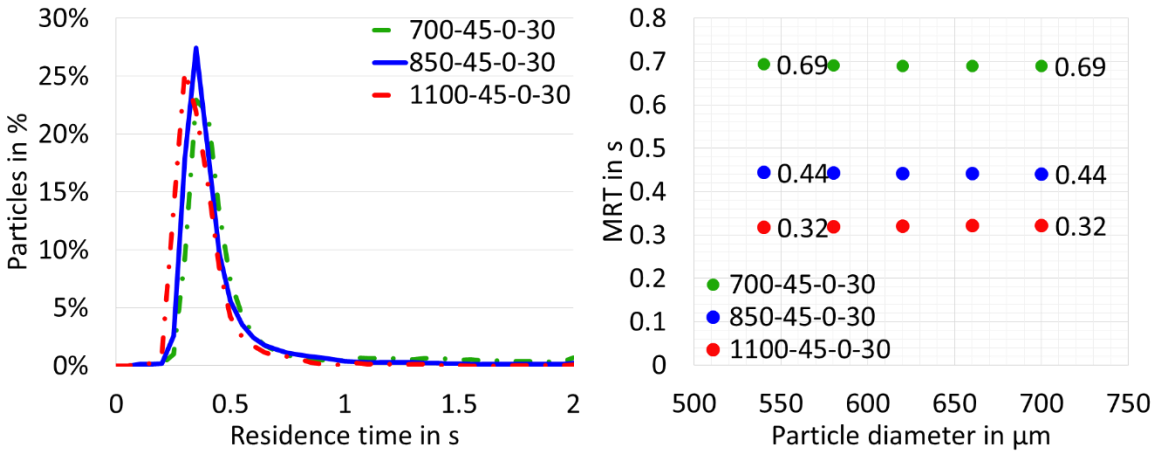

Figure 57: Residence time distributions (left) and mean residence times (MRT) (right) for three fluidization air flow rates and uncoated particles. Mean residence time is plotted for different size classes to show the influence of the particle size on the residence time. The first number in the legend description represents air flow rate in m³/h, the second one the atomization air flow rate in m³/h, the third one the particle size distribution (see Figure 6), and the last one the Wurster gap height in mm.

Figure 58a shows the RTD curves and Fig. 13b shows the mean residence times for five sizes classes at three atomization air flow rates, similar to the format presented in Fig. 12. Apparently, the atomization air flow rate has almost no influence on the RTD or the mean residence time in the Wurster tube zone. The reason is that only a few particles near the center of the tube are influenced by the larger air velocity from the nozzle; the majority of the particles are unaffected by changes in the atomizing air-flow rate. Although the RTD and CTD are not affected, the atomization air-flow rate is certainly of importance as it will influence the spray behavior and drying characteristics of beads in the spray zone. The bead size has no impact on the flow at all atomizing air-flow rates for the range of values investigated.

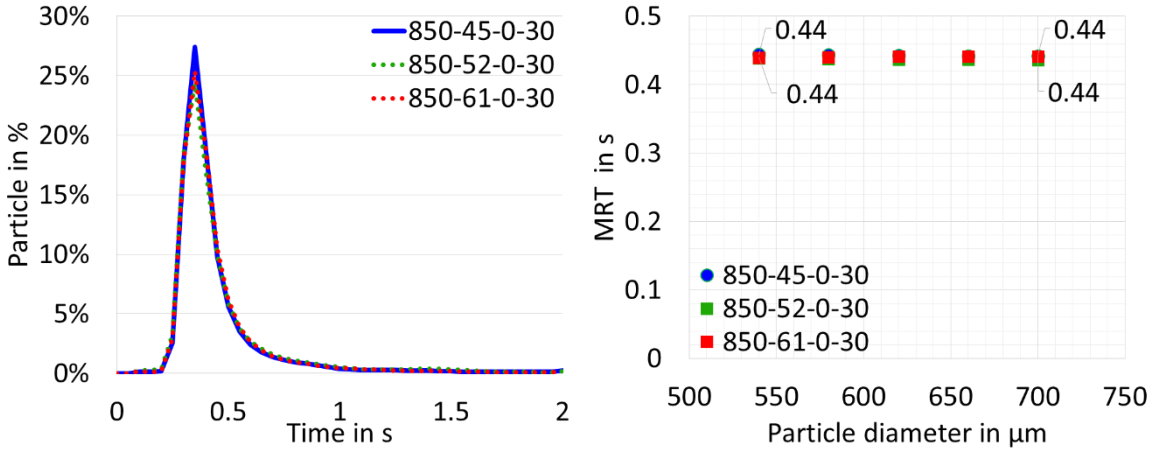

Figure 58: Residence time distributions (left) and mean residence times (right) for three atomization air flows and uncoated particles. Mean residence time is plotted for different size classes to show the influence of the particle size on the residence time.

Figure 59a and 14b show the RTD curves and the mean residence times of the five particle-sizes classes for varying Wurster gap height. The mean residence time increases significantly as the gap height is increased from 20 mm to 30 mm. This increase can be explained by the increase in particle recirculation through the tube as the inlet size to the tube is increased (see Figure 56 for an example of the particle recirculation). This effect can be also seen in the time-averaged particle velocity (Fig. 10c), where the velocity close to the inner Wurster wall is larger for the 20 mm gap compared to other Wurster gap heights. Subsequently, increase of the gap size from 30 mm to 40 mm or 50 mm does not have further impact on the mean residence time (Figure 59b). As before, the bead size has no noticeable impact on the flow for all Wurster gap heights investigated.

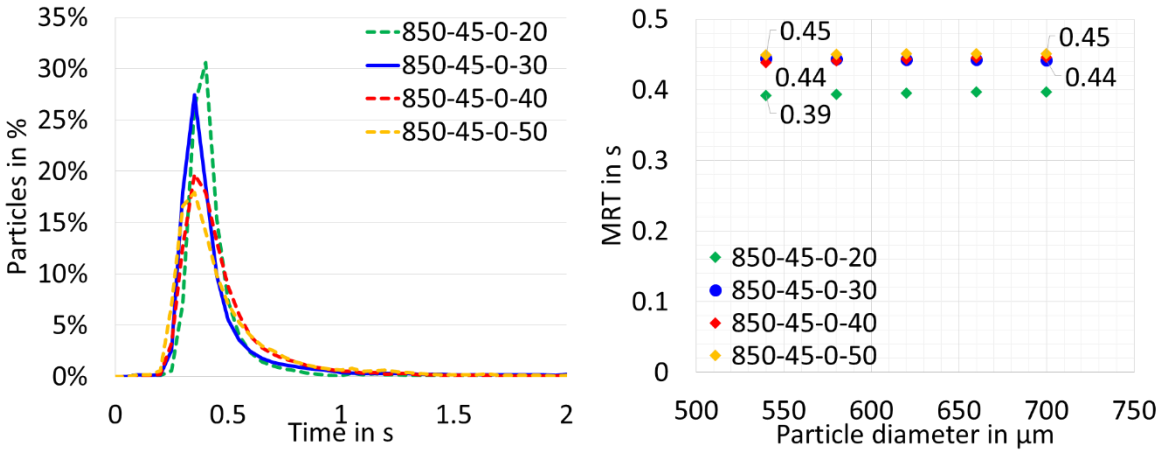

Figure 59: Residence time distributions (left) and mean residence times (right) for four Wurster gap heights and uncoated particles. Mean residence time is plotted for different size classes to show the influence of the particle size on the residence time. The first number in the legend description represents air flow rate in m³/h, the second one the atomization air flow rate in m³/h, the third one the particle size distribution (see Figure 6), and the last one the Wurster gap height in mm.

Figure 60 presents the RTD and the mean residence time for the five particle size classes for three particle size distributions, representing three stages of the coating. Recall that the first distribution (PSD 0) represents the uncoated beads, PSD 1 are the beads after the first coating stage, and PSD 2 are the beads after the second coating stage. These distributions are obtained from direct experimental measurements, along with the true density of the beads which change slightly from one stage to another.

As the particle sizes grow, the RTD shifts leftwards, i.e., the mean residence time decreases with increasing particle size. The reason for this observation has been explained earlier: particle velocities in the Wurster tube are larger for the bigger particles (PSD 1 and PSD 2), resulting shorter residence times. For the smallest particles (PSD 0), some backflow was observed (Fig. 11) which explains the disproportionately longer residence times. For any given distribution, the mean Wurster residence time does not vary noticeably with particle size.

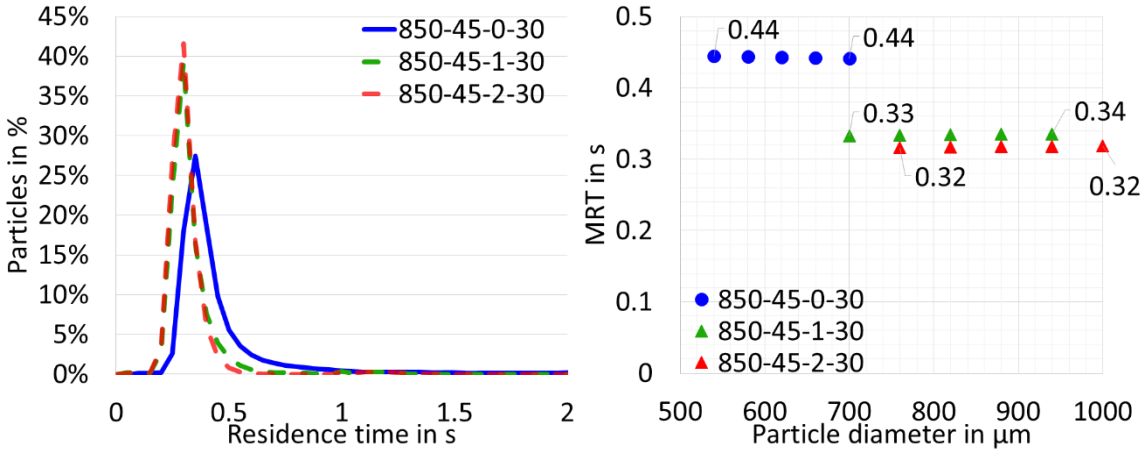

Figure 60: Residence time distributions (left) and mean residence times (right) for three particle size distributions for uncoated, once coated particles and twice coated particles. Mean residence time is plotted for different size classes to show the influence of the particle size on the residence time. The first number in the legend description represents air flow rate in m^3/h, the second one the atomization air flow rate in m^3/h, the third one the particle size distribution (see Figure 6), and the last one the Wurster gap height in mm.

E-6.4. Evaluation of the Cycle Time

The cycle time (CT) for a particle is the time between two successive visits to the spray zone, i.e., the entrance to the Wurster tube. It is strongly influenced by mixing dynamics in the denser, particle bed region. Figure 61a shows the CTD curves for varying inlet air-flow rate and Fig. 16b shoes the mean cycle times calculated for the five different particle-size classes at the three fluidization air-flow rates. As before, the range of particle sizes is sub-divided into the same five particles size classes as was

defined for the Wurster residence time calculations; the mean cycle time was computed for each individual particle-size class.

Similar to the trend for the Wurster residence time, the cycle time also decreases with increasing fluidization air-flow rates. However, it is interesting to note that the decrease between 700 m³/h and 850 m³/h is much more significant than that between 850 m³/h and 1100 m³/h, even though the change in the air flow rate $\Delta\dot{V}$ is higher in the latter case (150 m³/h vs. 250 ³/h). It can be also seen that the cycle time decreases slightly with an increasing particle diameter. Therefore, there is a subtle difference in the circulation rates of larger and smaller particles—the smaller particles experience fewer coating passes over the duration of the coating operation.

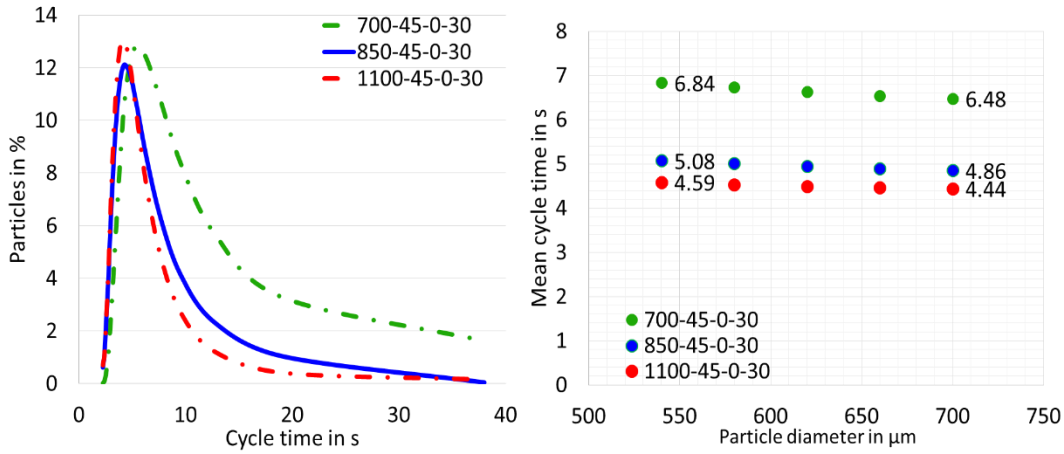

Figure 61: Cycle time distributions (left) and mean cycle times (right) for three fluidization air flows rates. Mean cycle time is plotted for different size classes to show the influence of the particle size on the cycle time. The first number in the legend description represents air flow rate in m³/h, the second one the atomization air flow rate in m³/h, the third one the particle size distribution (see Figure 6), and the last one the Wurster gap height in mm.

Figure 62 shows the CTDs of all particles and the mean cycle times of the five particle-size classes for three atomization air flow rates. As earlier, the difference between the atomization air flow rates is negligible since the atomization air flow rate only affects a small volume in the Wurster tube and does not significantly influence the particle bed dynamics. However, the difference between the Wurster residence time and the CTD lies in the influence of particle size: the mean Wurster residence time was unaffected by bead size, whereas the mean cycle time is found to decrease slightly with increasing particle diameter. Hence, smaller beads will experience fewer coating passes. This is consistent with the behavior observed in Fig. 16b.

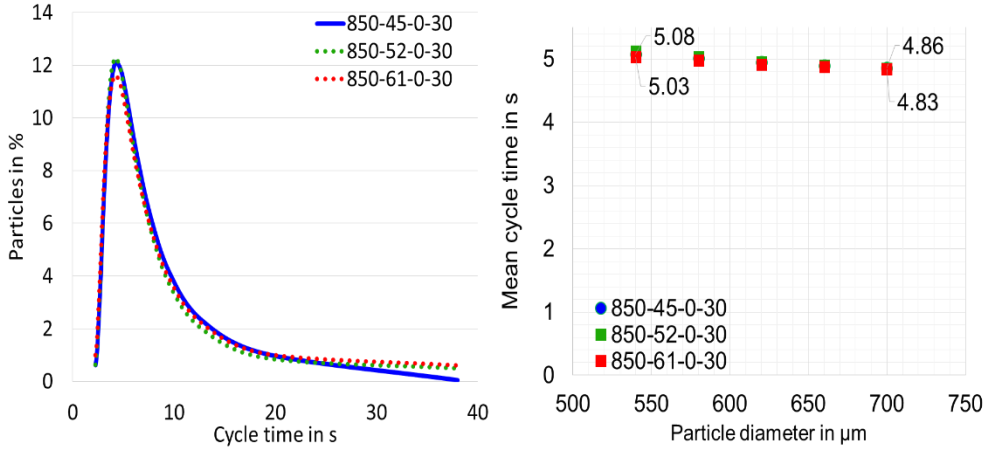

Figure 62: Cycle time distributions (left) and mean cycle times (right) for three atomization air flows and uncoated particles. Mean cycle time is plotted for different size classes to show the influence of the particle size on the cycle time. The first number in the legend description represents air flow rate in m³/h, the second one the atomization air flow rate in m³/h, the third one the particle size distribution (see Figure 6), and the last one the Wurster gap height in mm.

Figure 63 presents the CTD curves and the mean cycle times for five different particle-diameters classes for four Wurster-gap heights. The cycle time decreases systematically with increasing Wurster-gap height. This has been explained by the increased particle mass flow rate through the Wurster tube as the inlet gap size to the Wurster tube increases. The CTD data suggests that a larger Wurster-gap height should result in a better coating uniformity. According to our analysis, for a gap height of 50 mm, particles pass through the Wurster tube, i.e., the spray zone, approximately 820–850 times per hour; in contrast, for a gap height of 20 mm, number of passes lies in the wider range of 630—850. When the number of passes through the spray zone is more consistent, we can expect a more uniform mass gain among particles and, thus, better coating uniformity.

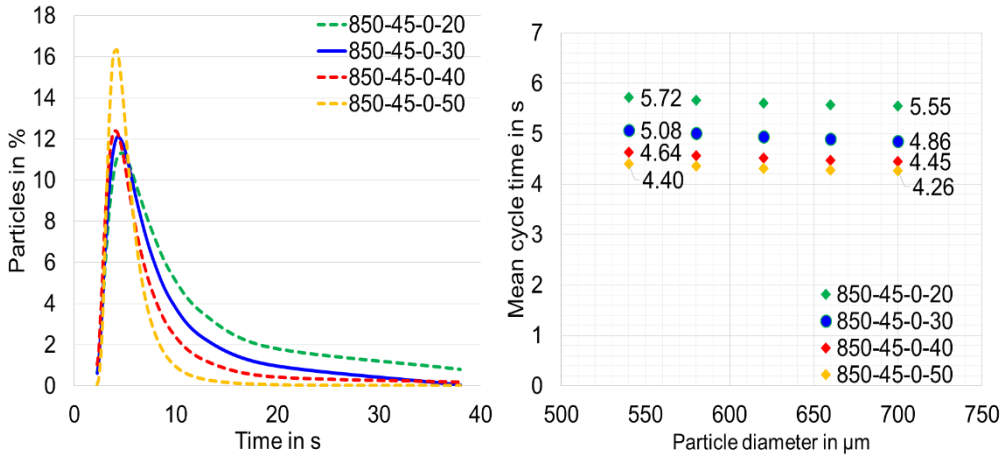

Figure 63: Cycle time distributions (left) and mean cycle times (right) for four Wurster gap heights and uncoated particles. Mean cycle time is plotted for different size classes to show the influence of the particle size on the cycle time. The first number in the legend description represents air flow rate in m³/h, the second one the atomization air flow rate in m³/h, the third one the particle size distribution (see Figure 6), and the last one the Wurster gap height in mm.

Figure 64 shows the CTD and the mean cycle times for the three coating stages (three different PSDs). The cycle time decreases with increasing particle diameters for all coating stages. The mean cycle time exhibits s a linear variation with particle diameter. This linear relationship between the mean cycle time and the particle size was observed for all coating stages. The width of the CTD decreases with the increasing particle size, even though some particles have not visited the Wurster tube after 40 seconds of simulated time for the case with PSD 1, and even more so for the particles from PSD 2.

It can be also surmised that the dependence on the particle size is more pronounced for the cycle time than for the mean residence time in the Wurster tube (see Figure 60). This can be explained by the fact that the denser, horizontal transport region is more prone to size-based particle segregation compared to the dilute, spray zone. This can be observed in Figure 65, which shows a snapshot of the particles colored by the particle diameter. It can be clearly seen that a segregated cluster of smaller particles (colored blue) exists in the horizontal transport region. These smaller particles are more likely to be back-mixed inside the horizontal transport region, thus leading to a longer cycle time.

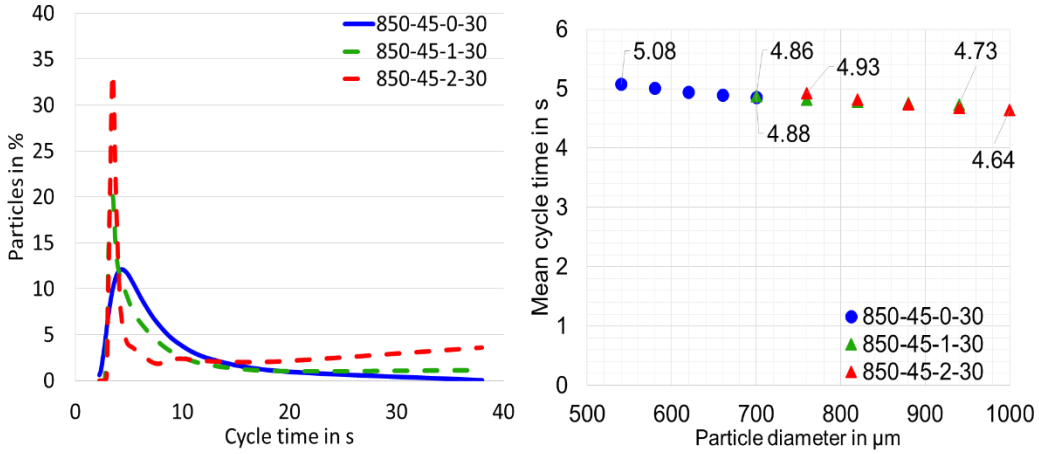

Figure 64: Cycle time distributions (left) and mean cycle times (right) for three particle size distributions for uncoated, once coated and twice coated particles. Mean cycle time is plotted for different size classes to show the influence of the particle size on the cycle time. The first number in the legend description represents air flow rate in m³/h, the second one the atomization air flow rate in m³/h, the third one the particle size distribution (see Figure 6), and the last one the Wurster gap height in mm.

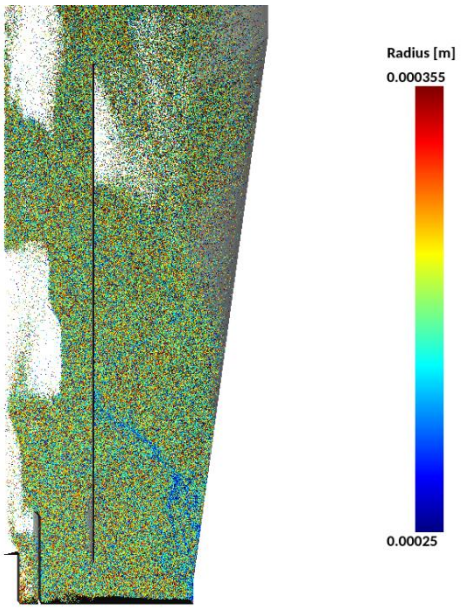

Figure 65: Snapshot of the simulation showing segregation inside the particle bed and no segregation (good mixing) in the Wurster tube. Particles are colored according to their radius.

E-6.5. Evaluation of Mass Flow Rate and Mass Holdup

The mass flow rate through the Wurster tube and the mass holdup of particles inside the Wurster tube for all parametric simulations are shown in Figure 66. The mass-flow rate is related to the mean Wurster-tube residence time and, as expected, the mass flow rate increases with increasing fluidization air flow rate, atomization air flow rate, and particle size. The particle size has the greatest influence, followed by the Wurster-gap height, followed by the fluidization air-flow rate. The mass holdup, which

dictates the number of particles in the spray zone that receive coating at any instant, decreases with the increasing fluidization air-flow rate and particle size and with the decreasing Wurster=gap height. It can also be seen that the mass holdup remains approximately constant when the Wurster gap height or the atomization air flow rate are varied.

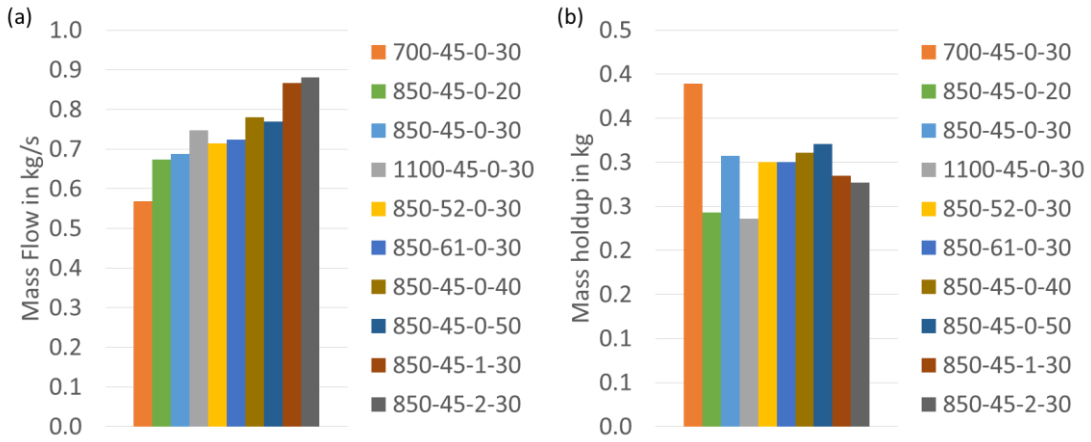

Figure 66: Mass flow rate (a) and mass holdup (b) in the Wurster tube for various process settings. The first number in the legend description represents air flow rate in m³/h, the second one the atomization air flow rate in m³/h, the third one the particle size distribution (see Figure 6), and the last one the Wurster gap height in mm.

E-7. Conclusions

In our study, an industrial-size Wurster coater, the Glatt GPCG 15/30, with a batch size of 40kg is analyzed using coupled CFD-DEM simulations. Several sets of varying process conditions are studied. First, the CFD-DEM simulation method was validated by a comparison of the model predictions with reference experimental and simulation results from Li et al. [15]. Our methods showed a good agreement with the published data regarding the particle residence time in different zones, the particle velocity profiles, and the particle cycle time. In order to apply CFD-DEM approach for an industrial size Wurster coater, a smaller axisymmetric 3-D sector (pie-slice) was considered. Almost identical results can be obtained by applying this pie-slice approach. Thereby significant reduction of computational time and especially the number of particles can be achieved, making it possible to simulate an industrial coating process containing a 40 kg batch size with an unmodified particle size distribution.

The primary goal of our work was to provide insights into the performance of an industrial-sized Wurster coater as a function of different processing conditions. For the analysis, the residence time within the Wurster tube (spray zone), the cycle time, and time-averaged radial velocity profiles were evaluated. The results of this computational investigation indicate that the particle flow behavior is

affected mostly by the fluidization air flow rate and the Wurster gap height. Although changing the atomization air flow rate has almost no influence on the particle flow, it could affect the spray properties and the spray coating. Since these effects were not considered in this study, the impact of the atomizing air-flow rate on bulk flow dynamics of beads is minimal.

We also established that the particle flow changes with the changing particle size and that, surprisingly, larger beads spend less time in the Wurster tube. A correlation between the particle size and cycle time was established, with a difference of around 4 % between the smallest and largest particles in one PSD. When the various coating stages were compared, the difference between the smallest particle size (530 µm) and the largest particle size (1000 µm) was 0.54 s (11 %). Overall, the Wurster coater process is robust in terms of residence time in the Wurster tube and cycle time. Since the change in the spray zone residence time was insignificant regardless of the process settings, the process design should focus on reducing the particle CT, leading to a faster, intensified process without affecting the product quality.

Based on the simulation results, correct process settings can be established to reduce the cycle time while preserving the residence time in the Wurster tube (i.e., the spray zone) as constant. This can be achieved by inducing recirculation of particles inside the Wurster tube zone and by setting the Wurster gap height to a value larger than 30mm. The negative vertical particle velocity close to the Wurster tube walls indicate recirculation of particles (see for instance Figure 56). Process settings with a fluidization air flow rate of 850-900 m^3/h and a Wurster gap height of 40 mm for the uncoated particles should give optimal process conditions. At later coating stages, the Wurster gap height should be kept at 40 mm and the fluidization air flow rate should be reduced to allow particle recirculation in the Wurster tube and to maintain the same overall particle behavior.

In the future, the results of the CFD-DEM simulations will be used to generate long-term coating prediction models based on the insights into the particle behavior associated with the investigated process parameters. In this way, a coupled CFD-DEM simulation of a large-scale Wurster Coater process can help to optimize the coating process and increase the yield of a unit operation.

E-8. Bibliography

[1] E. Teunou and D. Poncelet, “Batch and continuous fluid bed coating – review and state of the art,” *J. Food Eng.*, vol. 53, pp. 325–340, 2002.

[2] D. E. Wurster, “Air-suspension technique of coating drug particles. A preliminary report,” *J. Am. Pharm. Assoc.*, vol. 48, no. August, pp. 451–454, 1959.

[3] S. Fitzpatrick, Y. Ding, C. Seiler, C. Lovegrove, S. Booth, R. Forster, D. Parker, and J. Seville, "Positron emission particle tracking studies of a wurster process for coating applications," *Pharm. Technol.*, vol. 27, no. 9, pp. 70–78, 2003.

[4] S. Karlsson, I. Niklasson, S. Folestad, and A. Rasmuson, "Measurement of the particle movement in the fountain region of a Wurster type bed," *Powder Technol.*, vol. 165, pp. 22–29, 2006.

[5] F. Depypere, J. G. Pieters, and K. Dewettinck, "PEPT visualisation of particle motion in a tapered fluidised bed coater," *J. Food Eng.*, vol. 93, no. 3, pp. 324–336, 2009.

[6] M. Peglow and E. Tsotsas, "Continuous pellet coating in a Wurster fluidized bed process," *Chem. Eng. Sci.*, vol. 86, pp. 87–98, 2013.

[7] L. Liang, J. Remmelgas, B. G. M. van Wachem, C. von Corswant, M. Johansson, S. Folestad, and A. Rasmuson, "PEPT Study of Particle Cycle and Residence Time Distributions in a Wurster Fluid Bed," *Am. Inst. Chem. Eng. AIChE J.*, vol. 61, no. 3, pp. 756–768, 2015.

[8] N. G. Deen, M. Van Sint Annaland, M. a. Van der Hoef, and J. a. M. Kuipers, "Review of discrete particle modeling of fluidized beds," *Chem. Eng. Sci.*, vol. 62, no. 1–2, pp. 28–44, Jan. 2007.

[9] D. Gidaspow, *Multiphase Flow and Fluidization: Continuum and Kinetic Theory Descriptions*, 1st ed. Academic Press, 1994.

[10] P. A. Cundall and O. D. L. Strack, "A discrete numerical model for granular assemblies," *Géotechnique*, vol. 29, no. 1, pp. 47–65, Jan. 1979.

[11] F. J. Muzzio and M. G. Ierapetritou, "Scale-up strategy for continuous powder blending process," *Powder Technol.*, vol. 235, pp. 55–69, Feb. 2013.

[12] H. P. Kuo, P. C. Knight, D. J. Parker, Y. Tsuji, M. J. Adams, and J. P. K. Seville, "The influence of DEM simulation parameters on the particle behaviour in a V-mixer," *Chem. Eng. Sci.*, vol. 57, pp. 3621–3638, 2002.

[13] R. Kumar, B. Freireich, and C. Wassgren, "DEM–compartment–population balance model for particle coating in a horizontal rotating drum," *Chem. Eng. Sci.*, pp. 1–14, Jul. 2014.

[14] G. Toschkoff, S. Just, K. Knop, P. Kleinebudde, A. Funke, A. Altmeyer, D. Djuric, and G. Scharrer, "Design-of-Experiment based DEM simulation of an active tablet coating process ."

[15] L. Liang, J. Remmelgas, B. G. M. van Wachem, C. von Corswant, M. Johansson, S. Folestad, and A. Rasmuson, "Residence time distributions of different size particles in the spray zone of a Wurster fluid bed studied using DEM-CFD," *Powder Technol.*, vol. 280, pp. 124–134, 2015.

[16] L. Fries, S. Antonyuk, S. Heinrich, and S. Palzer, "DEM–CFD modeling of a fluidized bed spray granulator," *Chem. Eng. Sci.*, vol. 66, no. 11, pp. 2340–2355, Jun. 2011.

[17] J. Zhao and T. Shan, "Coupled CFD – DEM simulation of fl uid – particle interaction in geomechanics," *Powder Technol.*, vol. 239, pp. 248–258, 2013.

[18] R. Turton, "Challenges in the modeling and prediction of coating of pharmaceutical dosage forms," *Powder Technol.*, vol. 181, no. 2, pp. 186–194, 2008.

[19] M. Girardi, S. Radl, and S. Sundaresan, "Simulating wet gas – solid fluidized beds using coarse-grid CFD-DEM," *Chem. Eng. Sci.*, vol. 144, pp. 224–238, 2016.

[20] A. Ozel, J. Kolehmainen, S. Radl, and S. Sundaresan, "Fluid and particle coarsening of drag force for discrete-parcel approach," *Chem. Eng. Sci.*, vol. 155, pp. 258–267, 2016.

[21] S. Radl and S. Sundaresan, "A drag model for filtered Euler-Lagrange simulations of clustered gas-particle suspensions," *Chem. Eng. Sci.*, vol. 117, pp. 416–425, 2014.

[22] K. Takabatake, X. Sun, M. Sakai, D. Pavlidis, J. Xiang, and C. C. Pain, "Numerical study on a heat transfer model in a Lagrangian fluid dynamics simulation," *Int. J. Heat Mass Transf.*, vol. 103, pp. 635–645, 2016.

[23] T. Tsory, N. Ben-Jacob, T. Brosh, and A. Levy, "Thermal DEM–CFD modeling and simulation of heat transfer through packed bed," *Powder Technol.*, vol. 244, pp. 52–60, Aug. 2013.

[24] M. Sakai, M. Abe, Y. Shigeto, S. Mizutani, H. Takahashi, A. Viré, J. R. Percival, J. Xiang, and C. C. Pain, "Verification and validation of a coarse grain model of the DEM in a bubbling fluidized bed," *Chem. Eng. J.*, vol. 244, pp. 33–43, 2014.

[25] X. Sun, M. Sakai, and Y. Yamada, "Three-dimensional simulation of a solid–liquid flow by the DEM–SPH method," *J. Comput. Phys.*, vol. 248, pp. 147–176, Sep. 2013.

[26] P. Boehling, G. Toschkoff, K. Knop, P. Kleinebudde, S. Just, A. Funke, H. Rehbaum, and J. G. Khinast, "Analysis of large-scale tablet coating : Modeling , simulation and experiments," *Eur. J. Pharm. Sci.*, vol. 90, pp. 14–24, 2016.

[27] P. Boehling, G. Toschkoff, S. Just, K. Knop, P. Kleinebudde, A. Funke, H. Rehbaum, P. Rajniak, and J. G. Khinast, "Simulation of a tablet coating process at different scales using DEM," *Eur. J. Pharm. Sci.*, vol. 93, pp. 74–83, 2016.

[28] C. A. Radeke, B. J. Glasser, and J. G. Khinast, "Large-scale powder mixer simulations using massively parallel GPU architectures," *Chem. Eng. Sci.*, vol. 65, no. 24, pp. 6435–6442, Dec. 2010.

[29] M. Syamlal and T. J. O'Brien, "Computer simulation of bubbles in a fluidized bed," in *AIChE Symp. Ser*, 1989, vol. 85, no. 1, pp. 22–31.

[30] P. Toson and J. G. Khinast, "Impulse-based dynamics for studying quasi-static granular flows: Application to hopper emptying of non-spherical particles," *Powder Technol.*, vol. 313, pp. 353–360, 2017.

[31] N. Govender, D. N. Wilke, P. Pizette, and N. E. Abriak, "A study of shape non-uniformity and poly-dispersity in hopper discharge of spherical and polyhedral particle systems using the Blaze-DEM GPU code," *Appl. Math. Comput.*, vol. 319, pp. 318–336, 2018.

[32] L. Fries, S. Antonyuk, S. Heinrich, D. Dopfer, and S. Palzer, "Collision dynamics in fluidised bed granulators : A DEM-CFD study," *Chem. Eng. Sci.*, vol. 86, pp. 108–123, 2013.

[33] C. R. Müller, D. J. Holland, A. J. Sederman, S. A. Scott, J. S. Dennis, and L. F. Gladden, "Granular temperature: Comparison of Magnetic Resonance measurements with Discrete Element Model simulations," *Powder Technol.*, vol. 184, pp. 241–253, 2008.

[34] D. Jajcevic, E. Siegmann, C. Radeke, and J. G. Khinast, "Large-scale CFD–DEM simulations of fluidized granular systems," *Chem. Eng. Sci.*, vol. 98, pp. 298–310, Jul. 2013.

[35] Ding Jianmin and D. Gidaspow, "A Bubbling Fluidization Model Using Kinetic Theory of Granular Flow," *AIChE J.*, vol. 36, no. 4, pp. 523–538, 1990.

[36] L. G. Gibilaro, R. Di Felice, S. P. Waldram, and P. U. Foscolo, “Generalized friction factor and drag coefficient correlations for fluid-particle interactions,” *Chem. Eng. Sci.*, vol. 40, no. 10, pp. 1817–1823, 1985.

[37] S. Ergun, “Fluid flow through packed columns,” *Chem. Eng. Prog.*, vol. 48, no. 2, pp. 89–94, 1952.

[38] C. Wen and Y. Yu, “Mechanics of fluidization,” *Chem. Eng. Prog. Symp. Ser.*, vol. 62, no. 62, p. 100.

[39] M. S. van Buijtenen, W. J. van Dijk, N. G. Deen, J. A. M. Kuipers, T. Leadbeater, and D. J. Parker, “Numerical and experimental study on multiple-spout fluidized beds,” *Chem. Eng. Sci.*, vol. 66, no. 11, pp. 2368–2376, 2011.

F. Validating a numerical simulation of the ConsiGma® semi-continuous tablet coating process

Planned for publication: Böhling *et al.*, "Validating a numerical simulation of the ConsiGma® semi-continuous tablet coating process" TBD.

F-1. Abstract

Process understanding is the key element of process control. In this regard, computational tools can improve the fundamental understanding and process performance, especially those related to new processes, such as continuous tablet coating whose process mechanics remain a conundrum. In the last years, Computational Fluid Dynamics (CFD) and the Discrete Element Method (DEM) have increasingly been applied to analyze and understand processes in the pharmaceutical industry. GEA developed a semi-continuous tablet coater which can be integrated into a continuous tableting line, accelerating the switch from traditional batch production to the continuous mode of operation. The latter offers certain advantages over batch production, e.g., operational flexibility, increased process/product quality and decreased cost.

The goal of this work was to develop and validate a CFD-DEM simulation model of the tablet coating process in the GEA ConsiGma® coater. After the model development, simulation results for the tablet movement, coating quality, and heat and mass transfer during the coating process were validated and compared to the experimental outcomes. The experimental and simulation results agreed well on all accounts measured, indicating that the model can be used in further studies to investigate the operating space of the continuous tablet coating process.

F-2. Introduction

Continuous manufacturing (CM) is increasingly applied in the pharmaceutical industry [1], [2]. In comparison to batch production, it enables a higher throughput while simultaneously decreasing the waste and energy consumption and production costs [3]. Since the inline measurements are typically intrinsic to the process design, CM allows enhanced process control [4]. Above all, CM requires a high level of process understanding. Small, semi-continuous batches suffice for extensive exploration of the operating space, dramatically increasing the level of process understanding and making an extensive research on all kinds of CM production units possible [5]–[9].

In light of the transition fro2m batch to continuous manufacturing, GEA developed the ConsiGma® continuous processing line to process powder raw materials into tablets [10]. There are two types of ConsiGma® lines: the ConsiGma® continuous tableting line (CTL) and the continuous direct compression line (CDC). The advantages of both are a small footprint and reduced waste.

Tablets are the most commonly administered pharmaceutical dosage form and are often applied to add a color coating, a protective layer or a second active pharmaceutical ingredient, as well as to differentiate products and provide a delayed-release. All coating types have certain critical quality attributes that define the ultimate product performance. The most important ones are inter- and intra-coating variability [11], which should be low to ensure sufficient product quality, e.g. color uniformity. Coating variability (CoV) is defined through experiments and is typically confirmed using samples taken during production. Uniformity can be assessed by comparing the weight of the film-coated tablet to the mean tablet core weight or via spectroscopy methods e.g., terahertz or Raman probe.

Tablet coating experiments are performed on various scales [8], [12], [13], generally beginning with the smallest-scale equipment (laboratory scale) and only a few kilograms of tablets[12], [14], [15]. The benchtop laboratory equipment is typically scaled to the pilot scale in a piece of manufacturing equipment with a drum load of 10-50 kg [16]. Experiments on the industrial scale are carried out at the end of process development [17][18] using the intended commercial equipment. The product and technology transfer is accomplished and based on the existing scale-up rules and experience of the operating engineers [16], [19]. However, scale-up often causes problems due to changes in the coater geometry designs across the scales or completely different drum designs on the production scale. The general goal is to reduce the number of experiments required on a larger scale since they are expensive due to the time and material consumption [18].

Although continuous tablet drum coaters are still rarely used in the pharmaceutical industry, the increasing interest in end-to-end continuous manufacturing has created the need for integrated continuous tablet coaters [20]–[22]. Continuous tablet drum coaters typically have a similar shape and operating principles as traditional batch tablet coaters [20], [23]. The main difference is the design. For instance, in continuous tablet coaters, the baffles are constructed to direct the flow of the tablet bed from the inlet to the outlet region. The spray is applied from the top, and the drying airflow is either parallel or counter-current to the tablet movement. Therefore, a fully continuous tablet coater with an operating principle similar to the traditional batch pan coating process may require more space and additional equipment.

GEA has developed a tablet coater that should eliminate these shortcomings and can be integrated into both ConsiGma® continuous production lines [8][24]. It is a small semi-batch tablet coater, which can be nominally loaded with 2.5 to 7 kg of tablets depending on the drum insert. Compared to traditional batch tablet coaters, the ConsiGma® tablet coater operates at high rotation rates, with a Froude number close to 1. Streams of air (referred to as 'air knives') push the tablets away from the drum wall to form a cascade through the spray zone, allowing a very short coating cycle time (a total process time of about 10 minutes).

Simulations can be used to increase an understanding of the coating process, especially the Discrete Element Method (DEM) simulations that can provide a detailed analysis of the coating process [25], [26]. Nowadays it is possible to simulate the tablet coating process on every scale due to a relatively low number of tablets within the system (small batch size) and to analyze the process for a number of parameters [27]. Simulations can offer information about the inter- and intra-tablet CoV, tablet velocity, tablet bed dynamics (i.e., velocity, residence and cycle times) and forces acting on the tablets[19], [28]–[30].

Computational Fluid Dynamics (CFD) has been increasingly used in industrial applications to simulate fluid flow [31], [32]. In recent years, CFD and the DEM are coupled to model the interaction between granular and fluid materials. Initially, only the momentum term was exchanged [31], [33], [34]. Either only one phase was affected (one-way coupling) or both phases interacted with each other (two-way coupling). This allows simulating the movement of granular material, e.g., in a conveyor or fluidized bed coater. Further functionality is added by integrating the exchange of mass and heat into the simulation via a so-called four-way coupling [35]. The level of model complexity is determined by a particular problem statement.

A full simulation of the ConsiGma® tablet coating process requires the above-mentioned four-way coupling approach. Although existing models only consider the heat and mass transfer from a global perspective, they cannot resolve the local tablet wetness or coating quality [8][24]. The approach presented in this work involves the development of an algorithm for the coupling momentum, heat and mass transfer in the ConsiGma® film-coating equipment. Since most simulations consider only spherical particles, accounting for the momentum transfer is challenging due to the tablet shape. To that end, a model simulating the fluid forces acting on the tablets was introduced. Considering the heat and mass transfer is important for the prediction of wet and dry processes. The goal in this work was to develop a model (a so called *digital twin*) that simulates and predicts the entire coating process

inside the ConsiGma® coater in order to test the process parameters and optimize the performance without conducting experiments.

The focus of this work is the CFD-DEM model validation. First, the tablet bed dynamics are validated by comparing experimental and simulation results for the tablet acceleration. Next, the coefficient of inter-tablet CoV was compared. Finally, the heat and mass transfer in the simulation was compared to the experimental results. To that end, the outlet air temperature and humidity and the tablet moisture (measured via the loss on drying (LoD)) and temperature are analyzed. The goal of the validation was to establish if the CFD-DEM simulation can be used as a digital twin of the ConsiGma® coater and to recommend the testing of process points inside the coater. This work explores a novel method of defining the process operating space of a semi-batch film coating unit operation that can be integrated into the ConsiGma® lines to continuously produce film-coated tablets.

F-3. Simulation model

In the following Section, the CFD-DEM simulation model is briefly introduced. Next, the biconvex tablet model developed is explained. Finally, the models for the momentum-, heat- and mass-coupling are presented in detail.

F-3.1. CFD-DEM model

The code XPS (e**X**tended **P**article **S**ystem) based on Graphics Process Units (GPUs) and developed in-house was used to calculate the particle motion [36]. It solves Newton's second law by solving particle-particle and particle-wall interactions [37], [38]. This method was developed by Cundall and Strack [39] in 1979. For the motion of each particle, the following equation is solved:

$$m_P \frac{d\mathbf{v_P}}{dt} = -V_i \nabla \mathrm{p} + \vec{\boldsymbol{F}}_i^d + \sum_0^{N_P} \mathbf{F}_{P\rightarrow P} + \sum_0^{N_W} \mathbf{F}_{P\rightarrow W} + m_p \mathbf{g} \tag{28}$$

where m_P is the particle mass, $\mathbf{v}_P$ is the particle velocity, $-V_i \nabla p$ is the pressure gradient force, $\vec{\boldsymbol{F}}_i^d$ is the drag force, $\mathbf{F}_{P->P}$ is the particle-particle force, $\mathbf{F}_{P->W}$ is the particle-wall force and g is the gravity constant. The three-dimensional angular momentum of the particle is calculated as:

$$\mathbf{I}_P \frac{d\boldsymbol{\omega}_\mathrm{P}}{dt} = \sum_0^{N_c} \mathbf{M}_P + \mathbf{M}_W + \mathbf{M}_F \tag{29}$$

where $\boldsymbol{\omega}_P$ is the angular velocity, $\mathbf{M}_P$ is the torque coming from other particles, $\mathbf{M}_W$ is the torque coming from the tablet-wall interactions, $\mathbf{M}_F$ is the torque coming from the surrounding fluid and $\mathbf{I}_P$ is the moment of inertia. Details of the algorithm can be found in [36] and [40].

To calculate the gas phase, a commercially available CFD code AVL Fire© was used, which models the gas phase by solving the volume-averaged Navier-Stokes equations. All variables are locally volume-averaged quantities over control volume V, which must be at least one order of magnitude larger than particle volume V_P [40]. The conservation of mass is:

$$\frac{\partial}{\partial t}(\varepsilon_F \cdot \rho_F) + \nabla \cdot (\varepsilon_F \cdot \rho_F \cdot \mathbf{v_F}) = 0 \tag{30}$$

where ρ_f is the fluid density, ε_F is the local volume fraction of the fluid, $\mathbf{v}_F$ is the fluid velocity vector and t is time. Similarly, the conservation of momentum is:

$$\frac{\partial}{\partial t}(\varepsilon_F \cdot \rho_F \cdot \mathbf{v_F}) + \nabla(\varepsilon_F \cdot \rho_F \cdot \mathbf{v}_\mathrm{F} \cdot \mathbf{v}_\mathrm{F}) = -\varepsilon_F \cdot \nabla \mathrm{p} - \nabla \cdot (\varepsilon_F \cdot \boldsymbol{\tau}_F) + \varepsilon_F \cdot \rho_F \cdot \mathbf{g} - \mathbf{S}_M \tag{31}$$

$\mathbf{S_M}$ is the momentum transfer source term. The heat and mass transfer is identical to the momentum exchange. For detailed information about the coupling mechanism see Jajcevic et al. [40].

The thermal energy equation for the gas phase is:

$$\frac{\partial}{\partial t}\left(\varepsilon_F \cdot \rho_F \cdot C_{p,F} \cdot \mathrm{T}_F\right) + \nabla\left(\varepsilon_F \cdot \rho_F \cdot \mathbf{v}_\mathrm{F} \cdot C_{p,F} \cdot \mathrm{T}_F\right) = \nabla \cdot \left(\varepsilon_F \cdot k_F^{eff} \cdot \nabla \mathrm{T}_F\right) + \mathbf{S}_E \tag{32}$$

where $C_{p,F}$ is the gas heat capacity, T_F is the gas temperature, S_E is the inter-phase energy transfer and k_F^{eff} is the effective thermal conductivity calculated as follows:

$$k_F^{eff} = \frac{1 - \sqrt{1 - \varepsilon_F}}{\varepsilon_F} \cdot k_F \tag{33}$$

Various components of the vapor are solved considering the species transport model in the fluid phase. The transport of an arbitrary gaseous species "i" is described by the following equation:

$$\frac{\partial}{\partial t}\left(\varepsilon_F \cdot \rho_F \cdot \mu_{\boldsymbol{vap,i}}\right) + \nabla\left(\varepsilon_F \cdot \rho_F \cdot \mu_{\boldsymbol{vap,i}}\right) = \nabla \cdot \left(D_{eff} \nabla \cdot \left(\varepsilon_F \cdot \rho_F \cdot \mu_{\boldsymbol{vap,i}}\right)\right) + \mathbf{S}_{vap} \tag{34}$$

$\mu_{\boldsymbol{vap}}$ is the mass fraction of the vapor gas species, D_{eff} is the diffusion coefficient and $\boldsymbol{S_{vap}}$ is the vapor gas species source term. Forgber et al. [42] have provided an in-depth overview of the models used and validated the momentum, heat, and mass transfer models for spheres.

F-3.2. Bi convex tablet model

A biconvex tablet model was developed to accurately model the given tablet shape. The tablet has a diameter of 9.8 mm (L_3) and a height of 4.3 mm (L_2) with a rim thickness of 2.6 mm (L_1). For the purposes of CFD-DEM simulation, the tablet shape is modeled by overlapping three spheres and assumes that all tablets have the same size. The three spheres consist of one central smaller sphere describing the rim surface and two larger ones describing the cap. Figure 67 shows a sketch of the approximation via three overlapping circles.

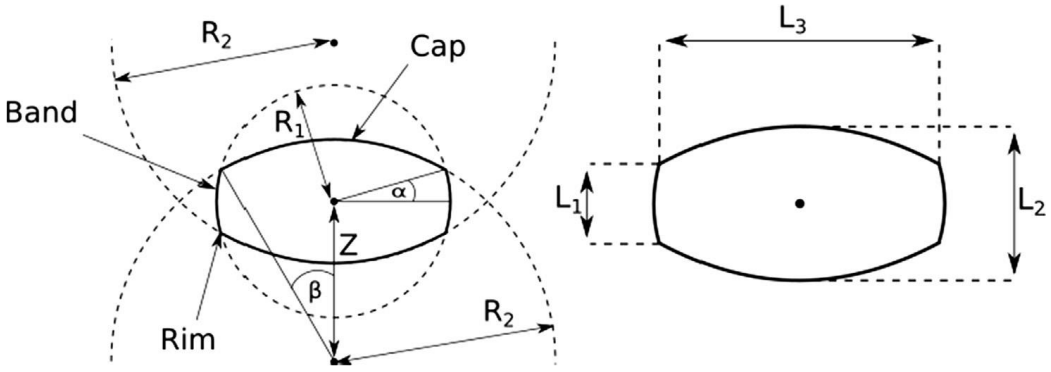

Figure 67: Construction of the biconvex tablet shape, including all symbols and expressions used. The image is taken from Kureck et al.[41].

Approximation via three overlapping spheres has advantages over other widely used shape approximations (e.g., the multi-sphere model and polyhedral shape model). Since only three spheres are needed to approximate the shape (vs. eight spheres typically applied under the traditional multi-sphere approach [30], [43]), the amount of memory required for the simulation is reduced, decreasing the computational expense while maintaining high accuracy of the simulation. Approximating the tablet shape without adding any artificial roughness required for the multi-sphere and polyhedral models enables fast simulations. For details of contact detection and force calculations see Kureck et al. [41]. Due to the symmetrical nature of the biconvex tablet, a drag model was developed for the coupling algorithms.

F-3.3. Drag force model

In contrast to spherical particles, the calculation of the drag force acting on a tablet requires special consideration. There are many ways to compute the drag coefficient for spheres in coupled CFD-DEM simulations[17], [44], [45]. A number of models are available for calculating the drag force acting on non-spherical elements [46], [47]. Typically these drag models only take into account a single particle in relatively dilute flows. However, for dense regimes of non-spherical particles, such as tablets, the correlation is not well established and is difficult to determine. Lattice Boltzmann Methods are often used to calculate the fluid forces acting on the particles [48], i.e., a model with varying numbers of fitting parameters is developed to correlate the drag on the particles. The problem with these approaches is that the fitting parameters have limited applicability to other shapes. Generally, a number of parameters have to be fitted to each particle shape. In this work, the drag coefficient calculation for non-spherical particles of Hölzer and Sommerfeld [47] for a single non-spherical particle is combined with the drag force model of Rong et al. [49], [50]. This model covers the single particle flow and the zones with a high packing fraction.

$$\vec{F}_i^d = \frac{1}{2} \cdot C_{D,0} \cdot \rho_F \cdot A_\perp \cdot \varepsilon_F^2 \cdot \varphi(d_i, x_i, \varepsilon_F) \cdot |\vec{u}_F - \vec{v}_i| \cdot (\vec{u}_F - \vec{v}_i) \cdot {\varepsilon_F}^{-(\beta(\varepsilon_F, \langle Re \rangle) + (\lambda(\phi, \langle Re \rangle)} \quad (35)$$

$A_\perp$ is the projected area perpendicular to the airflow direction and χ is a correction factor. $A_\perp$ is calculated based on an approximation algorithm, which interpolates the projected area of the tablets based on the mean angle and surface area computed at the beginning of the simulation. The drag coefficient is calculated as:

$$C_D = \frac{8}{Re} \cdot \frac{1}{\sqrt{\phi_\perp}} + \frac{16}{Re} \cdot \frac{1}{\sqrt{\phi}} + \frac{3}{\sqrt{Re}} \cdot \frac{1}{\phi^{\frac{3}{4}}} + 0.42 \cdot 10^{0.4(-\log(\phi))^{0.2}} \frac{1}{\phi_\perp} \quad (36)$$

ϕ is the sphericity of the tablet and $\phi_\perp$ is the crosswise sphericity. The sphericity is the ratio of the tablet volume to the sphere volume with the same surface area. The crosswise sphericity is calculated through $A_\perp$ and is the exposed surface area ratio of the tablet volume to the surface area of a sphere with the same volume.

Coefficient $\varphi(d_i, x_i, \varepsilon_F)$ depends on the particle characteristic diameter (d_i), particle type fraction x_i and void fraction ε_F. Since only one type of particle is considered in this work, α is set to 1. For simulations with different particle shapes or sizes, this parameter has to be defined via calibration with CFD simulations with varying packing fractions, void fractions, and diameters.

β is a correction factor for a low-void fraction, taking into account the void fraction and Reynolds number.

$$\beta(\varepsilon_F, \langle Re \rangle) = 2.65 \cdot (\varepsilon_F + 1) - (5.3 - 3.5 \cdot \varepsilon_F) \cdot {\varepsilon_F}^2 \cdot \exp\left[\frac{1}{2} \cdot (1.5 \cdot \log(Re))^2\right] \quad (37)$$

λ is a correction factor that takes the tablet diameter into consideration, as well as the Reynolds number.

$$\lambda(\phi, \langle Re \rangle) = (1 - \phi)\{C - D \cdot e^{-0.5 \cdot (3.5 - \log\langle Re \rangle)^2}\} \quad (38)$$

C is based on a linear regression of drag forces.

$$C(\phi) = 39 \cdot \phi - 20.6 \quad (39)$$

D is also based on the above linear regression.

$$D(\phi) = 101.8 \cdot (\phi - 0.81)^2 + 2.4 \quad (40)$$

In addition to the drag force, a CFD-DEM simulation of non-spherical particles has to consider the fluid lift force, C_L. To calculate it, the lift coefficient is computed. Correlations for the lift coefficient typically

link the lift coefficient to the drag coefficient and the relative angle of fluid velocity fields to the particle orientation, φ.

$$C_L = \mathrm{C_D}\sin^2(\varphi)\cdot\cos(\varphi) \tag{41}$$

Torque resulting from the non-sphericity of the tablets should not be neglected. To calculate it, the center of gravity, x_{cp}, has to be computed:

$$\mathrm{x_{cp}} = \mathrm{L}\cdot(3/4)\cdot(\sin(\varphi)/(4+\pi\cos(\varphi)) \tag{42}$$

Torque acting on the tablets due to the fluid-tablet interaction can be calculated by multiplying the center of gravity by the fluid forces:

$$\mathbf{M_F} = \mathrm{x_{cp}}(\vec{\boldsymbol{F}}_{Lift} + \vec{\boldsymbol{F}}_{Drag} + \vec{\boldsymbol{F}}_{other}) \tag{43}$$

F-3.4. Heat and mass transfer

The heat and mass transfer is realized via source terms, $\boldsymbol{S_E}$ and $\boldsymbol{S_{vap}}$. In this work, it is assumed that the air is not saturated and no condensation occurs during the coating process.

The energy source term, $\boldsymbol{S_E}$, is calculated based on the heat transfer coefficient, tablet surface A_P, and the difference between the tablet and film coating suspension temperatures $(T_P - T_F)$ as follows:

$$S_E = h_{FP}\cdot A_P\cdot(T_P - T_F) \tag{44}$$

$$h_{FP} = \frac{Nu_P\cdot\lambda_F}{d_P} \tag{45}$$

The heat transfer coefficient, h_{FP}, is a function of the Nusselt number, Nu_P, fluid heat conductivity, λ_F, and the specific particle diameter, d_P. For tablets, a specific diameter is the diameter of the area-equivalent sphere.

$$Nu_P = (7 - 10\varepsilon_F + 5\varepsilon_F^2)[1 + 0.7Re_P^{0.2}Pr^{0.33}] + (1.33 - 2.4\varepsilon_F + 1.2\varepsilon_F^2)Re_P^{0.7}Pr^{0.33} \tag{46}$$

The Nusselt number is a function of the void fraction Reynolds and Prandtl numbers. Mass transfer applies an algorithm similar to the heat transfer one:

$$\dot{m}_P = k_m\cdot A_{P,C}\cdot(w_P - w_F) \tag{47}$$

Mass transfer $\dot{m}_P$ is calculated via the mass transfer coefficient, k_m, the coated area, $A_{P,C}$, and the humidity difference between the tablet surface, w_P, and the surrounding gas, w_F.The wet surface area is calculated according to the model proposed by Kariuki et al. [51].

$$k_m = \frac{Sh_P\cdot D_{vap}}{L} \tag{48}$$

The mass transfer coefficient is a function of the Sherwood number, Sh, and the binary diffusion coefficient, D_{vap}.

$$Sh_P = (7 - 10\varepsilon_F + 5\varepsilon_F^2)[1 + 0.7Re_P^{0.2} \cdot Sc^{0.33}] + (1.33 - 2.4\varepsilon_F + 1.2\varepsilon_F^2) \cdot Re_P^{0.7} \cdot Sc^{0.33} \quad (49)$$

The Sherwood number (Sh_P) is a function of the void fraction and the Reynolds (Re) and Schmidt (Sc) numbers [52].

F-3.5. Spray coating model

To model the spray, an inline ray tracing algorithm similar to the approach proposed by Toschkoff et al. [53], [54] was used to detect the coated tablets. This algorithm requires a point of origin, opening angles, droplet size distribution, spray interval and direction vector as input variables. This way, a point of origin for each spray nozzle and the direction of the spray vector can be defined. The number of rays is a function of droplet size and spray interval time. This approach neglects the momentum and heat and mass transfer from the spray to the surrounding fluid. All mass and energy are only transferred between the spray and the tablet or between the tablet and the fluid. From the point of origin in the direction of the spray, tablets in the way of the spray vector are monitored. If a ray detects a tablet, the spray mass given by the droplet radius, the spray composition, and the density is transferred to the tablet. The spread is calculated via the spread function during the simulation run. The coated surface area is calculated using the above-mentioned algorithm of Kariuki et al. [51], which is also applied to calculate the evaporation rate. For more information about this approach, please refer to Forgber et al. [42].

F-4. ConsiGma® coater

In the following sub-Sections, the ConsiGma® coater is introduced in detail, from the coating geometry to an explanation of the process and experimental data.

F-4.1. Coater geometry

The coating process in the ConsiGma® coater involves small batches of consistent coating quality in series. This approach has several advantages over truly continuous and traditional processes. Experiments for setting up a new product or optimizing an existing one are fast and do not require a lot of material. Process settings are tested in small sub-batches, and a continuous process is achieved by recreating the optimal process conditions identified. Additionally, no start-up (e.g., pre-heating and cooling) or end effects typically associated with the continuous process are present and the equipment's footprint is smaller.

An overview of the most important ConsiGma® tablet coater parts is provided in Figure 68. The coating drum (b) is placed in a housing and loaded over a movable lid and chute (a). The adjustable spray nozzle is centrally mounted and is typically in a 12 o'clock position (d). It can be moved vertically and horizontally and rotated around its center. Air is introduced into the drum coater through a central pipe behind the coating wheel (e). Conditioned inlet air knives, which are installed outside of the drum coater between 2 and 3 o'clock (c), dislodge the tablets from the wall and guide them to the spray zone and provide additional drying air. When the coating process is finished, the tablets are discharged from the bottom of the drum (f,h). In addition, the sensors (g) measure the temperature and humidity of air exiting from the outlet air pipe (f) behind the drum coater. The CFD-DEM simulation performed only considers the drum interior (b). The drying air inlet was placed on the side of the drum, and the air knives were modeled as mass inlets on the drum surface. The remaining drum surface was set as the outlet region. The spray nozzle arm and the accompanying light source were included in the simulation volume. In the simulation, the surrounding housing and equipment were neglected, as well as the heat loss to the surrounding air.

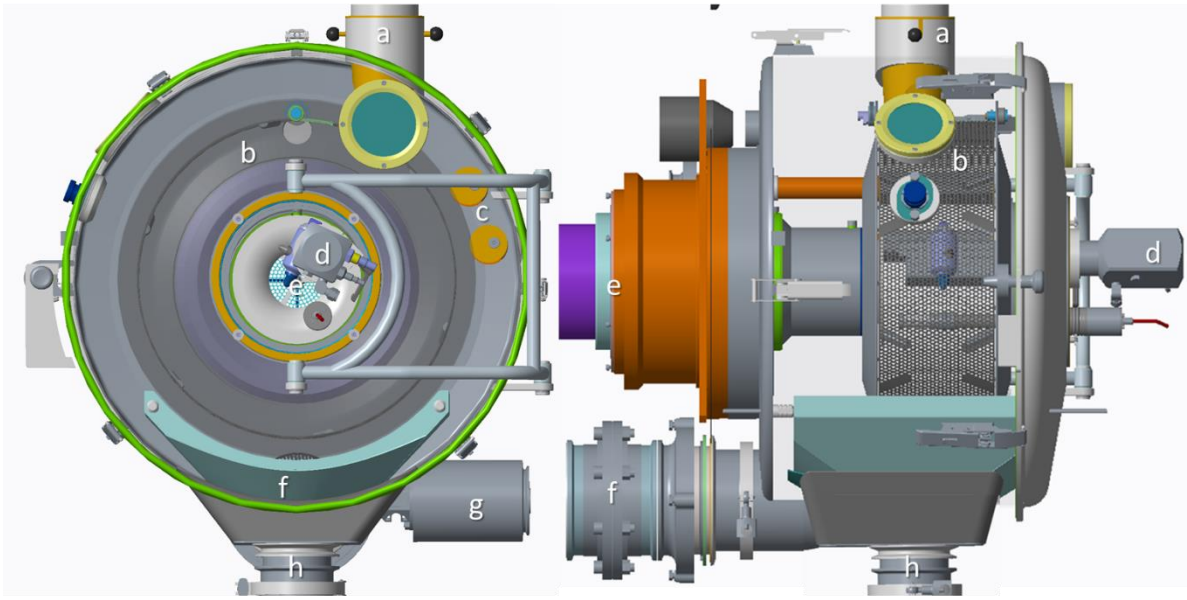

Figure 68: ConsiGma® coater, including the supporting surroundings: a) inlet funnel; b) drum; c) air knives; d) spray nozzle; e) air inlet; f) air outlet; g) temperature/ humidity sensor, and h) outlet funnel.

The ConsiGma® tablet coater drum has a diameter of 44.5 cm and a depth of either 160 mm or 320 mm (Figure 69) determined by the drum insert. The drums can be loaded with 2.5 to 7 kg of tablets depending on the tablet shape and the drum used. The 160 mm drum employs one spray nozzle (Figure 69), while the 320 mm coater uses two. The spray nozzle(s) are set up so that the spray zone covers

nearly the entire drum depth. This minimizes the need for fast axial tablet mixing, and only the radial tablet bed has to be mixed. ConsiGma® 320 has central gripper bars in addition to the gripper bars on the side of the drum to stabilize the tablet bed and accelerate the ring formation, as well as the lateral gripper bars.

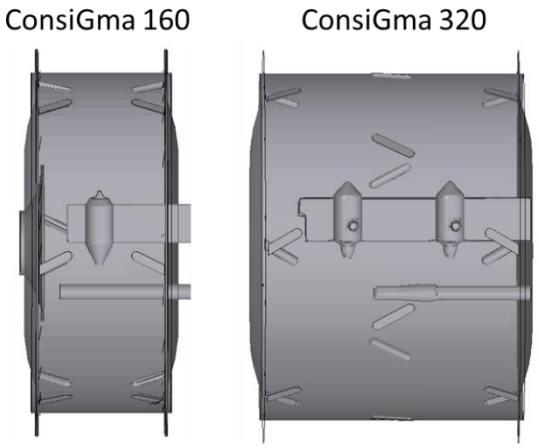

Figure 69: Coater Geometry of the ConsiGma 160 (left) and 320 (right) coater.

F-4.2. Process description

The coating process in the ConsiGma® coater can be divided into seven stages: loading, bed distribution, ring formation, cascade formation, spray coating, drying and discharging. The ConsiGma® coater is loaded via a hopper above the coater. When the loading stage is completed, the drum lid is closed and the coater is rotated at a low speed (ex. 5 rpm) to evenly distribute the tablet bed (A). After this, the drum accelerates to up to 115 rpm. High rotation rates enable the tablets to form a ring along the drum wall due to the centrifugal force that exceeds the gravitational force (B). When the tablet bed forms a steady ring, the rotation rate is reduced to 88-95 rpm depending on the tablet shape, the material properties, the drum load, and the drum type. The air knives inject air from the side and the tablet cascade is formed in preparation for spraying. Once a stable cascade is formed, the spray nozzle(s) are turned on to apply the coating solution (C) onto the tablets until the target quantity of suspension and the associated mass gain are reached. Finally, the tablets dry for a short time before the drum rotation stops and the tablet bed is allowed to collapse. After that, the lid at the bottom of the drum coater is opened and the coated tablet bed is discharged. The remaining tablets are emptied by slowly rotating the drum. A typical coating cycle lasts about 10 minutes depending on the target mass gain and the spray rate.

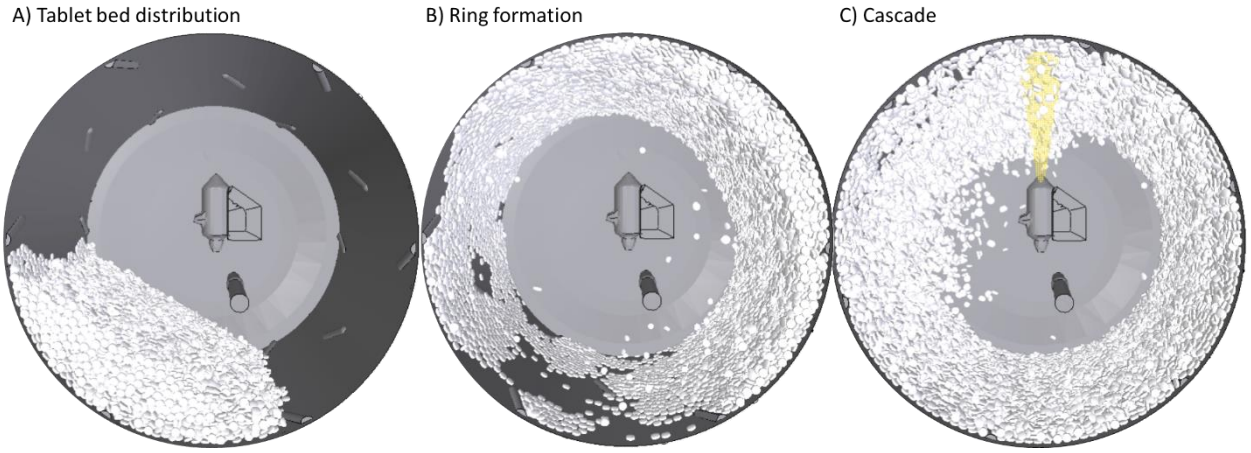

Figure 70: Stages of the coating process, loading/tablet bed distribution, ring formation and tablet cascade with spray.

Figure 71 shows the process output for a typical coating process in the ConsiGma® tablet coater. It provides the rotation rate, inlet air flow rate, air knife pressures, inlet temperature and humidity, and outlet air temperature and humidity. In the first 30 seconds, the tablets are loaded into the drum, which slowly rotates to distribute the tablet bed. After that, the rotation rate is increased to 115 rpm. In this phase, the tablets are distributed along the drum wall and form a ring. After 20 seconds, the rotation rate is reduced to 93 rpm and, shortly after, the air knives are started and the air knife pressure increases from its background pressure of 80mbar to 220mbar, which is kept constant during the coating process. In this example, the rotation rate is reduced in two steps from 93 rpm to 92 rpm and to 91 rpm by altering the tablet-drum friction. The friction between the tablet and the wheel changes in response to the coating applied. The outlet air temperature decreases from 70°C to 60°C and the air humidity increases from 6 g/kg to 14g/kg of air. After 11 minutes, the coating process is completed and the tablets are discharged from the coater wheel. After that, the outlet air temperature increases and the humidity decreases.

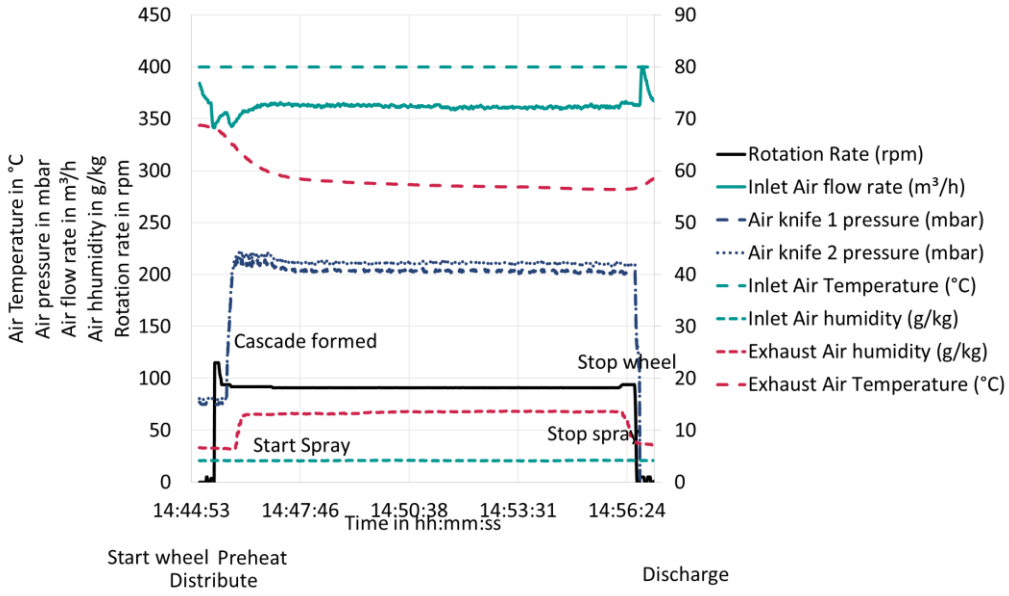

Figure 71: Typical coating process in the ConsiGma® coater.

F-4.3. Experimental setup and operating points

During the experimental runs, four parameters are tracked to validate the simulation model. First, the forces acting on the tablets are recorded to validate the tablet bed dynamics. Second, the coating quality is assessed by tracking the mass gain of 30 tablets across the coating process. Third, the influence of spray rate, drying air flow rate and temperature on the outlet air humidity is analyzed. Fourth, the influence of spray rate, drying air flow rate and temperature on the outlet air temperature is established.

In order to validate the tablet bed dynamics of the simulation model, accelerations of the model tablets are compared to the experimental results. To monitor the forces inside the ConsiGma® coater experimentally, an accelerometer from Maritime BioLogger (https://maritimebiologgers.com/) is placed in the system to track the accelerations in three dimensions every 0.02s. Due to the small size, it is assumed that the forces that the accelerometer experiences are similar enough to the accelerations experienced by the tablets during the coating process. The data are stored on a MicroSD and evaluated after the experiment is completed.

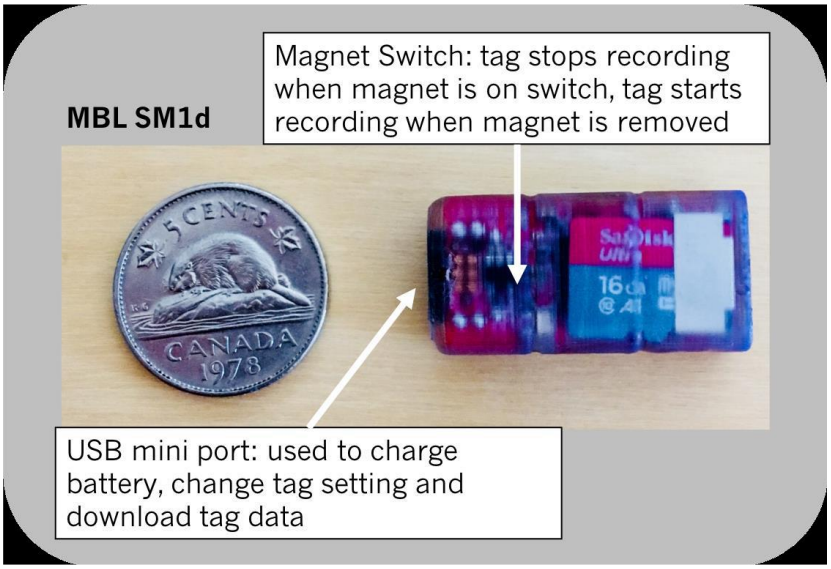

Figure 72: Size Comparison of the maritime bioLogger with a 5 cent coin (image from the manual).

Figure 73: Maritime BioLogger inside the tablet bed in the ConSigma® 320 tablet coater.

The coating quality is tracked by marking and weighing 30 individual tablets before starting the coating process. The tablets are coated for 1%, 2%, 3%, and 4% coating mass gain. After the coating process is finished, the marked tablets are weighed again and the coefficient of inter-tablet coating variation is calculated.

The outlet temperature and humidity are recorded automatically during the coating process inside the ConsiGma® coater. Both values are saved every 2 seconds and can be accessed either during the coating process or in subsequent analysis. The tablets are dried for up to 30 seconds and then discharged. The tablet temperature is measured after the coating process is finished using an infra-red camera and a distance thermometer.

Altogether, six experiments were performed to validate the simulation results for the heat and mass transfer. In the experiments, the drum load, rotation rate, and air knife pressure were kept constant, while the drying air flow rate, temperature, spray rate, and the coater size varied (Figure 69). The simulations were run until the tablet, air humidity and temperature reached a steady state. The design of experiment is provided in Table 18.

Table 18: Process parameters of the experiments and simulations performed.

Process Property DoE Number	**Coater Type**	**Load in kg**	**Rotation rate in rpm**	**Spray rate in g/min**	**Number of Nozzles**	**Drying air flow rate in m^3/h**	**Drying air temperature in °C**
1	160	3	90	75	1	180	60
2	160	3	90	60	1	180	80
3	160	3	90	45	1	210	90
4	320	6	93	75	2	300	60
5	320	6	93	60	2	360	80
6	320	6	93	45	2	420	90

F-5. Results

The primary goal of this work was to validate the CFD-DEM model of a representative coating process in the ConsiGma® tablet coater. The model was assessed with regard to the four most important process output parameters that define the tablet coating process. First, the tablet bed dynamics were analyzed. Changes in acceleration during the various phases were tracked using an accelerometer and compared to the simulation results. Second, the coating mass gain and distribution were assessed. Experiments were conducted tracking the coating mass of 30 tablets for 1%-4% coating mass gain. The mean coating mass and standard deviation were measured and used to calculate the coefficient of variation and compared to the simulation results. Third, the outlet air humidity was tracked. Six experiments were performed and recreated in silico. Process conditions were varied from wet to dry in two coater drum sizes. Additionally, the LoD of the tablets was tracked experimentally and compared to the simulation. Fourth, the outlet air temperatures were analyzed. In addition, the tablet temperature during the coating process was evaluated in the simulation (without being compared to the experimental results).

F-5.1. Forces

An accelerometer tracked changes in the acceleration during the various phases of the coating process. The results are shown in Figure 74, which illustrates the following four stages: loading, ring formation, cascade formation, and discharge process. The first row depicts the entire 260 seconds of the experimental run, including the transition from one phase to the next. In the second row, 5 seconds of the four phases of the coating cycle in the ConsiGma® coater are shown. The positions in the five seconds of interest are indicated by two black vertical lines. In this work, the acceleration is normalized using the gravity constant of 9.81m/s². During the load and tablet bed distribution phase, the accelerometer experiences accelerations of around 1g, i.e., mainly the gravitational pull. All other changes are minimal. During the ring formation, the drum coater is accelerated to 115 rpm and a regular sine wave-like behavior can be observed. During this phase, the tablet bed is in a steady-state and the movement of the tablets relative to each other is almost zero. The various accelerations tracked correspond to the position of the accelerometer. High acceleration values indicate the bottom of the drum coater, with the centrifugal and gravitational forces working in the same direction. The low values correspond to the top of the drum coater, with the centrifugal force counteracted by the gravitational force.

After the ring formation, the cascade phase begins. First, the rotation rate of the drum is reduced to 93 rpm. After 15 seconds, air knives are activated to push the tablets away from the drum wall and allow a wider cascade and enhanced mixing in the reentry zone. During this phase, peaks of up to 8g are observed, as well as periods of almost zero acceleration changes. Periods of high acceleration are due to rapid changes in the acceleration, indicating the reentry or contact of the accelerometer with the tablet bed and the drum wall after the free fall of the cascade. The periods of no acceleration relate to the free fall inside the cascade when the accelerometer appears to fall with a constant velocity. The period following the high peak zones is when the tablets are at the bottom of the drum coater. After the cascade, the tablet bed collapses and the drum rotation is reduced to 5 rpm. Again, mainly the gravitational force is acting on the accelerometer.

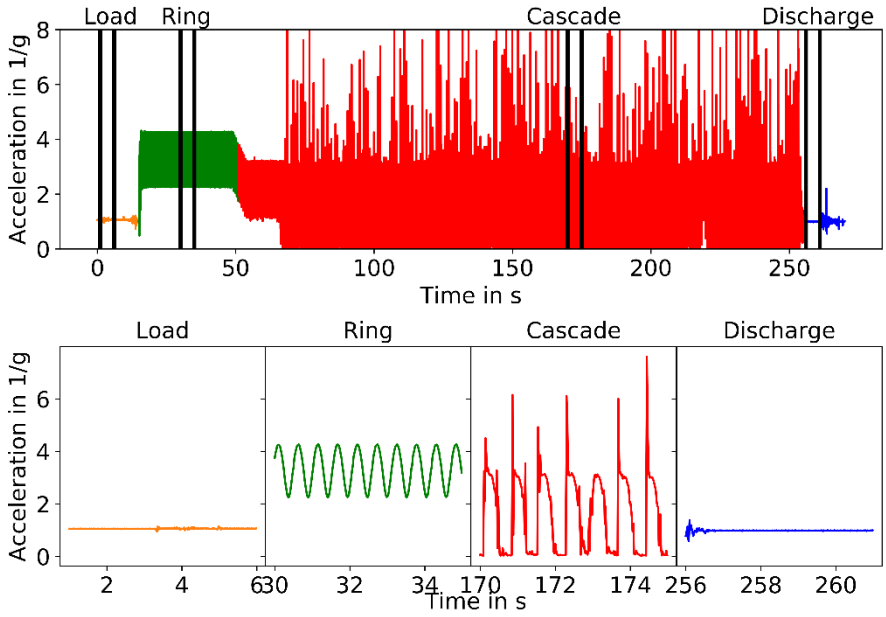

Figure 74: Accelerations recorded during an experimental run. The various phases of the coating process are shown in the subplots below: drum loading and tablet bed distribution, ring formation, cascade formation, and drum discharge.

Figure 75 shows the acceleration during the ring and cascade phases for ten individual rotations overlaid on each other. A full rotation in the ring phase is around 0.5 seconds, while in the cascade phase it lasts 0.7 seconds. In the ring phase, the acceleration changes recorded correspond well to the upper and lower limits of the drum wall. High values indicate the bottom of the drum, where the centrifugal and gravitational forces work in the same direction. Low values indicate the top of the drum, where the gravitational force works in the opposite direction from the centrifugal force. Between 0 and 0.1 seconds and 0.5 and 0.7 seconds, periods of no acceleration are observed. These periods represent the free fall of the accelerometer during the cascade. The accelerometer falls with the tablet bed cascade through approximately 1/3 of the drum coater with no change in the direction and velocity. The peaks at around 0.1 second indicate the end of the free fall and the reentry of the accelerometer into the tablet bed. The period of steady acceleration between 0.2 and 0.5 seconds represents the

acceleration after the reentry of the accelerometer into the tablet bed, up to the contact with the air knife zones. The air knife zones correspond to the smaller peaks in the acceleration at 0.45-0.5 seconds.

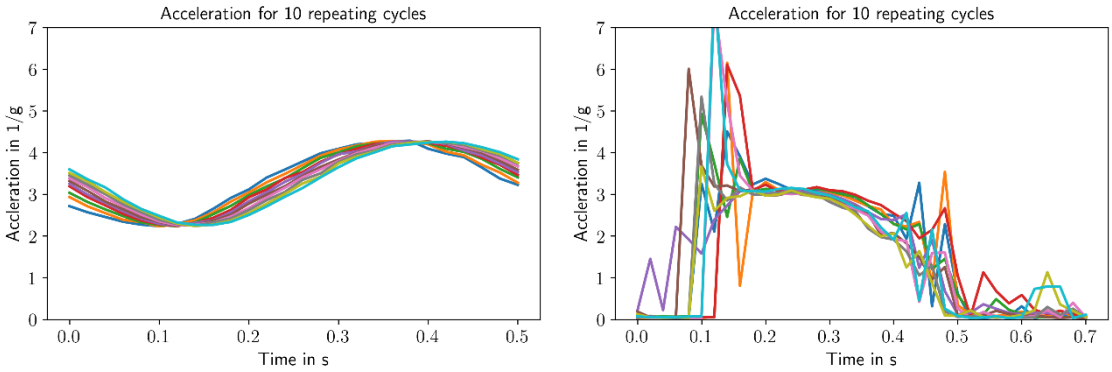

Figure 75: Forces acting on the accelerometer recorded during the ring (left) and cascade (right) phases over the coating cycle time.

Figure 76 shows an image of the simulated tablet bed during the cascade phase. The tablets are colored according to the forces acting on them, and the angle degree of the coater positions is shown around the drum. 0° is at the top of the drum and the angle is rotated counterclockwise, just as the tablets during the coating process do. The tablets experience low/no forces during the cascade phase, high forces during the reentry into the tablet bed and medium forces at the bottom of the drum.

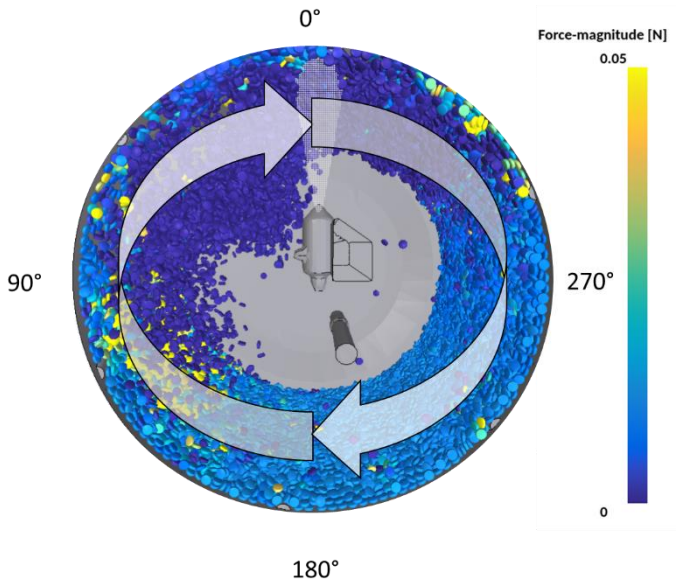

Figure 76: Visualization of the drum angle and the tablet forces.

Figure 77 shows the time-averaged acceleration values in the ring and cascade phases and a comparison between the simulation and experimental results. The simulation results are time- and

spatially-averaged across all tablets. On the left-hand side, the acceleration during the ring phase is shown. The experimental and simulation results agree well. An increase and a decrease in the acceleration from the bottom to the top of the drum and back are clearly visible, as well as the magnitude of the acceleration changes.

On the right-hand side, the acceleration during the cascade phase is shown, as well as the time-averaged acceleration changes of a single tablet during the simulation. The simulated and experimental results also agree well with regard to the overall shape of the curves. Once again, the value at the bottom of the drum (0°) is in good agreement. In the simulation, the zone of reentry into the tablet bed between 60° and 120° is wider and the maximal forces are higher. The zone of free fall/low acceleration is wider in the experimental results than it is according to the time- and spatially-averaged simulated results. In the simulation, some tablets adhered to the drum wall even during the cascade/free-fall period. Although this effect is also present in the experiments with single tablets, it was not recorded for the accelerometer. A possible explanation is that due to its different size, shape, and mass the accelerometer segregates in the inner layer of the tablet bed. The inner layer of the tablet bed always detaches during the free-fall phase. These tablets have higher acceleration forces acting on them since the centrifugal forces from the drum rotation are still contributing. Thus the mean force in this period is higher in the simulation. Since the shape and size of the accelerometer are different from those of the tablets, it tends to segregate and stay on top of the tablet bed. Thus, it is more likely to detach from the drum wall and be engaged in the free-fall phase, while not all tablets follow that pattern.

Regardless of these factors, the experimental and simulated results agree well and confirm the accuracy of the simulation results. This explanation seems to be valid if only the values for a single tablet are compared to the time-averaged experimental results. For a single tablet, the experimental and simulated accelerations are in good agreement even in the free-fall zone. In both cases, the acceleration values are time-averaged over ten cycles. Both the detached state during the free fall and the high acceleration in the reentry zones are captured in the simulation.

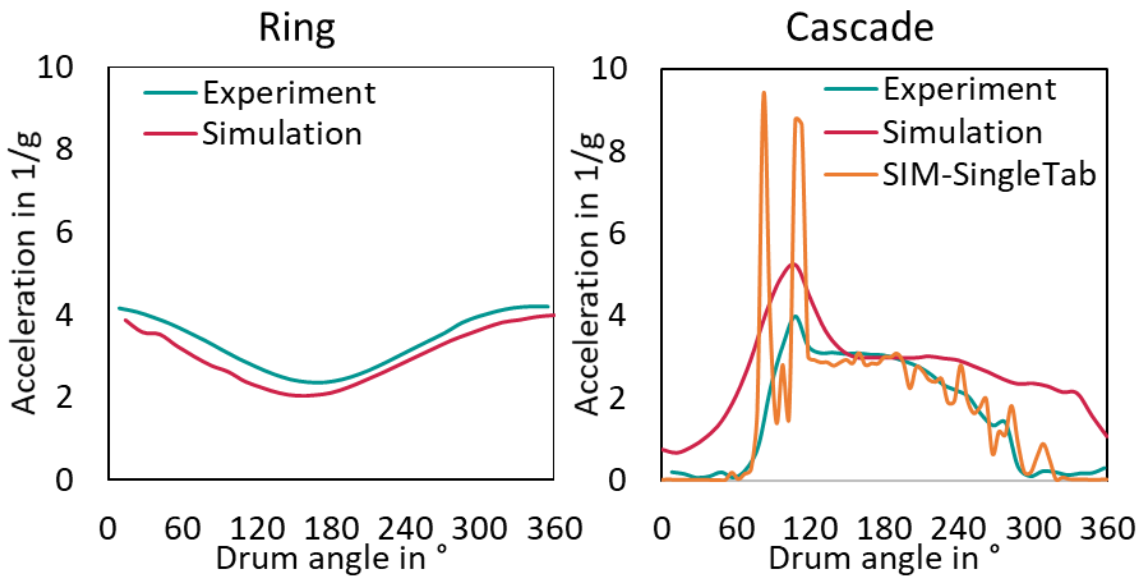

Figure 77: Experimentally time-averaged forces compared to time- and spatially-averaged forces acting on the tablets and time-averaged forces of a single tablet based on the simulation data.

F-5.2. Coefficient of inter-tablet coating variability

Figure 78 shows tablets coated with a mass gain of 1%, 1.7%, 2.5%, 3% and 4%. In the experimental run, 30 tablets were weighed and numbered, and the starting and final tablet weight were compared. The difference between the final and starting tablet weight is the coating mass gain. The Figure shows how the coating layers cover the marking as the coating mass gain increases. The mass gain of the marked tablets was used to calculate the mean coating mass and the standard deviation of the coating mass over time. In the case of 4% mass gain, the coating layer was thick, making it impossible to retrieve all marked tablets after the coating process was completed (although a change in the coating quality and uniformity is visible on the nine sample tablets). While 1% and 1.7% coated tablets show a clear difference in the coating quality as indicated by varying degrees of opacity, it is more difficult to visualize the difference between 2.5% and higher coating mass gains.

Figure 78: Uncoated and coated tablets with various mass gains.

Changes in the CoV over the processing time are shown in Figure 79. Six experiments with a process duration of 2.5, 5, 7.5 and 10 minutes were performed. This time corresponds to a coating mass gain of 1 – 4%. They are shown as black dots in the plot. The simulation results are represented by a solid red line for all tablets and a dotted blue line for 30 randomly selected tablets that were chosen to illustrate the influence of the number of tablets on the CoV variability. After an initial phase of 10 seconds, the simulation results show a steady decline with exponent over time of -0.5, indicating that the coating process in ConsiGma® adheres to the random mixing theory for a conventional batch tablet coating process [55]. The simulation results agree well with the experimental values for 2.5, 5 and 7.5

minutes. Only one simulation was run for 10 minutes. Figure 79 shows that a decline in the CoV is a steady process, which makes it unnecessary to simulate the entire process time.

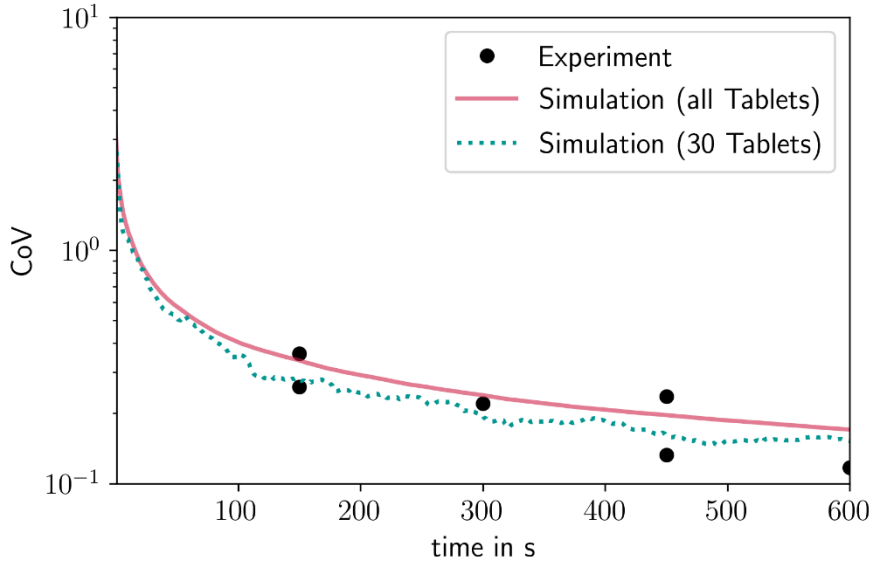

Figure 79: Evolution of the coefficient of variation and comparison between the experiment and the simulation.

Figure 80 shows the CoV for the six cases investigated in the simulation. The variants in the legend are: coater size in mm (ex. 160 in the first experiment); drying airflow rate in m^3/h (ex. 180); drying air temperature in °C (ex. 60); and spray rate in g/min (ex. 75). The results for the CoV follow a very similar trend. All simulations were run for a coating period of at least 120 seconds, with the CoV decrease reaching a steady state after about 20 – 30 seconds or 30 – 45 coating rotations. Additionally, the plot shows that the ConsiGma® 160 and 320 tablet coaters behave similarly in terms of coating quality.

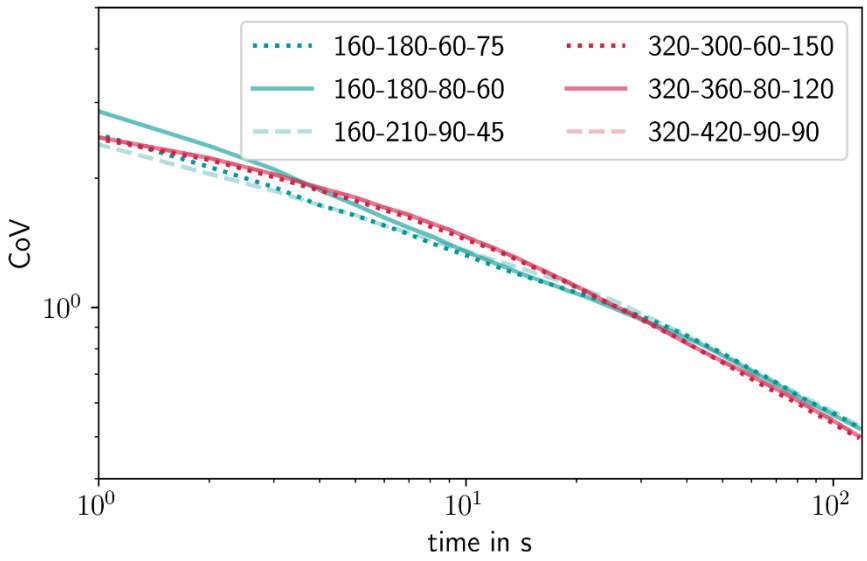

Figure 80: CoV in all simulated cases over time. The variants in the legend are: coater wheel type, drying air flow rate [m³/h], drying air temperature [°C] and spray rate[g/min].

F-5.3. Mass transfer

Figure 81 shows the outlet air humidity over time after the spray nozzle is activated. The left and right columns show the values for ConsiGma® 160 and for ConsiGma® 320, respectively, going from wet to dry cases. Experimentally, the humidity is measured at the outlet behind the tablet coater. In the simulation, the outlet air humidity is measured at the drum surface. In all cases, after 10 seconds the outlet air humidity increases from initial values of 2-6g/kg in the experiments to steady-state values of 15g/kg in the wet cases and 11g/kg in the dry cases. In the simulation, the inlet humidity value is set to 4g/kg in all cases, increasing at the same rate as the experimental results and with the steady-state values matching well in all cases, except for the wet case for ConsiGma® 160 (180m³/h, 60°C, 75g/min) in which the simulation underpredicts the outlet air humidity. In this case, the experimental inlet air humidity is higher than in the simulation, which explains the resulting higher outlet air humidity. The influence of process conditions on the air humidity was shown. The results indicate that the drying air flow rate and temperature together with the spray rate influence the outlet humidity and the evaporation rate. Since the values of all six conditions investigated are quite close, it can be concluded that the evaporation efficiency decreases with the decreasing temperature, airflow rate and temperature.

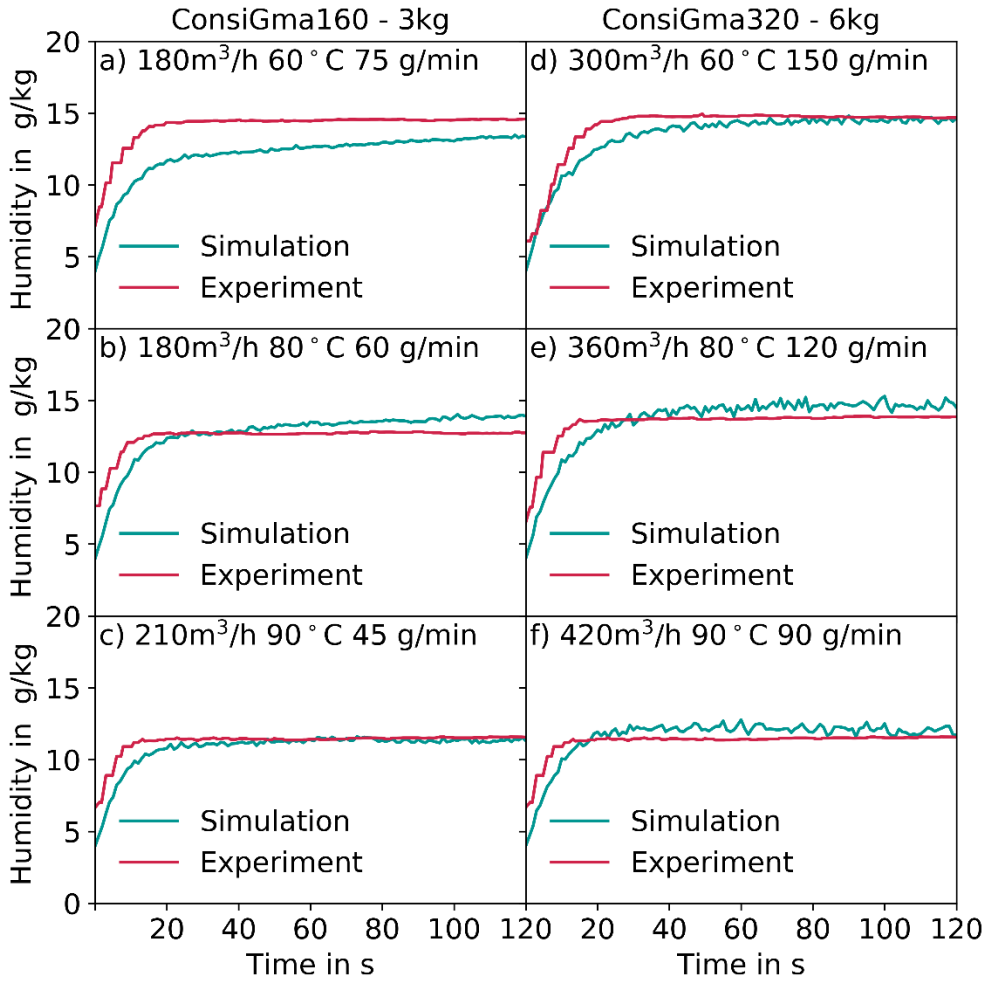

Figure 81: Comparison of the outlet humidity between the experiment and the simulation for ConsGima 160 with a drum load of 3kg: (a) drying air flow rate 180m³/h, air temperature 60°C, spray rate 75g/min; (b) drying air flow rate 180m³/h, air temperature 80°C, spray rate 60g/min; and (c) drying air flow rate 210³/h, air temperature 90°C, spray rate 45g/min, and ConsGima 320 with a drum load of 6 kg: (d) drying air flow rate 300m³/h, air temperature 60°C, spray rate 150g/min; and (e) drying air flow rate 360m³/h, air temperature 80°C, spray rate 120g/min; and (f) drying air flow rate 420³/h, air temperature 90°C, spray rate 90g/min.

The mean LoD of the tablets in the simulation in all six cases investigated is shown in Figure 82. In the simulations, the tablets are initialized without any liquid content. When spraying begins after 12 seconds of process time, the liquid mass on the tablets increases in all cases. After 10 seconds of spray coating, the mean liquid mass of the tablets reaches a steady-state under dry and medium conditions (160-180-80-60, 160-210-90-45, 320-360-80-120 and 320-420-90-90) and increases steadily under wet conditions (160-180-75-75 and 320-300-60-160). The steady-state mean LoD values in the dry case are 0.05%, 0.2% in the 160-180-80-60 case and 0.15% in the 320-360-80-120 case. Although neither of the wet cases (160-180-75-75 and 320-300-60-160) achieves a steady-state, the increase seems to get

shallower over time and reaches a LoD of 1%. This means that in the wet case, the water on the tablets accumulates and does not evaporate fast enough.

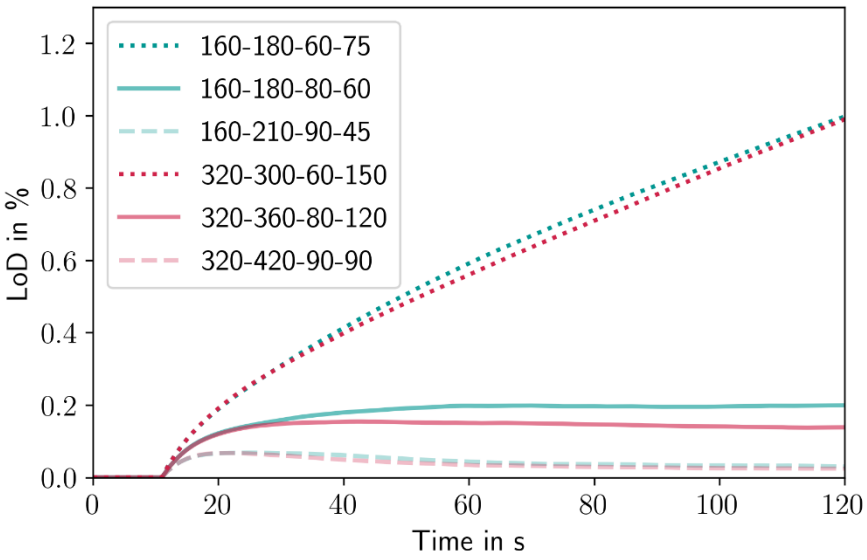

Figure 82: Mean liquid mass during the coating process inside the ConsiGma® coaters.

An increase in the LoD under wet coating conditions was also observed in the experiments. Figure 83 shows the LoD of the tablets before and after coating. The uncoated tablets have a LoD of 1% due to the previous process steps and the surrounding air. The initial tablet LoD is plotted as a dotted line. Silverman et al. defined a scaling parameter for the thermodynamics of a film coating process, N_{thermo}, as [56]:

$$N_{Thermo} = \frac{\dot{m}_{water}}{\dot{V}_{air} \cdot \rho_{air} \cdot (H_{sat,bed,T} - H_{inlet,dew,point,T})} \quad (50)$$

where $\dot{m}_{water}$ is spray liquid mass flow rate [g/h], $\dot{V}_{air}$is the drying air inlet volume flow rate [m³/h], ρ_{air} is the air density [kg/m³], $H_{sat,bed,T}$ is the specific humidity of the inlet air at tablet bed temperature [g/kg] and $H_{inlet,dew,point,T}$ is the specific humidity of the inlet air at the inlet air dew point temperature [g/kg]. Except for very wet coating conditions, the tablets leave ConsiGma® coater drier than when they entered it. Under very dry conditions, this means that the tablet LoD decreases from 1% to 0.5% and in the moderate cases to 0.8%. The tablets that leave ConsiGma® 320 are drier than those that leave ConsiGma® 160 at similar N_{thermo}. Under wet conditions, the tablets retain some of the coating suspension. The LoD increases to 1.5% in both cases, although in the wet cases N_{thermo} in ConsiGma® 160 is lower than in ConsiGma® 320, indicating an increased energy contribution from the surrounding equipment in ConsiGma® 320.

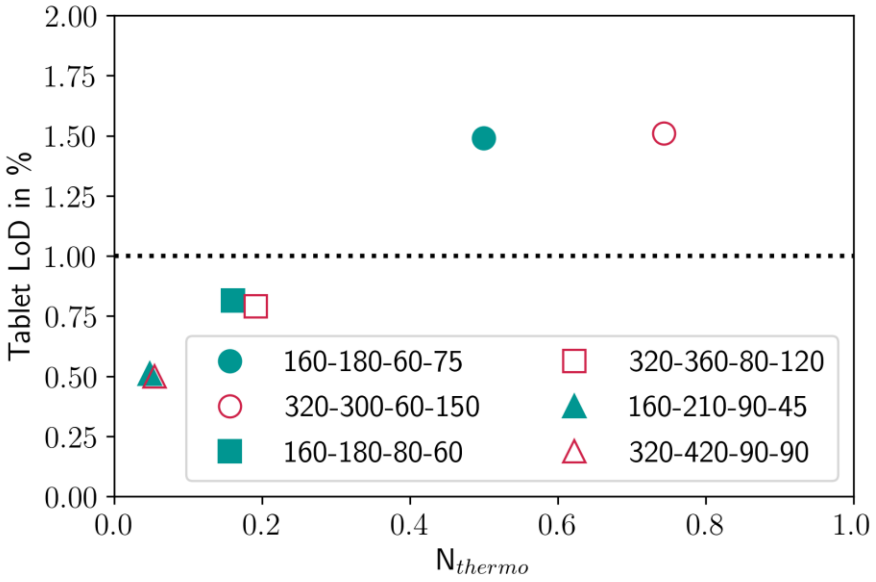

Figure 83: LoD of the tablets before and after the coating process.

F-5.4. Heat transfer

Figure 84 shows the outlet air state under all six conditions investigated. On the left- and right-hand sides, the results for ConsiGma® 160 and ConsiGma® 320 are shown, respectively, going from wet to dry conditions. The initial outlet temperatures in the experiments are higher than in the simulated cases. The reason is that the surrounding equipment is heated over time (also in between the coating experiments). The air cools due to the tablets and the coating spray while being heated due to the stored heat of the equipment. In the simulation, the energy input from the equipment and the heat loss to the surrounding air is neglected since only the drum inside the coater housing was considered. As such, the simulated air temperature increases while the experimental one decreases. Under wet conditions, the simulation underpredicts the outlet temperature. It seems that the simulations underestimate the energy input from the equipment and overestimate the evaporation rate. In the moderate and dry cases in ConsiGma® 160, the outlet air temperature is overpredicted in the simulation, which may suggest that the heat loss to the surrounding air in the smaller drum is higher due to longer residence times in the coater housing. In terms of the outlet air temperature, in the

moderate and dry cases in ConsiGma® 320 the experimental and simulated results match well. The residence time of the drying air is lower due to an increased volume airflow.

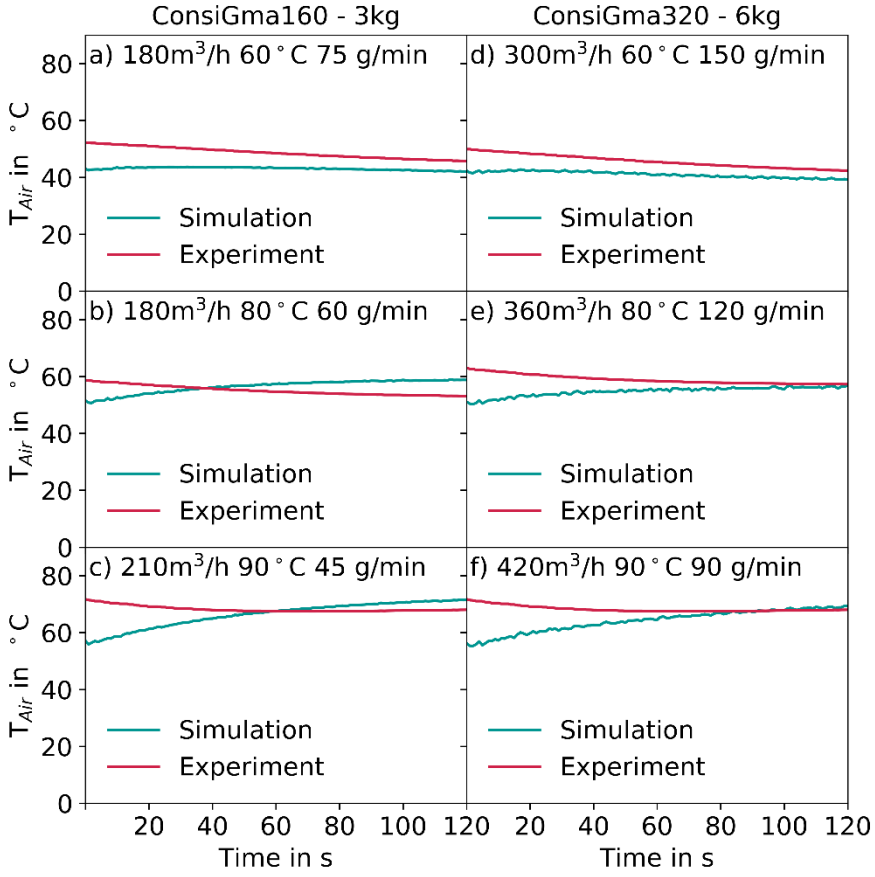

Figure 84: Comparison of the outlet air temperature between experiment and simulation for ConsGima 160 with a drum load of 3kg and a) drying air flow rate 180m³/h, air temperature 60°C, spray rate of 75g/min; b) drying air flow rate 180m³/h, air temperature 80°C, spray rate of 60g/min; and c) drying air flow rate 210³/h, air temperature 90°C, spray rate of 45g/min, and ConsGima 320 with a drum load of 6 kg and d) drying air flow rate 300m³/h, air temperature 60°C, spray rate 150g/min; e) drying air flow rate 360m³/h, air temperature 80°C, spray rate 120g/min; and f) drying air flow rate 420³/h air temperature 90°C, spray rate 90g/min.

Figure 85 shows the steady-state outlet temperatures using N_{thermo}. The steady-state temperatures for N_{thermo} below 0.2 fit well, with the best match observed for ConsiGma® 320. The simulation underpredicts the outlet air temperature for N_{thermo} values over 0.2, possibly due to neglecting the heat stored in the equipment which seems to reheat the outlet drying air. The largest difference between the outlet air steady-state temperature and the simulated outlet air temperature is 5K.

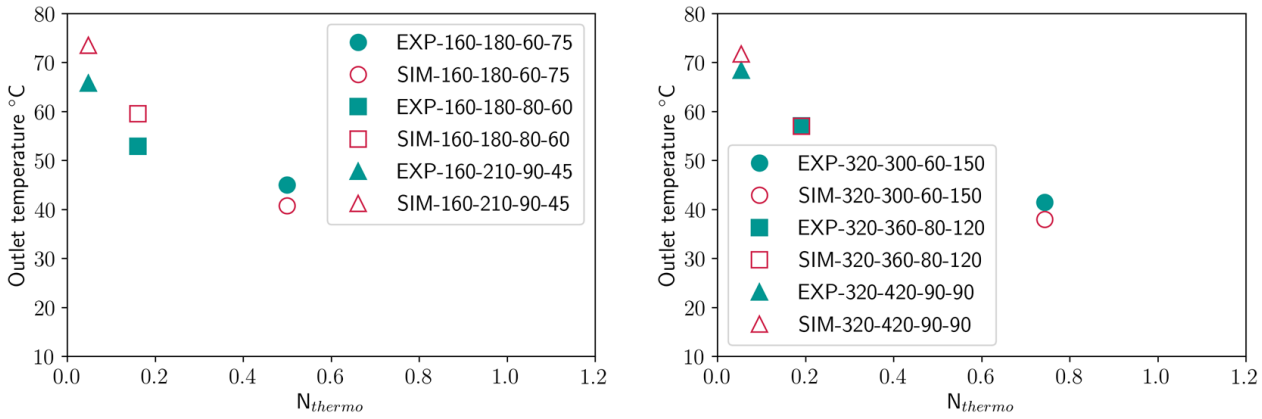

Figure 85: Mean tablet temperature comparison in the simulation after reaching steady-state using the Thermal number.

Figure 86 shows the evolution of the difference between the outlet air and tablet temperatures. After increasing during an initial peak for the first 10 seconds, the difference between the air and tablet temperature progresses towards a steady state. The initial peak indicates the time when the tablet bed is distributed, with most of the drying air bypassing it. After 5 seconds, the ring formation begins and the tablets are distributed along the drum wall. This enlarges the air-tablet interaction surface and increases the heat transfer to the tablets. After 12 seconds, the spray nozzle is activated and the tablet-air temperature difference reaches a steady state after 60 seconds between 8°C and 10°C. Clearly, the initial peak is due to the initialized tablet temperature of 30°C, i.e., the difference increases with the increasing air temperature. The steady-state does not clearly indicate how the tablet-air temperature difference is influenced by the thermal process settings since the highest temperature corresponds to the medium settings, followed by the wet settings and the dry settings that have the lowest temperature difference.

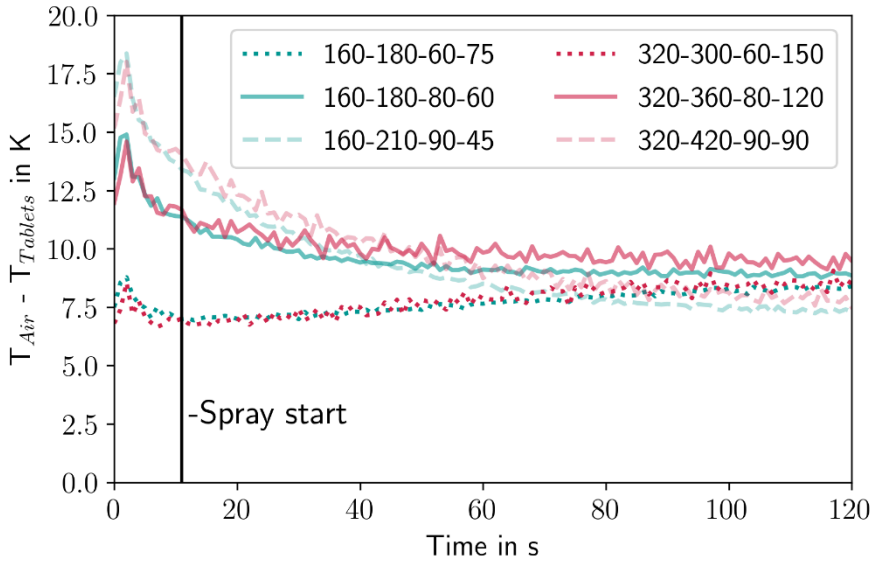

Figure 86: Mean temperature difference between the simulation and experimental results.

F-5.5. Conclusion

The goal of this work was to assess the validity of a CFD-DEM simulation model of the ConsiGma® tablet coater. Six experiments were performed in two coater sizes at varying spray rates, drying airflow rates and inlet temperatures. These experiments were repeated *in silico* using coupled CFD-DEM simulations that exchange the momentum, heat and mass between the tablet and the air phase. To validate the tablet bed dynamics, the tablet acceleration during the various process stages was evaluated and compared to the experimental results. Furthermore, the coating quality in terms of CoV, mass transfer (evaporation of the coating liquid) and heat transfer (between the gas and the tablet phases) were compared to the experimental results in order to validate the entire coating process.

Overall, the simulation and experimental results were in good agreement. During the ring formation stages, they match well with respect to the tablet acceleration. During the cascade stages, although the spatial- and time-averaged simulation values match well, the simulation overpredicts the acceleration during the free fall. In the simulation, the tablets adhered to the wall in this phase, while in the experimental run this phenomenon was not observed possibly due to the difference in the size and shape between the accelerometer and the tablets investigated (the accelerometer tends to segregate in the top or inner layer of the tablet bed and is more likely to detach during the free-fall period).

The coating quality was tracked in six experiments under constant conditions but with a variable coating mass gain target. In these experiments, the simulation was able to capture the evolution of CoV over time. In the simulation, since the spray drying and overwetting effects were not included, it was impossible to show or predict the coating defects.

The mass transfer was tracked through an increase in the outlet air humidity. The simulations matched the increase in the outlet air humidity during the ramp-up period and at steady-state. Moreover, the simulations were able to keep track of the liquid on the tablets, which can help to explain an increase in the LoD and can be used in future work to predict overwetting of the tablets. Finally, the heat transfer was validated by comparing the outlet air temperatures. The experimental and simulated values matched well at steady-state. During the ramp-up (transient) period, the outlet air temperature in the simulation was cooler than it was in the experiments. This can be explained by the heat stored in the equipment, which was not integrated into the simulation. The simulation also showed the temperature difference between the tablets and the outlet air temperature, which was around 10K in all cases. Since the outlet air temperature and humidity match well, it is assumed that this value is also valid for the ConsiGma® tablet coater.

The simulation model was able to replicate the movement and thermal behavior during the coating process inside the ConsiGma® tablet coater on various scales and in various process settings. This validates our simulation approach and confirms that the proposed model can be used to investigate the process space of ConsiGma® coating process. Furthermore, it can be applied to expand the design space of the ConsiGma® coater and reduce the total number of experiments during the development by excluding process settings that are predicted to fail.

Even though the model captured the main features of the coating process inside the ConsiGma® tablet coater, it can be improved. Three important issues will be addressed in its future iterations. The first one is the spray drying and evaporation of the liquid before a droplet is deposited on the tablet. This model extension will offer a more accurate prediction of the liquid deposition efficiency and identify drier and wetter runs even more accurately. The second one is the liquid absorption deposited from the surface and the tablet drying by diffusion. The third one the model equipment to account for the influence of heat transfer from the equipment to the tablets and drying air.

F-6. Bibliography

[1] FDA, “Quality Considerations for Continuous Manufacturing Guidance for Industry Quality Considerations for Continuous Manufacturing Guidance for Industry(draft),” no. February,

2019.

[2] "FDA Perspective on Continuous Manufacturing," *Scharmista Chatterjee*, 2012.

[3] S. Sacher, P. Wahl, M. Weißensteiner, and M. Wolfgang, "Shedding light on coatings : Real-time monitoring of coating quality at industrial scale," vol. 566, no. May, pp. 57–66, 2019.

[4] J. Rehrl, A. Karttunen, N. Nicolaï, T. Hörmann, and M. Horn, "Control of three different continuous pharmaceutical manufacturing processes : Use of soft sensors," vol. 543, no. February, pp. 60–72, 2018.

[5] L. Zema, G. Loreti, A. Melocchi, A. Maroni, and A. Gazzaniga, "Injection Molding and its application to drug delivery.," *J. Control. Release*, vol. 159, no. 3, pp. 324–31, May 2012.

[6] R. Singh, M. Ierapetritou, and R. Ramachandran, "An engineering study on the enhanced control and operation of continuous manufacturing of pharmaceutical tablets via roller compaction.," *Int. J. Pharm.*, vol. 438, no. 1–2, pp. 307–26, Nov. 2012.

[7] L. Saerens *et al.*, "In-line solid state prediction during pharmaceutical hot-melt extrusion in a 12 mm twin screw extruder using Raman spectroscopy.," *Eur. J. Pharm. Biopharm.*, Mar. 2014.

[8] I. C. Kemp, L. Iler, M. Waldron, and N. Turnbull, "Modeling, experimental trials, and design space determination for the GEA ConsiGma™ coater," *Dry. Technol.*, vol. 0, no. 0, pp. 1–11, 2018.

[9] A. F. Silva, J. Vercruysse, C. Vervaet, J. P. Remon, T. De Beer, and M. C. Sarraguça, "In-Depth Evaluation of Data Collected During a Continuous Pharmaceutical Manufacturing Process : A Multivariate Statistical Process Monitoring Approach," *J. Pharm. Sci.*, vol. 108, pp. 439–450, 2019.

[10] O. Goldstein, "ConsiGma ™ A platform for Continuouos Solid Dosage manufacturing enabling Quality by Design and Lean Manufacturing," 2017.

[11] E. Pharmacopoeia, "European Pharmacopoeia (PhEur) chapter 2.9.40 Uniformity of dosage units," *Eur. Pharmacop.*, vol. 8.8, pp. 3117–3120.

[12] J. M. A. Mauritz, R. S. Morrisby, R. S. Hutton, C. H. Legge, and C. F. Kaminski, "Imaging pharmaceutical tablets with optical coherence tomography.," *J Pharm Sci*, vol. 99, no. 1, pp. 385–91, Jan. 2010.

[13] P. Pepiot and O. Desjardins, "Numerical analysis of the dynamics of two- and three-dimensional fluidized bed reactors using an Euler–Lagrange approach," *Powder Technol.*, vol. 220, pp. 104–121, Apr. 2012.

[14] R. Dreu *et al.*, "Evaluation of the tablets ' surface flow velocities in pan coaters," *Eur. J. Pharm. Biopharm.*, vol. 106, pp. 97–106, 2016.

[15] S. Just *et al.*, "Optimization of Inter-Tablet Coating Uniformity for an Active Coating Process at the Lab and Pilot Scale," *Int. J. Pharm.*, vol. 30, no. 11, 2013.

[16] J. Ban, R. Kumar, and S. Agarwal, "Scaling Inter-Tablet Coating Variability in a Horizontal Rotating Drum," vol. 63, no. 9, pp. 3743–3755, 2017.

[17] F. Cello, A. Di Renzo, and F. P. Di Maio, "A semi-empirical model for the drag force and fluid-particle interaction in polydisperse suspensions," *Chem. Eng. Sci.*, 2010.

[18] S. Tanabe, H. Nakagawa, T. Watanabe, H. Minami, M. Kano, and N. A. Urbanetz, "Setting the process parameters for the coating process in order to assure tablet appearance based on multivariate analysis of prior data," *Int. J. Pharm.*, vol. 511, no. 1, pp. 341–350, 2016.

[19] P. Boehling *et al.*, "Simulation of a tablet coating process at different scales using DEM," *Eur. J. Pharm. Sci.*, vol. 93, pp. 74–83, 2016.

[20] D. Suzzi *et al.*, "DEM simulation of continuous tablet coating: Effects of tablet shape and fill level on inter-tablet coating variability," *Chem. Eng. Sci.*, vol. 69, no. 1, pp. 107–121, 2012.

[21] B. N. K. Thakral, "Continuous Tablet Coaters : Developments , Advantages and Limitations," pp. 70–73.

[22] C. Cahyadi, P. Wan, S. Heng, and L. W. Chan, "Optimization of Process Parameters for a Quasi-Continuous Tablet Coating System Using Design of Experiments," vol. 12, no. 1, 2011.

[23] R. Kumar and C. Wassgren, "Angular Circulation Speed of Tablets in a Vibratory Tablet Coating Pan," vol. 14, no. 1, 2013.

[24] B. Cha *et al.*, "A Thermodynamic Balance Model for Liquid Film Drying Kinetics of a Tablet Film Coating and Drying Process," *AAPS PharmSciTech*, pp. 1–13, 2019.

[25] C. Pei, H. Lin, D. Markl, Y. Shen, J. A. Zeitler, and J. A. Elliott, "A quantitative comparison of in-line coating thickness distributions obtained from a pharmaceutical tablet mixing process using discrete element method and terahertz pulsed imaging," *Chem. Eng. Sci.*, vol. 192, pp. 34–45, 2018.

[26] G. Toschkoff *et al.*, "Modeling of an Active Tablet Coating Process," *J. Pharm. Sci.*, vol. 104, no. 12, pp. 4082–4092, Dec. 2015.

[27] P. Toson and J. G. Khinast, "Impulse-based dynamics for studying quasi-static granular flows: Application to hopper emptying of non-spherical particles," *Powder Technol.*, vol. 313, pp. 353–360, 2017.

[28] P. Boehling *et al.*, "Analysis of large-scale tablet coating : Modeling , simulation and experiments," *Eur. J. Pharm. Sci.*, vol. 90, no. EuPAT 7 Special Issue, pp. 14–24, 2016.

[29] R. Kumar, B. Freireich, and C. Wassgren, "DEM – compartment – population balance model for particle coating in a horizontal rotating drum," *Chem. Eng. Sci.*, vol. 125, pp. 144–157, 2015.

[30] B. Freireich, R. Kumar, W. Ketterhagen, K. Su, C. Wassgren, and J. A. Zeitler, "Comparisons of intra-tablet coating variability using DEM simulations , asymptotic limit models , and experiments," *Chem. Eng. Sci.*, vol. 131, pp. 197–212, 2015.

[31] L. Li *et al.*, "Residence time distributions of different size particles in the spray zone of a Wurster fluid bed studied using DEM-CFD," *Powder Technol.*, vol. 280, pp. 124–134, 2015.

[32] M. Girardi, S. Radl, and S. Sundaresan, "Simulating wet gas – solid fluidized beds using coarse-grid CFD-DEM," *Chem. Eng. Sci.*, vol. 144, pp. 224–238, 2016.

[33] C. Bu, D. Liu, X. Chen, C. Liang, Y. Duan, and L. Duan, "Modeling and Coupling Particle Scale Heat Transfer with DEM through Heat Transfer Mechanisms," *Numer. Heat Transf. Part A Appl.*, vol. 64, no. 1, pp. 56–71, Jul. 2013.

[34] A. S. Peter Böhling, Dalibor Jajcevic, Conrad Davies, Alan Carmody, Pankaj Doshi, Johannes G.

Khinast, Mary T. am Ende, “Modeling an Industrial-Scale Fluidized Bed Wurster Coating Process Using CFD-DEM (2016 Annual Meeting).”

[35] K. Takabatake, X. Sun, M. Sakai, D. Pavlidis, J. Xiang, and C. C. Pain, “Numerical study on a heat transfer model in a Lagrangian fluid dynamics simulation,” *Int. J. Heat Mass Transf.*, vol. 103, pp. 635–645, 2016.

[36] C. A. Radeke, B. J. Glasser, and J. G. Khinast, “Large-scale powder mixer simulations using massively parallel GPU architectures,” *Chem. Eng. Sci.*, vol. 65, no. 24, pp. 6435–6442, Dec. 2010.

[37] P. Toson and J. G. Khinast, “Data in brief Particle-level residence time data in a twin-screw feeder,” *Data Br.*, vol. 27, p. 104672, 2019.

[38] P. Toson *et al.*, “Detailed modeling and process design of an advanced continuous powder mixer,” *Int. J. Pharm.*, vol. 552, no. 1–2, pp. 288–300, 2018.

[39] P. A. Cundall and O. D. L. Strack, “A discrete numerical model for granular assemblies,” *Géotechnique*, vol. 29, no. 1, pp. 47–65, Jan. 1979.

[40] D. Jajcevic, E. Siegmann, C. Radeke, and J. G. Khinast, “Large-scale CFD–DEM simulations of fluidized granular systems,” *Chem. Eng. Sci.*, vol. 98, pp. 298–310, Jul. 2013.

[41] H. Kureck, N. Govender, E. Siegmann, P. Boehling, C. Radeke, and J. G. Khinast, “Industrial scale simulations of tablet coating using GPU based DEM: A validation study,” *Chem. Eng. Sci.*, 2019.

[42] T. Forgber, P. Toson, S. Madlmeir, H. Kureck, J. G. Khinast, and D. Jajcevic, “Extended validation and verification of XPS / AVL-Fire ™ , a computational CFD-DEM software platform,” *Powder Technol.*, 2019.

[43] G. Toschkoff *et al.*, “Modeling of an Active Tablet Coating Process,” *J. Pharm. Sci.*, vol. 104, no. 12, pp. 4082–4092, Sep. 2015.

[44] D. Gidaspow, R. Bezburuah, and Ding Jianmin, “Hydrodynamics of Circulating Fluidized Beds: Kinetic Theory Approach,” *7th Fluid. Conf.*, 1992.

[45] Beetstra, R., van der Hoef, M.A., Kuipers, J.A.M., “Numerical study of segregation using a new drag force correlation for polydisperse systems derived from lattice-Boltzmann simulations,” *Chem. Eng. Sci.*, vol. 62, no. 1–2, pp. 246–255, 2007.

[46] B. Krueger, S. Wirtz, and V. Scherer, “Measurement of drag coefficients of non-spherical particles with a camera-based method,” *Powder Technol.*, vol. 278, pp. 157–170, 2015.

[47] A. Hölzer and M. Sommerfeld, “New simple correlation formula for the drag coefficient of non-spherical particles,” *Powder Technol.*, vol. 184, no. 3, pp. 361–365, Jun. 2008.

[48] S. S. K. P and J. a M. Kuipers, “Direct numerical simulations of fluid drag forces of non-spherical particle,” no. December, pp. 1–6, 2015.

[49] L. W. Rong, K. J. Dong, and A. B. Yu, “Lattice-Boltzmann simulation of fl uid fl ow through packed beds of spheres : Effect of particle size distribution,” vol. 116, pp. 508–523, 2014.

[50] L. W. Rong, K. J. Dong, and A. B. Yu, “Lattice-Boltzmann simulation of fluid flow through packed beds of uniform spheres: Effect of porosity,” *Chem. Eng. Sci.*, vol. 99, pp. 44–58, 2013.

[51] W. I. J. Kariuki, B. Freireich, R. M. Smith, M. Rhodes, and K. P. Hapgood, “Distribution nucleation:

Quantifying liquid distribution on the particle surface using the dimensionless particle coating number," *Chem. Eng. Sci.*, vol. 92, pp. 134–145, 2013.

[52] D. J. Gunn, *Transfer of Heat or Mass to Particles in Fixed and Fluidised Beds*, vol. 21. 1978.

[53] G. Toschkoff *et al.*, "Spray Models for Discrete Element Simulations of Particle Coating Processes," *Chem. Eng. Sci.*, vol. 101, pp. 603–614, 2013.

[54] P. Boehling *et al.*, "Analysis of large-scale tablet coating : Modeling , simulation and experiments," *Eur. J. Pharm. Sci.*, vol. 90, pp. 14–24, 2016.

[55] A. Kalbag and C. Wassgren, "Inter-tablet coating variability: Tablet residence time variability," *Chem. Eng. Sci.*, vol. 64, no. 11, pp. 2705–2717, 2009.

[56] A. R. Silverman, J. Givand, B. Holstine, and M. Gentzler, "Novel Scaling of Rotary Drum Film Coating Developed from Commercialization of Pharmaceutical Tablets."

[57] D. Niblett *et al.*, "Development and evaluation of a dimensionless mechanistic pan coating model for the prediction of coated tablet appearance," *Int. J. Pharm.*, vol. 528, no. 1–2, pp. 180–201, 2017.

G. Conclusion

Coating processes in the pharmaceutical industry are ubiquitous and yet rarely investigated. Typically they form the last process step. As most attention is put onto the synthesis and purification part during the initial process development, all granular process steps are often more of an afterthought. They "just have to work" and only minimal effort is expended to create mechanistic understanding and optimize the process after finding a working process point. Investigating and optimizing processes through simulations is a promising way to reduce the amount of actually needed experiments. Thus even in the past neglected or only marginally investigated processes can be optimized through state of the art simulation tools.

The goal of this work was to show the validity and possibilities to use detailed process simulation of coating processes to investigate and improve existing processes in the pharmaceutical industry. The first investigated process was a tablet-coating process. A tablet coating process is mainly governed by tablet bed behavior. The tablet bed has to move in a certain way to provide good axial and radial mixing as well as moderate forces to reduce tablet damage. Tablet coating processes are well suited for DEM simulations due to the size and weight of the tablets as the air drag on the tablets can be neglected. In the last two chapters, an advanced simulation algorithm was used which includes the fluid-particle interaction. A Wurster coater process was investigated taking momentum exchange between fluid and particle into account. Afterwards, the coupling algorithm has been extended to include heat and mass exchange between the granular and fluid phase as well. The application and validation example was a coupled simulation of a novel continuous tablet coater.

In chapter B, a combined study investigated experimentally and in silico the influence of the drum load, scale and rotation rate on the tablet bed surface velocity. First, the validity of the velocity measurements was demonstrated. For the DEM simulation, the influence of the material parameters on the tablet bed surface velocity was shown. The coefficient of friction and restitution do not influence the surface velocity. However, increasing the spring stiffness and time step size proved to influence the tablet surface velocity. After the tablet material parameters were calibrated to one process point the validity over the whole experimentally investigated process range and coater scales were shown. Overall the simulation and experimentally investigated results agreed well. At last, the influence of the material properties on the expected process outcome and tablet behavior was illustrated by comparing the starting range for the tablet stiffness of 2500N/m to the resulting tablet stiffness of 25000N/m. It was shown that the cycle time decreased with increasing spring stiffness but the predicted coating

quality decreases with increasing spring stiffness. Thus proving that the choice of the right material interaction parameters in DEM simulation is one of the utmost important impacts on the predicted process outcome. But false material properties still allow to compare different process settings and typically show the same trend as the correct properties. Predicted values will still be off up to a degree though.

After the importance of the material properties was shown DEM simulations were used to scale from the laboratory scale, which was extensively analyzed in previous work by Toschkoff et al. (Toschkoff et al., 2015) to the pilot and industrial scale (chapter C). Two scaling rules to scale the tablet bed dynamics were chosen and tested in silico. Either, the circumferential velocity or Froude number were kept constant. The drum load was scaled in both cases by the drum volume. We neglected thermal effects, e.g. tablet drying and heating due to changing spray rate, drying air flow rate or temperature due to computational constraints at that time. The effect of the scale-up rules on the tablet bed dynamics, spray zone velocity, spray residence time and cycle time were shown. Keeping the circumferential velocity constant keeps the tablet surface velocity constant but increases the cycle time and spray residence time which can have unforeseen consequences for product quality while keeping the Froude number constant increases the surface velocity, decreases the cycle time and keeps the spray residence time constant which should result in a similar coating quality across all scales. Higher surface velocities result from higher forces acting on the tablets in larger scales with the same Froude number. Overall scaling the tablet bed dynamics by keeping the Froude number constant results in shorter process times as the coefficient of inter tablet coating variation decreases faster and thus allows for faster process cycles.

Chapter D analyses an industrial scale tablet coating process in a multivariant study. In the simulations the drum load, rotation rate, spray rate, and the number of nozzles were varied and analyzed for the coating quality, cycle time, spray residence time and spray zone velocity. Coating quality for the base case simulation was compared to values measured experimentally. Experimental and simulated results agree well on the resulting coating quality although only 90s of the coating process were simulated while the real coating experiments took up to 5h. But it could be shown that even in the industrial scale the coating process reaches a steady state in which the CoV decreases with time to the power of -0.5. The simulation overall agreed with this value. Some simulation predicted faster coating processes with a calculated decrease of up to $t^{-0.6}$. It could be shown that increasing the spray zone width over the axial coater dimensions decreases the CoV. A possible explanation is that due to the increased coating zone width the influence of the axial mixing of the tablet bed is reduced. Thus, the internal radial mixing of

the tablet bed influences the process outcome which is independent of the number of nozzles. The final output of this work was a 4-dimensional process plot that visualizes the coating quality for all 4 investigated process input parameters. Additionally, we demonstrated that the simulation can help to investigate the tablet coating process at the industrial scale thus simplifying the process development process as the number of experiments can be reduced.

The simulation of an industrial scale Wurster coater, the Glatt 15-30 was performed using the CFD-DEM simulation tool (chapter E). The primary goal of our work was to provide insights into the performance of an industrial-sized Wurster coater as a function of different processing conditions. For the analysis, the residence time within the Wurster tube (spray zone), the cycle time, and time-averaged radial velocity profiles were evaluated. The results of this computational investigation indicate that the particle flow behavior is affected mostly by the fluidization air flow rate and the Wurster gap height. We also established that the particle flow changes with the changing particle size and that, surprisingly, larger beads spend less time in the Wurster tube. A correlation between the particle size and cycle time was established, with a difference of around 4 % between the smallest and largest particles in one PSD. When the various coating stages were compared, the difference between the smallest particle size (530 µm) and the largest particle size (1000 µm) was 0.54 s (11 %). Overall, the Wurster coater process is robust in terms of residence time in the Wurster tube and cycle time. Since the change in the spray zone residence time was insignificant regardless of the process settings, the process design should focus on reducing the particle cycle time, leading to a faster, intensified process without affecting the product quality.

In chapter F, the validity of a four-way coupling algorithm was shown on a novel continuous tablet coater. Experiments were performed in the coater to show the influence of the process parameters on the process output, including the drying air flow rate, spray rate and drying air temperature. It could be shown that the forces during the coating process and the decrease of the coating quality over time are in good agreement between the experiment and simulation results. Also, the novel heat and mass transfer in the experiment are in good agreement. Although the effect of the thermal capacity of the equipment on the outlet temperature was not integrated into the simulation the steady-state values were in good agreement.

Over the five performed studies the availability and accuracy of the large scale simulation were shown. Simulation proved to be able to realistically replicate and predict the behavior of granular material at every scale and thus can help to establish new processes or investigating the process space of existing

processes by eliminating the need for extensive experimental studies or enhancing the understanding of the process parameters influence.

H. Outlook

The accuracy and applicability of state of the art large scale process simulations have been demonstrated in this work. Nevertheless, it is important to further improve upon the accuracy and details simulation are able to recreate. As mentioned above it is possible to simulate thermal effects such as drying and heating, but they still need to be worked and improved upon. Incorporating drying and heating into large scale simulation and still be able to deliver fast results is no easy feat. To further increase the detail and accuracy of the simulations also effects like second stage drying, heat transfer between the geometry, tablets, and fluid have to be incorporated.

The goal of future projects should be to increase the accuracy and details of a coating process simulation. First, a simplified approach to calibrate the material properties in the simulations should be established. As could be shown, the material interaction properties influence the process results. Finding the right pair of material interaction materials is no easy task even for the simple contact laws used in this work. Even though tablet-tablet interaction can neglect effects that are present in other granular material e.g. cohesion, tribocharging, it is still challenging to find good experiments that can be on the one hand recreated in the simulation, on the other hand, give predictions about the real device – tablet behavior.

Intra tablet coating variability should be included in coating simulations in the future. It is already possible to track which side of the tablet the coating is applied. In future iterations, the tablet surface will be resolved in greater detail to predict the real intra-tablet coating variability. This is interesting especially for processes with a higher risk of unequal coating distribution on the tablet. Additionally, this system can be expanded to allow the three-dimensional resolution of the tablets to show the liquid uptake and heat transfer inside the outer and inner layers of the tablet.

Next tablet – fluid interaction coupling should be realized. This is important even though the fluid only has a limited effect on the tablet movement. There are only a few established algorithms to calculate the fluid forces acting on non-spherical particles such as tablets. Finding the right drag force models to support low and high void fraction for non-spherical particles is no easy task. A more general and more accurate model for the particle-fluid interaction of non-spherical particles would simplify the simulation process. A possible route would be to increase the resolution of the fluid domain when calculating drag, lift, and torque on the tablets. By incorporating polyhedral shapes in the simulation for the tablet-fluid interaction it should be possible to calculate the precise void fraction in each CFD cell and the fluid forces acting on the tablets would be more precise. Obviously, going this route would increase the

computational demand, but with increasing computational capacity should be a viable strategy when the computational time is kept constant, compared to the current state.

After the fluid-particle interaction is improved one should take a further look into the heat and mass transfer model. As the heat and mass transfer both benefit from improved tablet-fluid interaction calculation through a more precise resolution of the surrounding fluid. Most used models were developed a few decades ago and use dimensionless numbers. Nowadays detailed simulation should allow increasing the accuracy of the dimensionless models depending on the use case. Allowing to track the intra-tablet coating variability allows precise calculation of the wet surface area for evaporation. Introducing initial values for the LoD into the simulations and correctly predicting the drying curve of second and third stage drying allow even preciser predictions of the coating process. For the heat transfer model, a resolved tablet model that allows following the transient intra-tablet temperature at varying tablet depths would be practical for increasing process understanding. Such a model could be expanded to model the heat transfer between the geometry and the tablet more precisely.

Finally, a strategy should be developed that leads to simulation as an intrinsic part of the process development, especially for coating processes. The simulation should help developing new process control strategies that allow for more efficient processes and reduce waste due to error-prone processes. This can be realized by gaining insights from the simulation that leads to a better process understanding and thus increased process control. Incorporating simulation results in soft sensors and thus combining new PAT tools with simulation has the potential to extend the available operating space. In the midterm future, not only simplified models will be used to run digital twins in parallel to the actual process but process simulations will be fed with inline measured process data. This approach allows predicting the process outcome in real-time allowing for on the fly process optimization that will help to minimize rejected batches.

I. List of publication

I-1. Peer-reviewed paper – as the main author

Boehling, P., Toschko, G., Dreu, R., Just, S., Kleinebudde, P., Funke, A., & Rehbaum, H. (2017). Comparison of video analysis and simulations of a drum coating process. European Journal of Pharmaceutical Sciences, 104(March), 72–81. https://doi.org/10.1016/j.ejps.2017.03.031

Boehling, P., Toschkoff, G., Just, S., Knop, K., Kleinebudde, P., Funke, A., … Khinast, J. G. (2016). Simulation of a tablet coating process at different scales using DEM. European Journal of Pharmaceutical Sciences, 93, 74–83. https://doi.org/10.1016/j.ejps.2016.08.018

Boehling, P., Toschkoff, G., Knop, K., Kleinebudde, P., Just, S., Funke, A., … Khinast, J. G. (2016). Analysis of large-scale tablet coating : Modeling , simulation and experiments. European Journal of Pharmaceutical Sciences, 90, 14–24. https://doi.org/10.1016/j.ejps.2015.12.022

Böhling, P., Khinast, J. G., Jajcevic, D., Davies, C., Carmody, A., Doshi, P., … Sarkar, A. (2018). Computational Fluid Dynamics-Discrete Element Method Modeling of an Industrial-Scale Wurster Coater. Journal of Pharmaceutical Sciences, 108, 538–550. https://doi.org/10.1016/j.xphs.2018.10.016

I-2. Peer-Reviewed paper – as a co-author

Kureck, H., Govender, N., Siegmann, E., Boehling, P., Radeke, C., & Khinast, J. G. (2019). Industrial scale simulations of tablet coating using GPU based DEM: A validation study. Chemical Engineering Science. https://doi.org/10.1016/j.ces.2019.03.029

I-3. Book Chapters – as a co-author

Sarkar, A.; Shoemaker, B.; Doshi, P.; am Ende, M. T.; Jajcevic, D.; Böhling, P.; Toson, P.; Zadravec, M. & Khinast, J. G. 2019. “Multiscale Modeling of a Pharmaceutical Fuild Bed Coating Process Using CFD/DEM and Population Balance Models to Predict Coating Uniformity”. In: am Ende, D. J. & am Ende, M. T. (eds.), Chemical Engineering in the Pharmaceutical Industry, Hoboken, NJ, USA: John Wiley & Sons, Inc., pp. 419–450, ISBN: 978-1-119-60080-0, DOI: 10.1002/9781119600800.ch67, Available: <http://doi.wiley.com/10.1002/9781119600800.ch67>, [Consulted: August 22, 2019].

J. List of figures and tables

J-1. Figure captions

J-2. Table captions

K. Acknowledgement

I want to thank my colleagues at the RCPE to always be there ready to help, give advice or drink a coffee. It is a pleasure going to work in such a warm, welcoming and productive environment. The discussion about work and non work related topics bring new ideas and helped me to develop my scientific carreer. Worth mentioning are the working trips are fun and even though they are exhausting and sometimes boring. A special thanks goes to Dr. Dalibor Jajcevic who realy helped me a lot developing my scientific output and accuracy.

I want to thank my family for always supporting me in the my decisions and giving me the support I need even though I am so far away. At the same time I also want to thank my friends who are always there for me and help to take my mind from work and help me relax and recharge my batteries. It is nice to know that someone is there for you regardless what the topic is. I won't forget the RC Graz for providing me with good opportunities to get rid of my excess energy after long working days and the possibilities to always meet new people and hitting them hard. A special thanks goes to Marlene Grünberger for being there for me during the last month giving me support during the last phase of my PhD thesis.

At last I want to thank my supervisor Professor Johannes G. Khinast for having the patience and calmness to stay with me during my doctoral thesis.

This work was funded through the Austrian COMET Program by the Austrian Federal Ministry of Transport, Innovation and Technology (BMVIT), the Austrian Federl Ministry of Economy, Family and Youth (BMWFJ) and by the State of Styria (Styrian Funding Agency SFG)